A Network Approach to the Analysis of Mass Transfer from a Capillary Porous Medium

A Thesis Submitted to the Faculty of

Universidade Federal de Santa Catarina

In Partial Fulfillment of the Requirement for the Degree of

Doctor in Mechanical Engineering

by

YANG Xuefeng

Florianópolis, Santa Catarina

August 1995

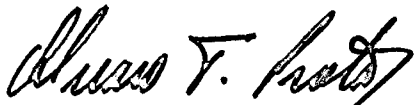# A Network Approach to the Analysis of Mass Transfer from a Capillary Porous Medium

Yang Xuefeng

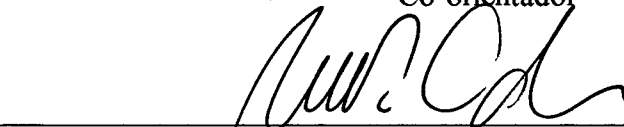Esta tese foi julgada adequada para a obtenção do título de

Doutor em Engenharia

especialidade Engenharia Mecânica, área de concentração Fluidos, e aprovada em sua forma final pelo Curso de Pós-Graduação em Engenharia Mecânica
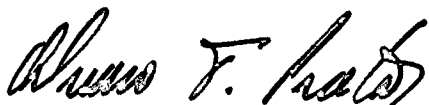

Prof. Álvaro Toubes Prata, Ph. D.
Orientador

Prof. Paulo César Philippi, Dr. Ing.
Co-orientador

Prof. Antônio Fábio Carvalho da Silva, Dr. Eng. Mec.
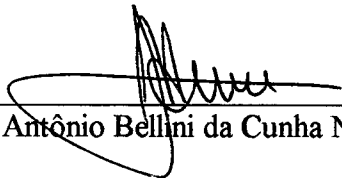Coordenador do Curso

Banca Examinadora:

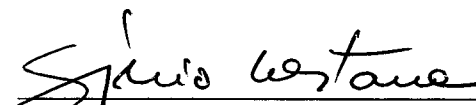Prof. Álvaro Toubes Prata, Ph. D.
Presidente
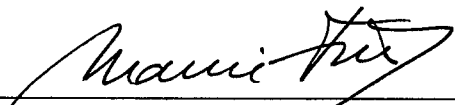
Prof. Paulo César Philippi, Dr. Ing.

Prof. José Antônio Bellini da Cunha Neto, Dr.

Prof. Silvio Crestana, D. Sc.

Prof. Mauri Fortes, Ph. D.

Florianópolis, 11 de agosto de 1995

To my lovely wife
Para minha querida esposa
献给我亲爱的妻子

LIU Li

For her love, constant support and company
Por seu amor, constante apoio e companhia
为了她的爱，支持和陪伴

To my loving parents
Para meus queridos pais
献给我亲爱的父母

YANG Xu & LIU Lanxin

For their love, education and encouragement
Por seu amor, educação e encorajamento
为了他们的爱，培育和鼓励

ACKNOWLEDGMENTS

ABSTRACT

A microscopic drying model for capillary porous medium is presented in this thesis. This microscopic model is based on a network approach for porous medium and is used to study the drying behavior inside the porous medium at the pore level during the drying process. The driving force for liquid transfer is the capillary force and the mass transfer in gaseous phase is the vapor diffusion. The Kelvin effect is considered in this model, i.e., the gas-liquid interface is treated as a meniscus. The gravity force is neglected because the size of the pores and throats in network are large enough (> 20 μm). Drying process is simulated using this model on various 100x20 square networks which contain 2000 pores and 4000 throats. The liquid used is alcohol. The drying process is assumed to be isothermal.

The phase distribution effect, the Kelvin effect and the influence of the velocity of the external flow upon the drying process are investigated. Three distinct regions are observed in all of the simulation results, i.e., dry region, unsaturated region and saturated region. The evaporating front region (unsaturated region) is relatively stable, although it is far from a flat surface. Many temporary liquid clusters appear in the unsaturated region and the cluster number increases with the distance of the evaporating front from the interface.

It is found that the phase distribution (moisture heterogeneities) has a great influence on the drying rate through the formation of funicular drying zones, specially at the beginning of the drying process. This influence decreases with the receding of the evaporating front from the interface. The drying process becomes vapor diffusion dominated after the interface is totally dried and the influence of phase distribution heterogeneities decrease. The evaporation-condensation mechanism is observed in the simulation, which confirmed the existence of such process in the drying of capillary porous medium.

Concerning to the microscopic model, it is found that Kelvin effect makes a very small difference in terms of the diffusion driving force caused by the curvature. The Kelvin effect, however, is very important from the point of view of the evaporation-condensation mechanism. The appearance of condensing clusters changes the drying path due to the liquid removing process, altering the phase distribution during the drying process. This influence is affected by the network formation.

The incoming velocity of the external flow over the interface of the porous medium has influence on the local mass fluxes as would be expected. But it is significant only while the interface is totally or partially wetted. This influence decreases with the receding evaporating front. Concerning the stability of the evaporating front, it seems that this is only important at the beginning of the drying period.

RESUMO

Um modelo de secagem microscópico para o meio poroso capilar é apresentado nesta tese. Este modelo microscópico é baseado em uma abordagem de rede para o meio poroso e é usado para estudar o comportamento da secagem no interior do meio poroso durante o processo de secagem em escala dos poros. A força motora para o transporte do líquido é a força capilar e a transferência de massa na fase gasosa é a difusão de vapor. O efeito Kelvin é considerado neste modelo, ou seja, a interface gás-líquido é tratada como um menisco. A força gravitacional é ignorada pois os tamanhos dos poros e gargantas da rede são relativamente grandes (> 20 μm). O processo de secagem é simulado usando este modelo em várias redes quadradas 100x20, contendo 2000 poros e 4000 gargantas. O líquido é álcool e o processo de secagem é assumido isotérmico.

O efeito de distribuição da fase líquida, o efeito Kelvin e a influência da velocidade do escoamento externo sobre o processo de secagem são investigados. Três regiões distintas são observadas em todas as simulações, isto é, região seca, região não saturada e região saturada. A frente de evaporação (região não saturada) é relativamente estável, mesmo que a superfície seja irregular. Muitas ilhas isoladas temporárias surgem na região não saturada e o número dessas ilhas aumenta com a distância da frente de evaporação da interface.

Constatou-se que a distribuição da fase líquida (heterogeneidade da umidade) tem uma grande influência sobre a taxa de secagem através da formação das zonas secas funiculares, especialmente no início do processo de secagem. Esta influência diminui com o recuo da frente de evaporação da interface. O processo de secagem torna-se dominado pela difusão de vapor após a secagem total da interface e a influência de heterogeneidade da umidade diminui. O mecanismo evaporação-condensação é observado na simulação, influenciando o processo de secagem através da mudança do caminho da secagem.

No que diz respeito ao modelo microscópico, o efeito Kelvin tem pouca influência com relação à força motora de difusão, causada pela curvatura. Entretanto, esse é muito importante do ponto de vista do mecanismo evaporação-condensação. O surgimento de ilhas isoladas em processo de condensação muda o caminho da secagem devido ao processo de retirada do líquido, alterando a distribuição da fase líquida durante o processo de secagem. Essa influência é afetada pela distribuição de poros da rede.

A vazão do escoamento externo tem uma influência na taxa de evaporação local, como era de se esperar. Entretanto, isso é importante apenas enquanto a interface está total ou parcialmente molhada. Esta influência diminui com o recuo da frente de evaporação no interior do meio poroso. A estabilidade da frente de evaporação parece ser importante somente no início da secagem.

LIST OF CONTENTS

LIST OF FIGURES

LIST OF TABLES

NOMENCLATURE

$\dot{m}$	flux density [kg s^{-1}]
$\bar{U}$	velocity vector [m s^{-1}]
$(\rho c)^*$	mass fraction weighted heat capacity [kcal kg^{-1} K^{-1}]
A	section area of throat [m^2]
a,b	coefficient
B	Bond number
Ca	capillary number
$\mathcal{D}$	binary mass diffusion coefficient [m^2 s^{-1}]
D	mass flux rate [kg s^{-1}]
D_T	non-isothermal mass diffusivity coefficient [m^2 s^{-1} K^{-1}]
D_v	isothermal mass diffusivity coefficient in vapor phase [m^2 s^{-1}]
D_{vT}	non-isothermal mass diffusivity coefficient in vapor phase [m^2 s^{-1} K^{-1}]
D_w	isothermal mass diffusivity coefficient [m^2 s^{-1}]
g	coefficient
J	diffusion flux density [kg m^{-2} s^{-1}]
k	convective mass transfer coefficient [m s^{-1}]
K	hydraulic conductivity [m s^{-1}]
$\mathcal{L}$	latent heat of vaporization [J kg^{-1}]
ℓ	typical pore size in Bond number
l	length of throat [m]
M	molecular weight [kg kmol^{-1}], also used as viscosity ratio in chapter 1
n	number of moles
P	pressure [Pa], also used as Peclet number in chapter 3
P_0	vapor pressure for a flat surface at temperature T [Pa]
P_r	vapor pressure for the curved surface of radius r [Pa]
r	radius [m]

R	universal gaseous constant [J mol^{-1} K^{-1}]
S	saturation, volume of liquid divided by empty volume
T	temperature [K]
t	time [s]
V	volume [m^3]
W	mass moisture content [kg kg^{-1}]
x,y	spatial coordinates

GREEK SYMBOLS

Γ	conductance
ρ	density of mixture [kg m^{-3}]
ϕ	general variable
ν	kinematic viscosity [m^2 s^{-1}]
ω	mass fraction
σ	surface tension [N m^{-1}]
μ	viscosity [kg m^{-1} s^{-1}]
λ^*	effective thermal conductivity [kcal m^{-1} s^{-1} K^{-1}]
ρ_l	liquid density [kg m^{-3}]
ρ_s	density of dry material [kg m^{-3}]

SUPERSCRIPTS

0	values at time t
H	horizontal throats
V	vertical throats

SUBSCRIPTS

A	vapor
B	air
l	liquid
sat	saturated
P	central grid point
E	east grid point

N	north grid point
S	south grid point
W	west grid point
e	east face of control volume
n	north face of control volume
s	south face of control volume
w	west face of control volume
x	local value

CHAPTER 1   GENERAL INTRODUCTION

1.1 BACKGROUND

Many processes involve heat and mass transfer between a fluid and a porous medium. The convective drying of porous materials and the thermal insulation of buildings are two examples. Especially, drying is an essential operation unit in the industrial production and one of the most energy-intensive processes in industry. There is hardly a product in the processing industries that does not have to be dried one or more times during the course of its production. Sometimes, the drying operation cost can affect the economics of all process. To improve process performance and energy utilization, new drying technologies have been studied and applied, such as fluidized and spouting bed drying, freeze drying, spray drying and dielectrically-assisted convective drying, with emphasis on increasing the heat and mass transfer area and the transfer coefficient at the interface between external flow and porous material. Although these drying technologies have been used in industry production, the drying model for prediction of the processes are generally empirical or semi-empirical. From the theoretical point of view, even the simplest situation, such as the convective drying of a bed of glass beads at room temperature is still a challenging problem for the modelers. One of the reasons which precludes the existence of a general model for the prediction of drying of porous material is the great variety of the materials encountered in practice and the geometric complexity of their structures. Porous media include a lot of materials which are encountered literally everywhere in everyday life. A material or a structure must pass at least one of the following two tests in order to qualify as a porous medium (Dullien, 1979).

(1) It must contain spaces, so-called pores or voids, free of solids, imbedded in the solid or semisolid matrix. The pores usually contain some fluid, such as air, water, oil, etc., or a mixture of different fluids.

(2) It must be permeable to a variety of fluids, i.e., fluids should be able to penetrate through one face of a septum made of the material and emerge on the other side.

Capillary flow   Evaporation-Condensation   Vapor flow
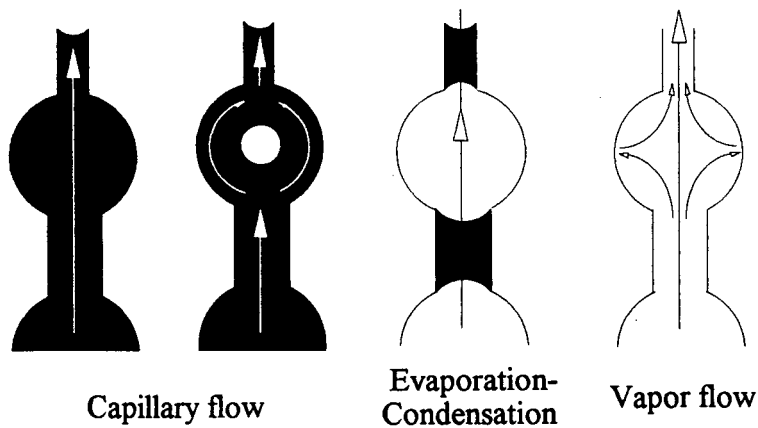
Fig. 1-1   Moisture movement at various stages in the
drying of a porous material (from Bories, 1991)

When a sample of wet porous material dries under constant external conditions, that is, temperature, humidity and air-velocity held constant during the drying process, four phases of moisture movement within the material may be distinguished (Fig. 1-1). In the first phase, the sample is saturated with the liquid, the moisture flows as liquid towards the interface under a hydraulic gradient due to the difference of capillary force. There is no vapor or air inside the porous medium, or it can be neglected. In the second phase, a part of the sample has been dried, the moisture has withdraw from the waist of the pores, and moisture can migrate either by creeping along the capillary walls or by successive evaporation and condensation between liquid bridges (Fig. 1-2). The evaporation-condensation mechanism through liquid bridges works as following:
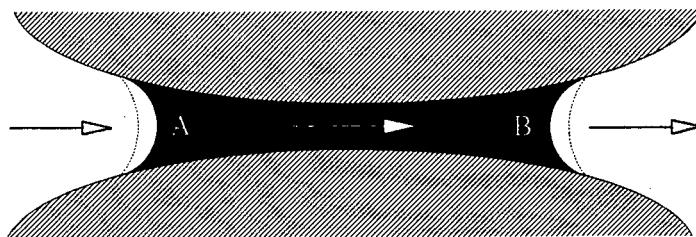
Fig. 1-2   A liquid bridge at a narrow throat

Initially, the menisci curvature at the two sides of the liquid bridge are equal due to the thermodynamic equilibrium condition (indicated by solid line). The vapor flows in the direction

indicated by the arrow due to the gradient of partial pressure caused by the difference of menisci curvatures and the temperature. Vapor condenses at the surface of meniscus A, resulting in a decreasing of the meniscus curvature (plotted by dashed line) and the unequilibrium of capillary force between two sides. The meniscus B (solid line) has a higher curvature than meniscus A. This curvature difference of menisci at the two end sides of the liquid bridge results in a pressure difference inside the liquid phase, i.e., a gradient of hydraulic pressure from A to B is established. As a consequence, liquid flows from high to low pressure and a new equilibrium tends to establish at the two end sides of the liquid bridge (dashed line). If the vapor pressure at the side B is lower than that of side A, the liquid at meniscus B will evaporate causing an increasing in curvature. Vapor will condense on side A and evaporate on side B, and liquid is transported through the bridge. The liquid bridge can last if the condensation rate at one side is equal to the evaporation rate at the other side. Of course, the liquid bridge could have two evaporating or condensing menisci at its both sides depending on the moisture content adjacent to the menisci. If the two menisci are evaporating, the liquid bridge will become smaller and smaller until it disappears. On the other hand, if the two menisci are condensing, the liquid bridge will become bigger and bigger until its menisci reach the throat edges.

On a latter drying stage, the liquid bridges evaporate entirely leaving only adsorbed moisture behind. During this last phase, moisture moves by unhindered diffusion. The final stage of the porous medium is one of desorption-adsorption during which any moisture evaporated is condensed and the body is in hygrothermal equilibrium with its environment.

The internal moisture flow may be affected by several factors depending on the structure of the solid matrix, the type of moisture bonding, the moisture content, temperature and pressure in the capillaries, etc. The main mechanisms which cause internal moisture flow are:

(1) Capillary forces
(2) Diffusion due to concentration difference
(3) Phase change (evaporation - condensation mechanisms taking place in the pores)
(4) Surface diffusion of moisture on adsorbed liquid layer at the capillary surface
(5) Difference in total pressure
(6) Gravity
(7) Thermo-diffusion

Several of these mechanisms dominate at a given time during drying, and their importance are not the same for different porous materials. It depends on many factors such as material composition, period of drying, pore size etc. No matter which mechanism controls the drying

behavior, the drying rate curve is almost common to all materials (Fig. 1-3). A general drying process will now be described (Peishi and David, 1989, Bories, 1991)

If the initial moisture content of the porous medium is high enough, almost all material surface is covered by a liquid film and the internal moisture transfer is mainly attributable to capillary flow of free liquid. The drying rate is then generally controlled by the convective heat and mass transfer coefficient of the external flow. If the external conditions are constant, the drying rate is constant in this period. It is also known that if all the heat needed for evaporating the liquid is supplied by the air, the temperature of the material surface will take on a value very close to the ambient wet-bulb temperature (Prata and Sparrow, 1985a, 1985b and 1988)
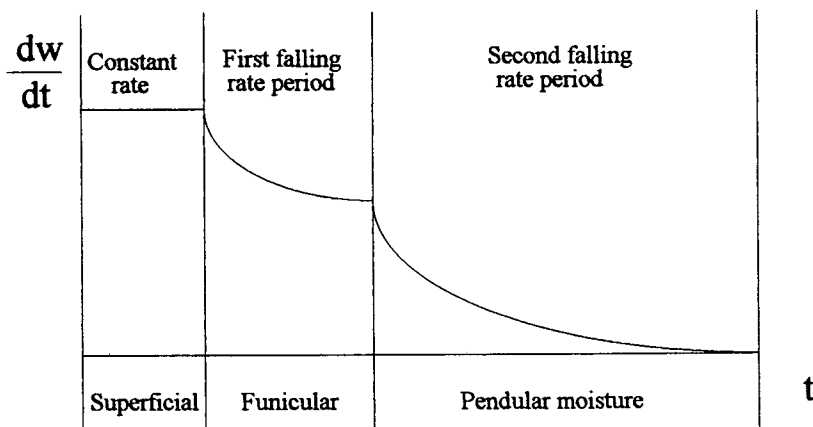
Fig. 1-3   Variation of drying rate with time

As drying proceeds, the liquid supplied to the surface by capillary forces becomes insufficient to replace the liquid being evaporated. When the moisture content reaches a certain critical value, discontinuous wet patches will occur at the material surface. Thus, the mass transfer coefficient decreases with the surface free liquid content and the first falling rate period starts. In the first falling rate period, a new energy balance will be reached at the surface, accompanied by a slowly rising of the surface temperature. Free liquid still exists at the surface, the 'dry' patches still contain bound liquid, and the vapor pressure at the surface is determined by the Clausius-Clapeyron equation.

When the surface moisture content reaches its maximum sorptive value, no free liquid exists at the surface. The surface temperature will rise rapidly, signaling the start of the second falling rate period, and evaporation takes place only inside the material.

The main difficulty in modeling the drying behavior lies in the prediction of the falling rate period which is, in fact, the essential period of drying. Such a prediction requires a rigorous and detailed physical and mathematical description of internal mechanisms and boundary conditions.

1.2 LITERATURE REVIEW

The description of heat and mass transfer is usually based on the transport equations resulting from the differential balance laws. To predict the mass and heat flux from a given material requires detailed information on the surrounding velocity and temperature fields. For a continuous medium, this information is extracted from the solution of the associated microscopic equations subject to pertinent boundary conditions.

For porous media, these local or microscopic equations are generally still valid within the pores. However, the geometric complexity of the pores medium precludes a general solution of the detailed velocity and temperature fields.

To overcome these difficulties, the continuum approaches are generally used to obtain 'macroscopic' equations, valid at a Representative Elementary Volume (R.E.V.). In these models, the porous medium is treated as a fictitious continuum medium and the variables of interest (moisture contents, temperature, etc.) are not representative at the pore scale but at the scale of small volumes containing a sufficient number of pores (R.E.V.) (Bachmat and Bear, 1986). The majority of these models are based on the work of Philip and de Vries (1957), Luikov (1966) and Whitaker (1977). The fundamental hypotheses for all macroscopic models are the continuum approach involving generalized Darcy's and Fick's laws and the relative permeability concept. The macroscopic equations for heat and mass transfer in porous medium have the following form (Bories, 1991):

$$\frac{\partial w}{\partial t} = \nabla \cdot (D_w \nabla w + D_T \nabla T) - \nabla \cdot (\frac{\rho_l}{\rho_s} K \nabla y) \qquad (1\text{-}1)$$

$$(\rho c)^* \frac{\partial T}{\partial t} = \nabla \cdot ((\lambda^* + \ell \rho_s D_{VT}) \nabla T + \ell \rho_s D_V \nabla w) \qquad (1\text{-}2)$$

in which w and T denote the local moisture content and temperature in the porous medium, respectively. All coefficients of equations (1-1) and (1-2) are dependent variables of moisture content and temperature and must be specifically determined for each porous medium. For more details, one can refer to Crausse (1983) or Crausse.et al. (1981).

As have been pointed out by Masmoudi et al. (1991), these equations have not yet been derived from the microscopic equations by means of a rational approach such as, for instance, the volume averaging method (Whitaker, 1977) in a completely satisfactory way. Doubt remains with regard to the validity of these equations from a theoretical point of view. It has been shown that one cannot expect to describe certain two-phase flow processes in porous media according to a continuum approach because of the occurrence of large-scale heterogeneities in the fluid distribution within the porous medium. These heterogeneities are associated with the action of the capillary forces in a system containing a sufficient distribution of pore size. In some cases, moisture content heterogeneities could also be associated with macroscopic heterogeneities of the structure (Maneval and Whitaker, 1988).

Some macroscopic equations are derived from microscopic equations through volume averaging techniques (Slattery, 1970, Gray, 1983, Whitaker, 1986a,b, Moyne et al., 1988, Bear and Bensabat, 1989 and Moyne et al., 1990). These equations are assumed to be valid, on the R.E.V., of average volumes of microscopic quantities. The main advantage of this kind of approach is to provide a clear physical significance of the macroscopic coefficients, relating energy and moisture fluxes and temperatures and moisture content gradients.

Bories (1991) reviewed some theoretical, numerical and experimental studies published during the last decade on simultaneous heat and mass transfer during the drying of capillary-porous bodies and concluded that despite the limitations of the theory and the underlying assumptions, the macroscopic model is a good tool to describe and to analyze the drying of capillary-porous bodies. However, many doubts still remain regarding the macroscopic models. For example:

- What are the transport properties of the material in question?
- What are the appropriate values of the convective heat and mass transfer coefficients to be used at the interface between the porous medium and the external flow?
- What is the minimum size of the averaging volume or Representative Elementary Volume for the material and transport phenomena in question?
- How the liquid is distributed inside the porous medium during the drying process?
- To what extent is the heterogeneity of liquid phase distribution?
- To what extent is the influence of the heterogeneity of liquid phase distribution upon the drying process?
- What is the importance of Kelvin effect on the drying process?

In a number of studies (Whitaker and Chow, 1983, Plumb et al., 1985), it has been found that the heat and mass transfer coefficients at the interface must be allowed to vary during the

drying process in order to obtain satisfactory agreement between experimental and numerical results. The heterogeneities of moisture content at the interface has a great influence upon heat and mass transfer coefficient. Traditional one-dimensional simulation is not suitable to describe this phenomenon. Two-dimensional or three-dimensional simulation is needed to improve the accuracy of the numerical results.

In the falling rate period, the fraction of wet area decrease with decreasing interface moisture content. However, the continuum approach model can not answer how the fraction of the wet area varies with the interface moisture content and where is the wet and dry patches at interface.

Furthermore, most of the macroscopic models have a common resolution of drying, i.e., interface is the first part to be dried, then the dried region proceeds inside the porous medium. In other words, there is always a positive moisture gradient from the bottom of sample to the interface; the moisture at the bottom is always higher than that at the interface. This is probably true for some of the porous media, but not for all.

Lee et al. (1992) reported some surprising phenomena in the drying of 65μm and 120μm glass beads. They observed that in all cases these beads had the lowest saturation at the bottom and very close to the investigated drying surface. In this case sufficient suction potential is developed to lift the entire water column in the packed bed towards the drying surface, resulting in two drying fronts: one at the top of the bed and one at the bottom. This observation is contrary to any of the model predictions that are available in literature. One can note from Lee et al. results that the moisture gradient can be negative at some place and positive at other place from bottom to surface.

Lee et al. also measured the pressure at the bottom of the sample for the 65μm beads. It was found that the pressure dropped very quickly to 0.305 cm (vacuum) of water as the bed began to dry but after a short period rose to atmospheric. This implies that air broke through from the surface of the bed even at high liquid saturation.

It is also well-known that strong heterogeneities in the fluid phase distribution may occur during drying process (trapped clusters of fluid) (Lenormand et al., 1988). However, in its standard form, the model of Philip and de Vires cannot account for the occurrence of such heterogeneities, which is not surprise because of the fundamental hypotheses of such kind of model — continuum approach. One cannot expect to describe the heterogeneous phenomena by using a continuum concept.

To answer some of the questions posed previously, percolation theory seems to be a good alternative. Percolation theory, developed over the last decades, is ideally suited as a conceptual framework for interpreting the morphology and transport properties of disordered composite materials. In several papers (Larson, 1977, Pathak, 1980 and Larson et al., 1981), it is shown that percolation ideas provide the basis of an unified theory of the properties of porous media and fluids therein.

Many transport process may be successfully idealized as transport of an abstract 'fluid' through an abstract 'medium'. Diffusion of a solute through a solvent is an example of such a process. If, as in this example, the 'fluid' (solute) is imagined to 'flow' randomly, the process is termed a diffusion process. If, on the other hand, the 'fluid' flow paths are determined by the 'medium', but the 'medium' itself is in some sense random, the process is called a percolation process. This classification, and the introduction of percolation theory, are due to Broadbent and Hammersley (1957).

In percolation theory, the porous medium is really treated as a 'porous material', i.e., parts of solid and parts of pores are identified. It is almost impossible to describe the geometry of porous media exactly because of their complexity and to overcome this difficulty, many simple geometric descriptions of porous media through percolation theory have been employed in previous studies. The most used method is the network model. In this model, the pores can be represented by spheres (for 3-D representation) or cylinders (for 2-D representation) and connected by throats. The liquid and vapor can migrate from one pore to others through the throats. This approach will be discussed in more details in Chapter 2.

Network models of pore structure were first pioneered by Fatt (1956). More recently, pore-level physics have been combined with percolation theory concepts to predict the macroscopic transport and capillary equilibrium properties of porous medium, such as capillary pressure curves and relative permeability curves. One of the early attempts in this direction was the work of Chatzis and Dullien (1977), who applied bond percolation to regular two-dimensional and three-dimensional lattices in order to simulate the mercury intrusion porosimetry curves of sandstones. Bond-correlated site percolation in random networks was latter introduced by Chatzis (1980) as a more realistic model for the simulation of immiscible displacement in sandstones. Other contributions applying percolation theory concepts to capillary displacement in two- and three- dimensional networks include the works of Mohanty et al. (1980), Larson et al. (1981), Mohanty and Salter (1982), Chander et al. (1983), Wilkison and Barsony (1984), Guyon et al. (1984) and Yanuka et al. (1989). Network models consisting of unit cells of the constricted-tube type, have been developed by Payatakes et al. (1973,1980). Models of this type were used to study single-phase flow (Constantinides and Payatakes, 1989) and two phase immiscible

displacement (Dias and Payatakes, 1986) in porous media. Network models of spheres-and-capillaries have been used by Lapidus et al. (1985), Conner et al. (1983), Conner and Lane (1984) and Tsakiroglou and Payatakes (1990) in simulations of mercury porosimetry. Most of the above cited studies are parametric investigations of the effect of model parameters on model predictions. The network models can be used to predict the structure and transport properties of porous media which are used in the macroscopic model for drying of porous media (Ioannidis and Chatzis, 1993). However, few works have been done to predict the drying process of capillary porous media directly by using the network model.

Masmoudi et al. (1991) used the invasion percolation theory to predict the drying of capillary porous media. In their model, drying is considered as an immiscible displacement process at low capillary number where air and water are displacing and displaced fluid, respectively. In absence of gravity, immiscible displacement can be characterized by two dimensionless numbers, the viscosity ratio M and the capillary number Ca which are defined as following,

$$M = \frac{\mu_{(displacing\ fluid)}}{\mu_{(displaced\ fluid)}} , \qquad Ca = \frac{m_{(displaced\ fluid)}V}{\sigma}$$

where V and σ denote the displaced fluid average velocity and the interfacial tension, respectively. Ca represents the ratio of viscous forces to capillary forces. Depending on the values of Ca and M, three main flow pattern have been identified (Lenormand et al., 1988)

- viscous fingering
- capillary fingering
- stable displacement

In the case of drying, for air as the displacing fluid and water as the displaced one, $M = 1.8 \times 10^{-2}$ and typical value of capillary number are smaller than 10^{-10}. At very low capillary number, such displacement can be associated with invasion percolation as statistical model (Lenormand et al., 1988, Wilkison, 1984). The invasion process is entirely controlled by the capillary mechanisms that take place at the microscopic scale, and the randomness due to the different size of pores. During the invasion process, the non-wetting fluid can only enter the throat associated with the largest radius of curvature (which corresponds the smallest capillary pressure). Invasion percolation is thus a local model. At each step, the displacing fluid invades one pore according to the size of the throats along the boundary between the two fluids within the material. In the work of Masmoudi et al. (1991), the main efforts were devoted to characterizing the trapped fluid clusters. The experimental results were obtained using a two-dimensional transparent etched network which containing about 10,000 ducts with seven classes of width

(from 0.1~0.6 mm) distributed at random. It was found that liquid clusters of various size appeared during the drying process. The number and size of the clusters depend on the relative importance of capillary and gravity. The occurrence of clusters affects the interfacial transfer coefficient. The width of the trapped cluster region tends to increase with the average distance from the interface.

Plumb and Prat (1992) developed two microscopic models for describing transport phenomena in capillary porous media. The first consists of a two dimensional array of square particles having a log-normal size distribution. The randomly sized particles are placed on a Cartesian grid with centers distributed uniformly resulting in a network of non-uniformly sized pores. In the second model, the porous medium is represented using two sets of elements: pores and throats, located respectively at the sites and bonds of a two-dimensional Cartesian lattice. All sites and pores have the same size, however, the width of the throats is selected randomly according to a log-normal distribution. The prediction of liquid transport due to capillary action and diffusion in the vapor phase were made using both models. It was found that the prediction of capillary pressure and vapor phase diffusivity agree with results available in the literature qualitatively and that the Representative Elementary Volume for such properties is larger than that traditionally accepted for other properties such as porosity and dry diffusivity. The maximum array or network size used in their study was 40x40. The studies of Plumb and Prat are introductory and deals only with transport phenomena inside the porous matrix. External flow was not considered in their model.

In the more recent work of Prat (1993), an isothermal drying model of capillary porous media was presented based on a modified form of invasion percolation theory. The porous medium is conceptualized as a network of pores connected by narrow throats. In addition to capillary and gravity effects, evaporation at the microscopic gas-liquid interface and vapor diffusion in the gases phase were taken into account. This leads to a modification of the invasion rules associated with invasion percolation. In this model, the trapping cluster phenomenon was considered. Contrary to the standard invasion percolation, permanent trapping cluster does not occur because of the evaporation at the border of each cluster during the drying process. Some drying simulations on a two-dimensional network containing 5000 ducts were carried out using this drying model. The phase distribution inside the network was presented and compared favorably with experimental results obtained using a two-dimensional micromodel (Masmoudi and Prat, 1991). The Kelvin effect was not taken into account in this model, i.e., the gas-liquid interface was treated as plane.

1.3   OBJECTIVE OF PRESENT WORK

The purpose of this work is to develop a microscopic model for capillary porous media by using the network approach to simulate the drying process, and to study the influence of the heterogeneity of the porous media from a microscopic point of view, such as liquid distribution heterogeneity and the trapped cluster phenomenon. The final goal of this work is to describe the heterogeneities of moisture at the surface and inside of porous media, to obtain the liquid distribution at each step of the drying process, and to study the influence of dry patches phenomenon on the mass transfer at the interface between a fluid and a capillary porous medium.

CHAPTER 2   PROBLEM FORMULATION

2.1   PROBLEM CONFIGURATION

The problem studied here focus on the convective drying of capillary porous media (Fig. 2-1). It consists of two parts: external flow (dry air flow) and internal flow (porous media). The external flow could be considered here as a steady laminar flow with zero incidence at the surface. The vapor mass fraction and velocity of the external flow are denoted by ω and U, respectively. The porous medium is assumed to be saturated initially and can be represented by a network model. The liquid in porous medium can only evaporate from the top open edge. Other three edges are impermeable.

For simplicity, only the isothermal drying of non-hygroscopic capillary porous medium is considered. The terminology "capillary porous medium" implies that capillary effects are the main mechanism of internal moisture transfer in the liquid phase (Prat, 1993). In these materials, contrary to the hygroscopic materials, the liquid moves through the pores and not the solid phase, i.e., the liquid sorption phenomena may be neglected. The mechanism for vapor transfer inside the porous medium is the vapor diffusion through the empty pores. There can be an adsorbed liquid film on the solid surface (Rogers and Kaviany, 1992) which is due to the van der Waals' dispersive forces, and is significant when the pores are very small (smaller than 1 μm). The surface adsorption/desorption will not be addressed here since only pores larger than 1 μm will be considered.

The traditional approach to attack such a problem can be summarized by the following steps:

(i) the external flow is determined by assuming a no-slip condition at the porous surface.

(ii) heat and mass transfer is obtained by coupling the equations describing transports in both media by expressing continuity of temperature, mass fraction, and heat and mass normal flux densities at interface.
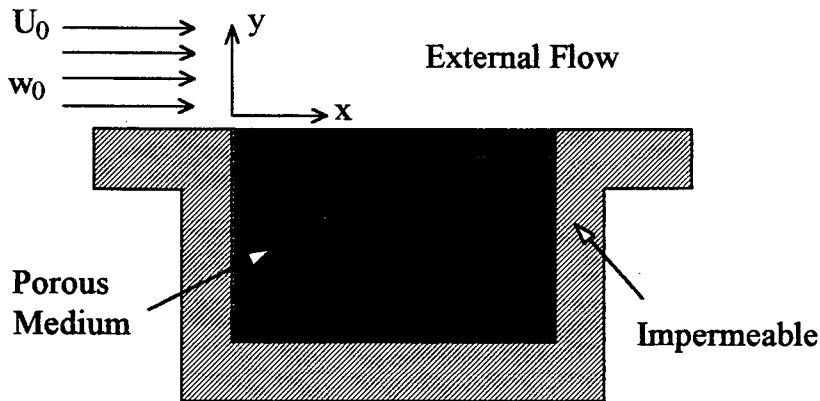
Fig. 2-1   Configuration of the problem

Considering that a microscopic model will be used here to describe the drying of the porous medium, one could understand that the traditional approach for this configuration is no longer suitable. The difficulties appear both inside the porous medium, and at the interface between the external flow and the porous medium. The question is how to deal with the phase change inside the porous medium. In the present model, the liquid is evaporated at the air-liquid interface and then transported to the top open edge by vapor diffusion. There is an evaporating front inside the porous medium and its form change continually during the drying process. It is difficult to simulate the real transient process of drying because of this evaporating front inside the porous medium. This will be discussed in more details in the section of boundary conditions for the porous medium.

For the convective drying of the porous medium, it was first assumed that both external flow and the flow inside the porous medium are in an equilibrium at each time interval of drying process, i.e., the evaporating rate at the interface is constant for each time interval. The no-slip boundary condition is employed at the interface between the external flow and porous medium. Thus the external flow problem is analogous to a boundary layer problem over a flat plate. For each time interval, the species concentration problem is solved independent of the mass transfer in the porous medium. The mass transfer in the porous medium (diffusion fluxes in empty throats and the evaporating rate at the evaporating front) were determined with the obtained moisture content profile at the interface. The evaporating front inside the porous medium keeps the same

form during this time interval. In this way, the mass transfer of the external flow and porous medium is solved separately in a segregate manner. To update the moisture content field of the external flow at each time interval, the information of the mass transfer of porous medium is passed to the external flow. The coupling between the mass transfer of porous medium to the external flow will be discussed in more details in chapter 3.

2.2   PROBLEM FORMULATION

2.2.1   External Flow Problem

As have been discussed before, use will be made of the continuum approach to the external flow, with the no-slip condition at the interface. For a detailed discussion of the validity of a no-slip condition at the porous surface, one can refer to the work of Masmoudi and Prat (1991). In this respect the external flow is similar to the boundary layer problem over a flat plate. This is a well studied problem, and the governing equations are given by

$$\nabla \cdot \bar{U} = 0 \tag{2-1}$$

$$\bar{U} \cdot \nabla \bar{U} = -\frac{1}{\rho}\frac{\partial p}{\partial x} + \upsilon\frac{\partial^2 U_x}{\partial y^2} \tag{2-2}$$

$$\bar{U} \cdot \nabla \omega = \vartheta_{AB}\frac{\partial^2 \omega}{\partial y^2} \tag{2-3}$$

where $\bar{U} = U_x\hat{i} + U_y\hat{j}$ is the velocity vector, p is the pressure, υ is the kinematic viscosity, ρ is density, ϑ_{AB} is the binary diffusion coefficient and ω is the mass fraction of the vapor of the evaporating liquid.

There is no time derivative in equations (2-2) and (2-3) because it is assumed that the external flow reaches a steady state at each time interval of drying process. The time evolution for the external flow can thus be viewed as a succession of steady states.

2.2.2   Boundary Conditions for the External Flow

The boundary conditions at the interface depend upon what kind of model is used for the porous medium. For the case of a macroscopic model, the boundary conditions are somewhat simple. However, for the case of a microscopic model, different boundary conditions at the interface will be required for the solid, full throats and empty throats,

The boundary conditions for equation (2-2) are given as following,

$$\vec{U}_i = 0 \qquad \qquad \text{at the solid surface} \qquad \qquad (2\text{-}4)$$

$$U_{yi} = \frac{\rho \mathcal{B}_{AB}}{\rho_{Ai}} \frac{\partial \omega_{Ai}}{\partial y} \qquad \qquad \text{at full throats} \qquad \qquad (2\text{-}5)$$

$$U_{yi} = -\mathcal{B}_{AB} \frac{\partial \omega_{Ai}}{\partial y} \qquad \qquad \text{at empty throats} \qquad \qquad (2\text{-}6)$$

where the subscript A, B and i denotes the vapor, air and interface respectively. Equation (2-5) represents the vertical velocity of vapor at the interface (Prata and Sparrow, 1988). In accordance with the impermeability condition, the naturally occurring diffusive flow of air to the interface must be balanced by a convective flow of air away from the interface, this is taken care of by the ratio ρ/ρ_{Ai} in equation (2-5), as will be discussed later in section (2.2.3.3). Equation (2-6) is Fick's law and gives the vertical velocity of the vapor at the interface between the porous media and the external flow.

For equation (2-3), the boundary conditions are,

$$\frac{\partial \omega_{Ai}}{\partial y} = 0 \qquad \qquad \text{at solid surface} \qquad \qquad (2\text{-}7)$$

$$\omega_{Ai} = \omega^* \qquad \qquad \text{for full throats} \qquad \qquad (2\text{-}8)$$

$$J_{Ai} = -\rho \mathcal{B}_{AB} \frac{\partial \omega_{Ai}}{\partial y} \qquad \qquad \text{for empty throats} \qquad \qquad (2\text{-}9)$$

where the ω^* is the vapor mass fraction at the system temperature for corresponding throat radius and the J is the vapor diffusion flux density within the empty throats. With given boundary conditions, one can solve the governing equation numerically by using the control volume method (Patankar, 1980), for instance.

2.2.3   Microscopic Model for Porous Medium

2.2.3.1   Network Model for Porous Medium

The structure of most real porous media is too complex for an exact mathematical description. For this reason, simplified geometrical models of the porous media are usually employed. Based of such simplified models, transport process in porous media can be predicted. One can refer to Dullien and Batra (1970), van Brakel (1975), and Payatakes and Dias (1984) for reviews of different models based on pore network used for various classes of porous media.
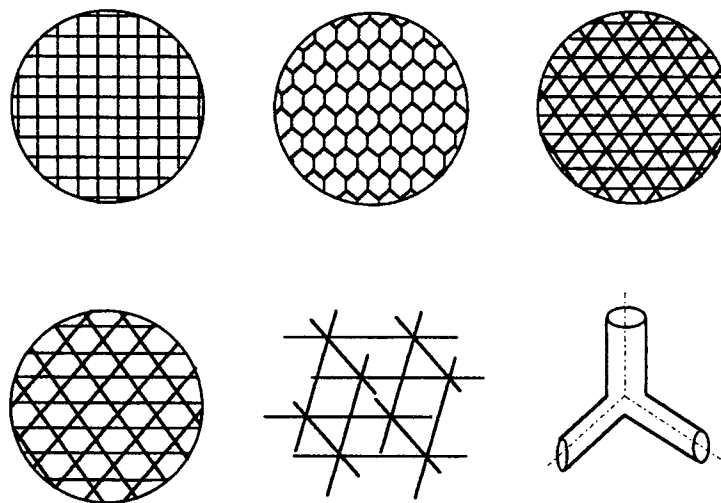
Fig. 2-2   Some example of lattices and pore network

Different network models (square, hexagonal, triangular, Kagomw, cubic, and node of a pore network, for example, Burganos and Sotirchos, 1987, Fig. 2-2) should be used to describe the structure of different porous media. The geometrical structure of a packed bed of sand, for instance, is different from that of a piece of wood. Therefore, a very important step is to select an appropriate network model for a given porous medium. To some extent, the choice of the network is a factor that can determine the success of a microscopic model. Generally, the image analysis technique should be used to study the structure of porous media. The distribution of pores can be obtained and the appropriate network can be selected by using this technique.

For simplicity, we could consider the porous media as a network consisting of pores and throats. Thus, the porous media will be treated here as a cubic (for three-dimensional) or square (for two-dimensional) network of spherical (or cylindrical) pores interconnected by cylindrical (or

rectangular) throats. The distance between the centers of two adjacent pores will be held fixed. The diameters of pores and throats could be chosen randomly from preselected distribution (Gaussian or log-normal, for instance). This makes the network model adopted here different from that of Plumb and Prat, 1992. In their model, only the throat diameter a log-normal distribution but the diameter of pores was kept the same. Where two adjacent pores are found to intersect during the network construction, one of them is randomly interchanged with another pore of the network. A similar interchange is made if a throat is found to be larger than one of the two pore at its ends. One can refer to Constantinides and Payatakes (1989) for more details on the computer-aided construction of the network.

2.2.3.2   Liquid Transport in Porous Medium

In the present model, the driving force for liquid transport is the difference of the capillary pressure. For the convective drying problem treated here, the immiscible displacement concept is not appropriate to describe the drying process because all the liquid which were taken from the porous media is in vapor state. In other words, the liquid have to become vapor before it is transported to the external flow. For the immiscible displacement process (Kaviany,1991), there is no mass exchange through the air-liquid interface, and the liquid is displaced simply by the air, i.e., the liquid is taken from the porous media in liquid state. That is the case in the work of Masmoudi et al. (1991) and Plumb and Prat (1992), where the drying is treated as an immiscible displacement process. The present author is in doubt about this approach.

The description of the liquid transport adopted here will now be presented. At the beginning of drying, all of the pores and throats are filled with liquid, and only the throats adjacent to the surface are in contact with the external dry air flow. The evaporation of liquid takes place at the throats which have an air-liquid interface. As drying proceeds, the curvature of menisci of the throats adjacent to the interface decrease. When the curvature of the menisci reach a critical value, i.e., the meniscus of the biggest throat is approximately hemispherical, its curvature stops changing. As a result of evaporation, the meniscus of the biggest throat adjacent to the surface recedes inwards the porous matrix, and all others menisci remain at the same position because their suction potential are higher than that of the biggest throat. The liquid which evaporated from the smaller throats are replaced by liquid from bigger throats which have an air-liquid interface. In other words, bigger throats lose their liquid in two ways, by evaporation and by liquid flow caused by difference of capillary pressure. Smaller throats virtually do not lose liquid because they can get liquid from bigger throats to replace their evaporated liquid. There is a balance between the rate of evaporation and liquid flux caused by difference of capillary pressure. The menisci of smaller throats do not recede as long as this balance holds. For a discussion of the

influence of gravity and viscosity in this balance, the reader is referred to Prata and Prat, 1995. At the later period of drying, the difference of capillary pressure become smaller, and liquid evaporated from small throats can not be replaced by liquid transported by difference of capillary pressure, and the menisci of the small throats begin receding. At this moment, all of the menisci recede either because of evaporation or liquid flow.

Fig. 2-3 gives a simple example of the liquid transport in the porous medium. The menisci A and E are plate at the initial. Liquid evaporate from both menisci A and B and their curvature decrease. When their curvature reach the critical value of meniscus A, their curvature stop changing. The meniscus A recedes to the position B. The meniscus E remains at the interface because it can take the liquid from larger throat to replace the evaporated liquid. After throat 1 is empty, the meniscus recede to the position C and throat 3 still has condition to take liquid from throat 2 to replace its evaporated liquid. Meniscus E begin to recede inside the porous medium only after the meniscus from throat 2 reaches the position D because there is no more larger full throat from which throat 3 can take liquid. As a result of evaporation, the menisci E and D change their position in the same time until throat 3 is empty.
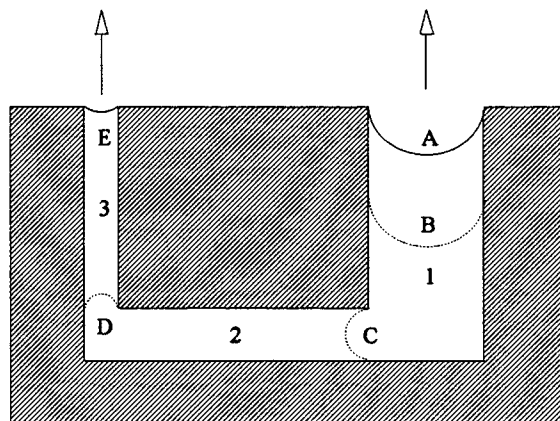
Fig. 2-3   An example of liquid transport in porous medium

As mentioned before, the trapped liquid phenomena can occur at some period of the drying process. Several liquid clusters can appear in the porous media. For each trapped liquid cluster, the liquid evaporated from smaller throats can only be replaced by the liquid of the biggest throat of the corresponding cluster because there is no connection between trapped clusters.

The liquid inside the pores have priority to evaporate in each cluster as soon as one of its connecting throats is empty because the pore radius is always bigger than that of its connecting throats due to the basic rule in construction of networks. If one of the pore connecting throat is the largest throat at the evaporating front, the pore has to be the biggest one after the liquid in that throat was evaporated. This will be taken as a rule in the present simulation.

2.2.3.3   Evaporation Rate at the Air-Liquid Interface

In the present model, liquid evaporation takes place at all pores having an air-liquid interface inside the porous medium during the drying process. The evaporated vapor are transported to the surface only by vapor diffusion. It should be noted that the porous medium is isothermal and that the liquid evaporation rate is controlled by the rate of diffusion, i.e., vapor transported by diffusion have to be balanced by vapor evaporated. The balance between diffusion and evaporation yields (Prata and Sparrow, 1988)

$$\rho_{Ai} U_{yi} = \rho \vartheta_{AB} \frac{\partial \omega_{Ai}}{\partial y}$$

(2-10)

where ρ_{Ai} is the vapor density at the air-liquid interface, U_{yi} is the vapor velocity, ρ is the mixture density, ϑ_{AB} is the binary diffusion coefficient and ω is the vapor mass fraction; subscript A and i denote vapor and interface respectively. Equation (2-10) can be rewritten as

$$U_{yi} = \frac{\rho \vartheta_{AB}}{\rho_{Ai}} \frac{\partial \omega_{Ai}}{\partial y}$$

(2-11)

Equation (2-11) will be used to calculate the evaporation rate at the interface between the external flow and the porous medium.

2.2.3.4   Diffusion of Vapor

The vapor diffusion takes place between two adjacent empty pores while the connecting throat is empty. It is assumed that the vapor diffusion between empty pores can be treated as an one-dimensional binary diffusion. Thus, the diffusion of vapor can be described by Fick's law

$$J_A = -\rho \vartheta_{AB} \frac{\partial \omega_A}{\partial y}$$

(2-12)

where, except for J_A which is the vapor flux density, all other symbols appearing in equation (2-12) have been already explained and is also in the nomenclature.

Diffusivities of gases at low density are almost composition independent, increase with the temperature, and vary inversely with pressure. In the present work, the gaseous pressure in the porous medium is atmospheric pressure and the temperature virtually constant. Therefore, the binary diffusion coefficient, $\mathcal{D}_{AB}$, will be assumed constant.

2.2.3.5   Partial Pressure of Vapor within the Pores

During the drying process, the pores can have only two states: full of liquid or empty. For a full pore, it is not necessary to calculate the partial pressure of liquid because there is no vapor diffusion through it. But for empty pores, the situation is somewhat complex because the connecting full throats could belong to different trapping clusters. There are two possible situations and the way to determine the partial pressure of the vapor for each situation is different. Those situations will now be discussed.

1. Empty pore connecting with empty throats

In this case, the partial pressure of vapor in the pore is determined by the diffusion rate of adjacent throats. There is a mass balance that has to be satisfied and the vapor partial pressure can only be calculated by solving the diffusion equations of adjacent throats all together. Note that the partial pressure of this pore depends upon the four adjacent pores, that is, it is not an independent variable. This will be discussed later in more details.

2. Empty pore connecting with more than one full throats

The vapor partial pressure in the pore is not uniform. Consideration is given to an empty pore connecting with more than one full throats which belong to different trapping clusters. For each trapping cluster, the menisci radii of all throats which are on its border have to be the same, and is determined by the Kelvin's law. If there are difference of menisci radii at the border of a trapping cluster, there would be difference of Kelvin force between them. This force unbalance will cause liquid flow inside the trapping cluster until equilibrium is established. The menisci radii at the border will tend to be the same and equal to the radius of the biggest full throat. In other words, the partial pressure of vapor at a trapping cluster have only one value and is determined by the biggest throat at the border.
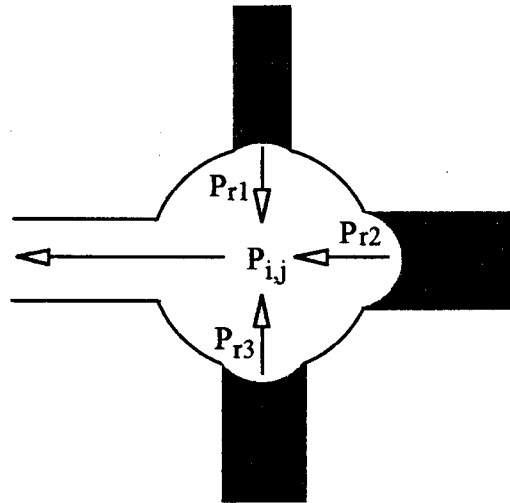
Fig. 2-4 Diagram showing an empty pore with three full throats;
the vapor partial pressure is determined by the balance between
evaporating rate at interface and diffusion fluxes of empty throats

The vapor partial pressure at the menisci of the full throats which are connected to the empty pore, thus, can have different value since they belong to different trapping clusters (Fig. 2-4). Kelvin's equation can then be used to determine the vapor partial pressure at the border of each trapping cluster. The vapor partial pressure at the center point of the empty pore ($P_{i,j}$) can be calculated by mass balance assuming an equilibrium state. One should recall Kelvin's equation,

$$RT \ln \frac{P_r}{P_0} = -\frac{2\sigma M}{r \rho_l}$$

(2-14)

where

R	Universal gas constant
T	Absolute temperature of the system
σ	Surface tension
M	Liquid molecular weight
ρ_l	Liquid density
r	Radius of curvature
P_0	Vapor pressure for a flat surface at temperature T
P_r	Vapor pressure for a curved surface of radius r

For simplicity, it is assumed that the contact angle is equal to zero, i.e., the meniscus radius is equal to the throat radius. The mass fraction ω is then calculated by using the state equation for ideal gases,

$$P_r V = n_{vapor} RT \tag{2-15}$$

$$\rho_A = \frac{n_{vapor} M_A}{V} = \frac{P_r M_A}{RT} \tag{2-16}$$

$$\rho_B = \frac{P_B M_B}{RT} = \frac{(P_{Total} - P_A) M_B}{RT} \tag{2-17}$$

$$\omega_A = \frac{\rho_A}{\rho_A + \rho_B} \tag{2-18}$$

where the V is the volume, n is the number of moles and P_{Total} is the total pressure in the empty pores. All other symbols have already been explained and is also listed in the nomenclature.

2.2.3.6   Resistance Network for Vapor Diffusion
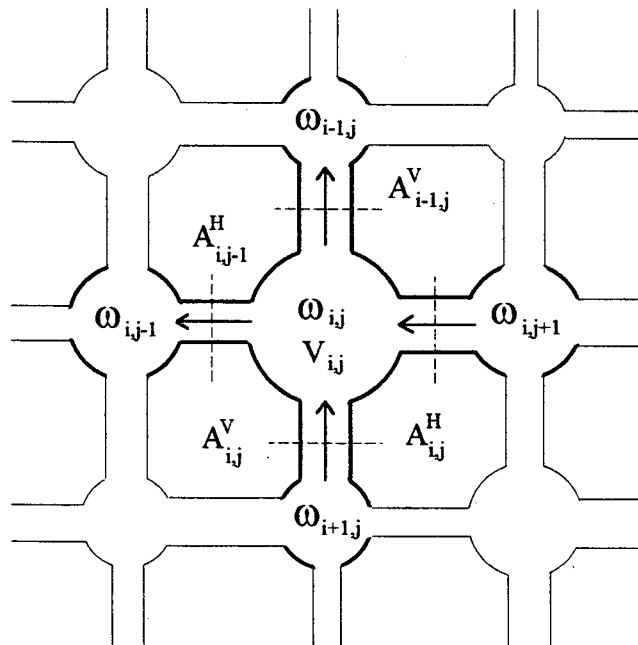
Fig. 2-5 Resistance network for vapor diffusion

The vapor evaporated from the evaporating front inside the porous medium is transported to the top open edge by diffusion through empty pores and throats. The vapor cannot be transported through a full throat by diffusion but evaporation-condensation mechanism. The vapor mass fraction in empty pores are not independent variables, but are determined by the diffusion fluxes of neighbor empty throats. There is a mass balance for each empty pore that must be satisfied. The number of empty pores and throats change at each time interval, and, therefore, the resistance network for vapor diffusion change its form during the drying simulation.

For a square network, each pore is connected with four throats, i.e., the coordination number is four. Generally, we consider the situation sketched in Fig. 2-5. At a time interval Δt, the vapor mass balance for pore (i,j) is given by

$$\left[(\omega_{i,j}\rho_{i,j})^{t+\Delta t} - (\omega_{i,j}\rho_{i,j})^{t}\right]V_{i,j} / \Delta t = \dot{m}^{V}_{i,j} - \dot{m}^{V}_{i-1,j} + \dot{m}^{H}_{i,j} - \dot{m}^{H}_{i,j-1} \tag{2-19}$$

where $\omega_{i,j}$ is the vapor mass fraction in pore (i,j), $\dot{m}^{V}_{i,j}$ is the vapor flux in vertical throat (i,j) and $\dot{m}^{H}_{i,j}$ is the vapor flux in horizontal throat (i,j). From Fick's law, the vapor flux in vertical throat (i,j) is calculated from

$$\dot{m}^{V}_{i,j} = A^{V}_{i,j}\rho^{V}_{i,j}\mathcal{S}^{V}_{i,j}\frac{\omega_{i+1,j} - \omega_{i,j}}{l^{V}_{i,j}} \tag{2-20}$$

where

$A^{V}_{i,j}$	Cross sectional area of vertical throat (i,j)
$\rho^{V}_{i,j}$	Gaseous density in vertical throat (i,j)
$\mathcal{S}^{V}_{i,j}$	Binary diffusion coefficient
$l^{V}_{i,j}$	Length of vertical throat (i,j)

For simplicity, equation (2-20) will be written as,

$$\dot{m}^{V}_{i,j} = g^{V}_{i,j}(\omega_{i+1,j} - \omega_{i,j}) \tag{2-21}$$

where

$$g^{V}_{i,j} = A^{V}_{i,j}\rho^{V}_{i,j}\mathcal{S}^{V}_{i,j} / l^{V}_{i,j} \tag{2-22}$$

Similarly, for the others mass fluxes,

$$\dot{m}^V_{i-1,j} = g^V_{i-1,j}(\omega_{i,j} - \omega_{i-1,j}) \tag{2-23}$$

$$\dot{m}^H_{i,j} = g^H_{i,j}(\omega_{i,j+1} - \omega_{i,j}) \tag{2-24}$$

$$\dot{m}^H_{i,j-1} = g^H_{i,j-1}(\omega_{i,j} - \omega_{i,j-1}) \tag{2-25}$$

where

$$g^V_{i-1,j} = A^V_{i-1,j}\rho^V_{i-1,j}\vartheta^V_{i-1,j} / l^V_{i-1,j} \tag{2-26}$$

$$g^H_{i,j} = A^H_{i,j}\rho^H_{i,j}\vartheta^H_{i,j} / l^H_{i,j} \tag{2-27}$$

$$g^H_{i,j-1} = A^H_{i,j-1}\rho^H_{i,j-1}\vartheta^H_{i,j-1} / l^H_{i,j-1} \tag{2-28}$$

Substituting equations (2-21), (2-23)-(2-25) into equation (2-19), one obtains

$$\left[(\omega_{i,j}\rho_{i,j})^{t+\Delta t} - (\omega_{i,j}\rho_{i,j})^t\right]V_{i,j} / \Delta t = g^V_{i,j}(\omega_{i+1,j} - \omega_{i,j}) -$$

$$-g^V_{i-1,j}(\omega_{i,j} - \omega_{i-1,j}) + g^H_{i,j}(\omega_{i,j+1} - \omega_{i,j}) - g^H_{i,j-1}(\omega_{i,j} - \omega_{i,j-1}) \tag{2-29}$$

After rearrangement it follows,

$$\left[(\omega_{i,j}\rho_{i,j})^{t+\Delta t} - (\omega_{i,j}\rho_{i,j})^t\right]V_{i,j} / \Delta t = g^V_{i,j}\omega_{i+1,j} + g^V_{i-1,j}\omega_{i-1,j}$$

$$+ g^H_{i,j}\omega_{i,j+1} + g^H_{i,j-1}\omega_{i,j-1} - (g^V_{i,j} + g^V_{i-1,j} + g^H_{i,j} + g^H_{i,j-1})\omega_{i,j} \tag{2-30}$$

It should be noted that the diffusion flux in each throat was assumed to be constant during time interval Δt. The value of ω in empty pores at each time interval are obtained by solving equation (2-30).

2.2.4   Boundary Conditions for the Porous Medium

The boundary conditions at the interface for the external flow have already been given in equation (2-4)-(2-9). For the porous medium model, the boundary conditions at the interface between the external flow and the porous medium is somewhat simple. The throats adjacent to the interface were considered either full or empty. For full throats, equation (2-11) is used to obtain the evaporation rate and for empty throats, equation (2-12) is used to calculate the diffusion flux. The coupling between the external flow and the internal flow will be discussed in more details in the next Chapter.

The situation inside the porous medium is more complex, since the problem encompasses phase change, that is, there is an evaporating front inside the porous medium. Different from the macroscopic model, this evaporating front is not plane but has a complex geometric form. Moreover, the evaporating front changes its form and place during the drying process. At late drying periods, the formation of liquid clusters complicates the situation. Clearly, one can not expect to deal with the continuous change of the evaporating front during the drying simulation because it is difficult to calculate the diffusion fluxes of empty throats with a changing evaporating front inside the porous medium. This is the main reason that it is difficult to simulate the real transient process of drying. The form of resistance network for vapor diffusion has to be fixed in order to have a fixed boundary condition at the evaporating front. Therefore, the evaporating front is assumed to be fixed during a time interval. For each new time interval Δt, the position of the evaporating front for each cluster have to be updated to get the new resistance network for vapor diffusion. The vapor mass fraction at the evaporating front is the saturated value corresponding to each trapped cluster, i.e., the mass fraction at the border of one trapped cluster are the same and is determined by the radium of the biggest throat at its border.

CHAPTER 3   SOLUTION METHODOLOGY

After the formulation of the external flow problem, the introduction of the boundary conditions and the discussion of the microscopic model for porous medium explored in last chapter, the next step is to solve the governing equations numerically and to develop a simulator for the porous medium according to the microscopic model described foregoing. As have been discussed before, the external flow can be treated as a boundary layer problem and is a well studied subject. That is particularly true for the problem of the boundary layer over a flat surface (see for instance Schlichting, 1968). In the present work the main attention is focused on the flow pattern and the drying behavior of the porous medium, and on the coupling between the external flow and the internal flow. Most of the present chapter will be devoted to this purpose.

3.1 NETWORK CONSTRUCTION FOR THE POROUS MEDIUM

The first task is to construct a network for the porous medium on which the microscopic model as discussed in section 2.2.3 can be applied. As have been mentioned in Chapter 2, the geometric structure of the porous medium is complex and drying strongly depends upon this structure. In this regard, it is very important to select an appropriate network model for studying the porous medium. Reconstruction of porous medium has been receiving much attention in recent years and the reader is referred to Fernandes (1994) and Adler (1992) for a more elaborate discussion on that. In the present work, the attention is not paid to the reconstruction of the porous medium. For simplicity, the network used here is a square network of pores and throats. Each pore is connected to four throats. The distance between the centers of two adjacent pores is fixed, but the radii of pores and throats have a known distribution. In order to give a more real radii distribution of pores and throats to the network, experimentally measured data is used to obtain the parameters for the network construction. For a given porous medium, the volume of

pores of different radii can be measured, for example, by mercury porosimetry (Kloubek, 1981 and van Brakel et al., 1981). The experimentally measured volume distribution of the sand-caulim medium to be used here is shown in Fig. 3-1. From this figure, the radii distribution of pores and throats is calculated.
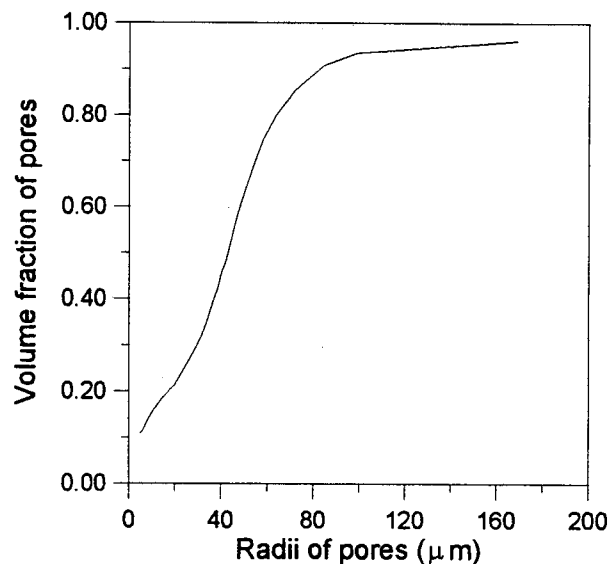
Fig. 3-1 Pore distribution of the sand-caulim mixture used
as the porous medium in the present work (Quadri, 1988)

In a real porous medium, it is difficult to say what is pore and what is throat. Generally, the bigger voids inside the porous medium are treated as pores and the smaller voids are treated as throats. Indeed, it is unknown how much empty volume in a porous medium is pores or throats, since all empty volume can be treated either as pores or as throats. In the present work, the empty volume will be treated as spherical pores to obtain the radii distribution of the pores.

To facilitate the network construction, the isonumber method (Philippi, 1995) is used to obtain the distribution of pores radii, i.e., each class of pores has the same number of pores. From the data of volume fraction of pores (Fig. 3-1), the accumulated pores number is calculated. The curve of accumulated pores number *versus* pores radii is drawn in Fig. 3-2. From this curve, ten classes of pores radii are obtained (Table 3-1).
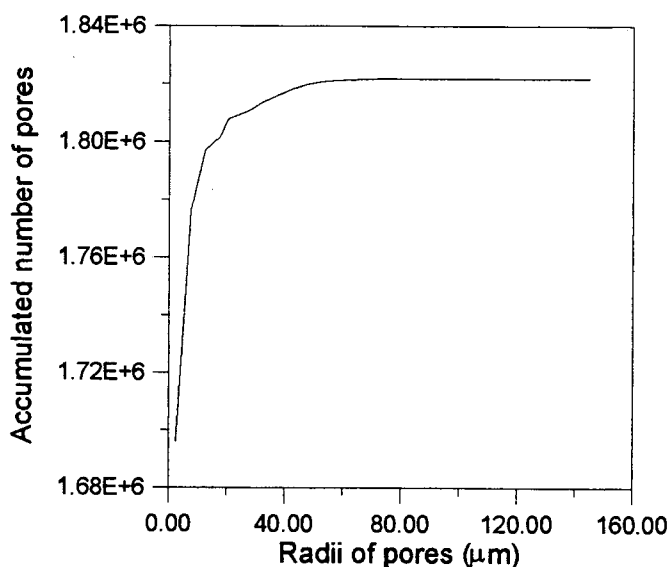
Fig. 3-2   Accumulated pores number *versus* the pores radii

As have been mentioned before, the voids can be treated either as pores or throats. In other words, the distribution of the radii of throats should be the same of the pores. To obtain the radii distribution of the throats, therefore, it is assumed that the throats have the same kind of distribution of the pores but have a different radii range. The radii range for the pores is 14.3~178.2 μm and the radii range for the throats, thus, can be obtained by using a factor to all classes (the factor is chosen between 0.5 ~ 0.9). The porosity of the network can be changed by using different factors and the distance between the pores. It should be noted that the network diffusive resistance for the vapor is assumed to be only due to the throats and that there is no resistance due to the pores; the pores resistance is somehow inserted into the throat resistance through an equivalent length. The distance between the centers of two adjacent pores is chosen to be large enough to avoid the intersection of two adjacent big pores. There may be an overlap of radii range of pores and throats, i.e., some throats may have a bigger radius than that of some pores. During the network construction, therefore, if a throat is found to be larger than one of the two pores at its end, it is randomly interchanged with other throat of the network.

Table 3-1   Radii classes of pores and throats obtained
from the experimental data

Radii of pores $\times 10^5$ (m)	17.82	9.190	5.565	4.105	3.475	3.065	2.655	2.300	1.840	1.430
Radii of throats $\times 10^5$ (m)	8.910	4.595	2.783	2.053	1.738	1.533	1.328	1.150	0.920	0.715

3.2   SOLUTION PROCEDURE

3.2.1   Solution Procedure for the Porous Medium

3.2.1.1   Identification of Trapped Clusters and Location of the Evaporating Front

In the present model, the trapped cluster phenomena is taken into account during the drying process. The evaporating front recedes gradually inward the porous medium and its form changes continually during the drying process. This evaporating front has to be located inside the network in order to calculate the vapor diffusion fluxes for the empty throats. Therefore, the first important step is to develop an algorithm to scan the trapped clusters within the network. The task of this scanning procedure is to find out the trapped clusters from the information of the state of pores and throats (empty or full). Then, a number is given to each cluster to identify it since liquid evaporated from each cluster can be taken off only from the corresponding cluster. In fact, the cluster phenomena takes places soon after some of the throats adjacent to the external interface are dried. Clearly, it strongly depends on the radii distribution of throats in the porous medium. The more the smaller throats are located near the surface, the sooner the clusters appear.

Other task to be achieved is to identify the throats which are located on the boundary of each cluster. It is on those throats that evaporation and condensation take place. As drying proceeds, the number of clusters and their boundary change. It is necessary, therefore, to run the program at each time interval to update the information about the trapped clusters and the evaporating front. The algorithm for scanning clusters and some illustrative results will be presented in Chapter 4, together with its validation.

3.2.1.2   Diffusion Fluxes in Resistance Network

After the clusters have been identified and the evaporating front has been located, the next step is to determine the diffusion flux in each empty throat. This is attained by solving equation (2-30) on the resistance network for the vapor diffusion with the prescribed boundary conditions at the interface (profile of mass fraction for the external flow near the interface) and the evaporating front (saturated mass fraction at the menisci surface of the throats which are on the border of the trapped clusters).

It is well known that equation (2-30) which gives the mass fraction of pore(i,j) can be written in two different formulations, explicit and implicit, depending on which time the mass fraction of the neighboring pores are determined. If the values used are those of the last iteration

(known), the equation is an explicit one. In this case, the equation for each pore is independent of the other equations and can be solved one by one. If the values used to evaluate the mass fraction of the neighboring pores are those of the present iteration (unknown), the equation is implicit. In this formulation, it is necessary to solve a linear system of equations to determine the mass fraction for each pore. A solution of this system of equations can be obtained by a direct or iterative way. Some direct methods are: Matrix inversion, elimination of Gauss, Fourier transformation, etc. The iterative methods are: Jacobi method, Gauss-Seidel, Successive Over-Relaxation (S.O.R.), etc. (Patankar, 1980, Press et al., 1992). Clearly, the explicit formulation is simpler to be adopted than the implicit one. However, the convenience of the explicit method is offset by a serious limitation: the time step Δt for each iteration have to be small enough to ensure stability. In present model, the implicit scheme is adopted and it is assumed that the vapor diffusion between the empty pores in the porous medium is in equilibrium, i.e., the vapor entering an empty pore is equal to the vapor leaving the pore during a time interval Δt. To this extent equation (2-30) is simplified as

$$\omega_{i,j} = \left(g^V_{i,j}\omega_{i+1,j} + g^V_{i-1,j}\omega_{i-1,j} + g^H_{i,j}\omega_{i,j+1} + g^H_{i,j-1}\omega_{i,j-1}\right) / \text{GSUM} \tag{3-1}$$

where

$$\text{GSUM} = g^V_{i,j} + g^V_{i-1,j} + g^H_{i,j} + g^H_{i,j-1} \tag{3-2}$$

The mass fraction of each empty pore is calculated one by one in the resistance network for vapor diffusion by using the equation (3-1). This is done iteratively, and convergence is reached rapidly. After convergence has been reached, the mass fraction of the vapor in the empty pores is taken to be constant during the drying time interval, in accordance with the implicit scheme. Thus, during Δt the vapor fluxes to and from the pores are taken to be constant.

The next step is to obtain the evaporation (or condensation) rate on the border of each cluster. In fact, the evaporation (or condensation) rate of the full throats which are on the border of the clusters is obtained when the resistance network for vapor diffusion is solved. To obtain the evaporation rate of a cluster, one just needs to sum the evaporation rate of the throats on its border. It should be noted that some of the throats are evaporating and some condensing (Fig. 3-3a). It is defined here that the evaporation rate is positive and the condensation rate is negative. Thus, if the sum of the evaporation rate is positive, it means that this cluster is losing liquid by evaporation. If the sum is negative, the cluster is gaining liquid by condensation. The amount of liquid evaporated from each cluster in a given time interval can be obtained multiplying the evaporation rate by the time interval. It is worthy mentioning that an empty pore can lie on the border of various clusters, as indicated in (Fig. 3-3b).

The condensing throats at the border of the clusters are marked in order to distinguish them from the evaporating throats. It is important to do so because, of course, the evaporated liquid of a cluster cannot be removed from a condensing throat even if it is the biggest throat on the border of cluster. This will be a rule in choosing the biggest throats on the evaporating front.
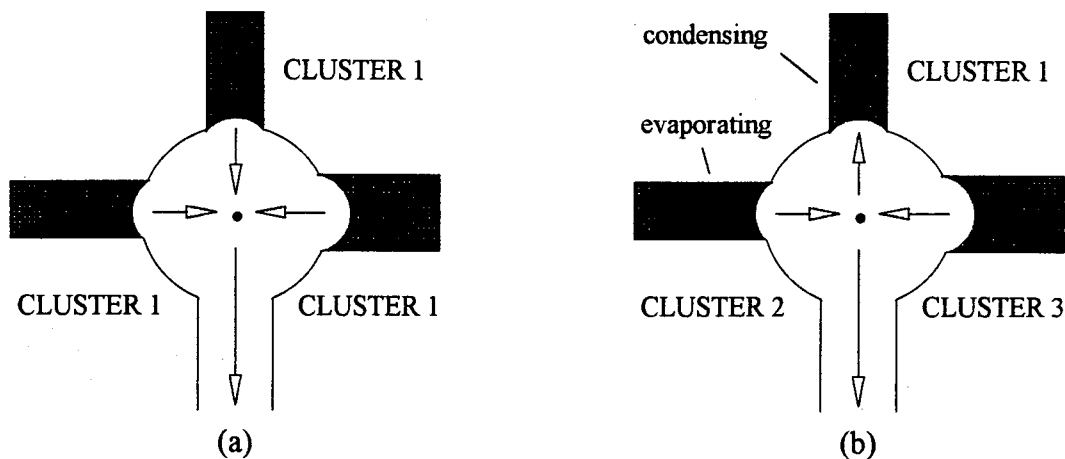
Fig. 3-3   (a) pore on the border of one cluster

(b) pore on the border of three clusters

3.2.1.3   Determination of the Time Interval

At each time interval, it is assumed that the network is in an equilibrium, that is, the mass fraction at the empty pores and the diffusion fluxes through the empty throats remain constant. Clearly, the time interval used to calculate the quantity of the liquid evaporated from each cluster has a great influence on the drying process simulation. The smaller the time interval, the better the approximation of drying process. Generally, the problem becomes independent of the time interval if liquid of only one or two throats and pores is removed in each time interval. The time interval is not fixed during the simulation because the drying rate decreases sharply after the interface is dried. Since the evaporating rate is bigger at the earlier times, the time interval starts with a small value, and with the receding of the evaporating front, the evaporating rate decrease and bigger time intervals can be used to accelerate the marching procedure.

If the time interval were chosen arbitrarily, it could happen that some small clusters would have less liquid to be removed than that that would be evaporated from them during the time interval. To avoid this problem, the time interval is chosen as following,

- after the clusters and their borders are located, the evaporation (or condensation) rate for each cluster is calculated
- the amount of liquid in each cluster is obtained
- for each evaporating cluster, the time to evaporate all liquid of cluster is calculated
- the smallest time is chosen to be the time interval and is used for all clusters to calculate the amount of liquid evaporated or condensed

In this way, it is ensured that all clusters have sufficient liquid to be removed in each time interval. At the beginning of simulation, the network is saturated , i.e., there is only one cluster in the network and it is obvious that one cannot choose the time to evaporate all liquid in this cluster (the whole sample) as the first time interval. To avoid a too big time interval at the beginning and during the simulation, a criterion is used to control the maximum time interval for different drying stages. The time interval increases gradually as drying proceeds since the drying rate decrease for larger times.

3.2.1.4   Removal of Liquid from Clusters

So far, it is known how much liquid is evaporated from the border of each cluster and transported to the surface of porous medium or, reversely, how much vapor is condensed to each cluster during a time interval Δt. The attention now is turned to the removing of the liquid from each cluster. The questions are how to remove the evaporated liquid from each cluster, when and where the liquid removing process stops.

Inspection is carried out from left to right and from top to bottom of the network during the liquid removal process. If there is only one biggest throat at the evaporating front of each cluster in each time interval, there is no doubt that this throat loses its liquid first. Difficulties appear when there are more than one biggest throat on the cluster border at the same time interval. One has to determine, thus, from which throat the liquid should be removed first. According to the mechanism for liquid transfer of the present model (capillarity), the biggest throats can lose their liquid because they have the same radius, regardless of their location on the cluster border. There are various ways to remove the evaporated liquid from each cluster. For a given cluster, for example, the first biggest throat encountered at the cluster border during the inspection can be chosen as the throat from which the liquid is removed first. As soon as the liquid of this throat is removed, the liquid of the connecting pore is also removed because, as have been mentioned before, the pores have priority to evaporate. After the liquid from the pore is removed, other three connecting throats become located on the evaporating front. The removal process for this throat can stop and the inspection goes on, or, the process can only stop when the radii of the

O.241.159 - 1

three connecting throats are smaller than that of the other throats that lie on the border. The way employed to simulate the drying process, of course, can affect the simulation result in a significant extent. Since only a little amount of liquid (of one or two throats or pores) is removed from a cluster in a time interval, this influence is strong. The left top part of the porous medium will be dried more rapidly than the right part because the inspection routine is always started from the left top part of the network.

In the present model, the liquid removal from a given evaporating cluster is performed by the following steps:

1. The biggest throat radius is obtained by comparing the radii of the evaporating throats on the border of cluster. The condensing throats are not considered during the inspection.
2. The first biggest full throat encountered on the border of a cluster during the inspection is taken as the first throat from which the liquid is removed.
3. The liquid of this throat is removed if it is an evaporating throat. Contrarily, the inspection goes on to encounter the next biggest throat.
4. After the liquid of this throat is removed, the liquid within the pore which is connected to the biggest throat (at other end) is removed.
5. The other three full throats are marked as the throats on the border and the liquid removal process in this throats stops.
6. The inspection goes on to find out other biggest full throat on the border.
7. Steps 1-6 is repeated until all the evaporated liquid is removed from this cluster.

If the given cluster is a condensing one, condensed liquid is given to it by the following steps:

1. The biggest throat radius is obtained by comparing the radii of the throats on the border of cluster, regardless of it is evaporating or condensing.
2. The first biggest full throat encountered on the border of the cluster during the inspection is taken as the throat on which the condensed liquid is put.
3. The liquid is given to this throat, and what is changed is the amount of the liquid in the throat. The meniscus position is considered the same.

For simplicity, the liquid volume within the throats is calculated considering a plane menisci surface.

The liquid removal process is performed cluster by cluster until all of the evaporated liquid is taken off from the evaporating cluster and the condensed liquid is placed on the condensing cluster.

For an evaporating cluster, the amount of evaporated liquid during a time interval is hardly equal to the amount of liquid in the chosen throats and pores. At the end of the time interval, the amount of evaporated liquid to be removed may be less than that of a biggest throat or a pore. Under this circumstance, some liquid is left in the throat or pore after the evaporated liquid is taken off from this throat or pore. If this occurs for a throat, the throat is treated as a full one in the next iteration but the quantity of liquid in it is less than before. Thus, the meniscus will not be at the end of the throat. Instead, the meniscus recedes inside the throat as shown in Fig. 3-4a. For a throat having two empty pores at its ends (liquid bridge), the menisci of both side recede inside the throat (Fig. 3-4b). It should be noted that evaporation-condensation mechanism can take place at this kind of throats. In fact, the liquid bridge in the throat is a small trapped cluster. For a big trapped cluster, the evaporation-condensation mechanism can also take place because one can look all trapped clusters as liquid bridges. The difference is that for a small trapped cluster (one throat), there is only one evaporating meniscus and one condensing meniscus, for a big trapped cluster, however, there may be various evaporating and condensing menisci.

(a)   (b)

Fig 3-4   Diagram showing the possible position of menisci of throat

As have been shown in Fig 3-4, there are various possible positions for menisci inside the throats. Regardless of where the menisci are, this kind of throat is treated in the same manner as a completely full throat in the next time interval, and the evaporating rate at receded menisci is obtained in the same manner of that at menisci at the ends of throat.

If the liquid removing process is terminated in a pore and the amount of liquid left to be removed is less than the existing amount of liquid within this pore (Fig. 3-5), then the evaporated liquid is removed from this pore and this pore is treated as an empty one in the next iteration. The full throats connected to this pore are taken to be on the evaporating front in the next iteration. This kind of pore will be taken as the first one to be evaporated in next iteration, that is, it is

treated as the biggest throat on the evaporating border at the next time interval. It should be noted that in the last time interval, this pore and its three connected full throats belong to the same cluster. As it becomes an "empty" pore during the next time interval, it no longer link the three full throats. In this circumstance, the three full throats may be in three different clusters. Considering that the vapor diffusion flux in the empty throat is the result of evaporation from three full throats, the liquid left in this pore should be distributed among the different clusters to which the three throats belong. The liquid left in this pore, is then equally divided and distributed among the different clusters.
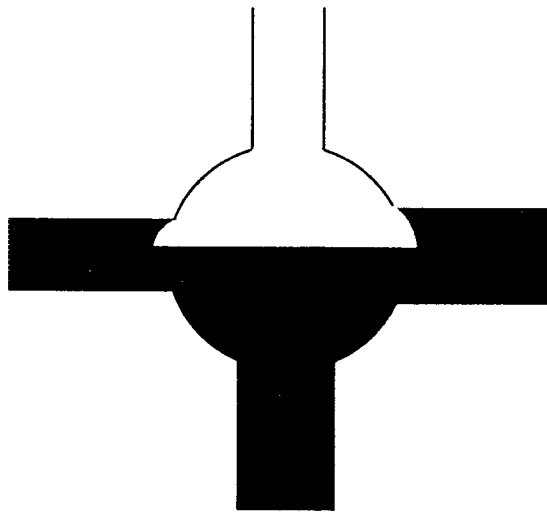
Fig. 3-5   Diagram of pore with left liquid

All procedures performed during a time interval within the porous medium is completed at this point. Next, the network is inspected again to identify trapped clusters and evaporating fronts for the next time interval. To obtain the vapor fluxes in the resistance network, a new boundary condition has to be given at the interface between the porous medium and the external flow. Therefore, the mass fraction field of the external flow should be updated. The calculation of the mass fraction in the external flow will be explored next.

3.2.2   Solution for External Flow

The mathematical model for external flow is given by equations (2-1)-(2-3). To solve those differential equations, use is made of the control volume methodology due to Patankar (1980). In this methodology, the calculation domain is divided into a number of nonoverlapping control volumes such that there is one control volume surrounding each grid point (Fig. 3-6). The governing equation is then integrated over each control volume and a set of algebraic equations is obtained as explored in the next section.
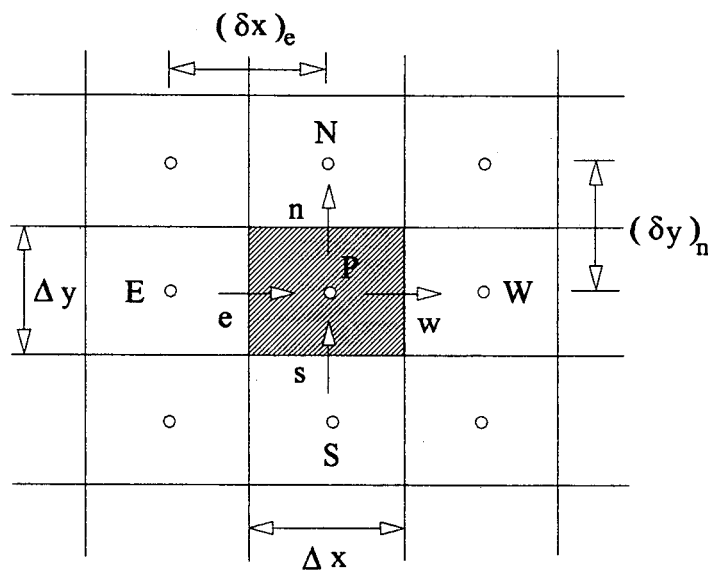
Fig. 3-6   Control volume for the two-dimensional situation

3.2.2.1   *Discretization of Differential Equations*

The governing differential equations are integrated over each control volume. Piecewise profiles expressing the variation of the variables of interest (such as U_x, U_y and ω, etc.) between adjacent grid points are used to evaluate the required integrals. The outcome is algebraic equations containing the value of the variables of interest for a group of grid points. The value of the variable in each control volume is taken as constant and equal to the value of the grid point at the center of control volume.

Equation (2-2) and (2-3) can be written in the general form as

$$\frac{\partial}{\partial t}(\rho\phi) + \frac{\partial}{\partial x_i}(\rho u_i \phi) = \frac{\partial}{\partial x_i}\left(\Gamma \frac{\partial \phi}{\partial x_i}\right) + S \tag{3-3}$$

where the ϕ is the general variable (U_x, U_y and ω, for example), Γ is the diffusion coefficient and the S is the source term. The two-dimensional discretization equation for this general differential equation can be written as (for the details of discretization, one can refer to Patankar, 1980)

$$a_P \phi_P = a_E \phi_E + a_W \phi_W + a_N \phi_N + a_S \phi_S + b \tag{3-4}$$

where

$$a_E = D_e A(|P_e|) + [| -F_e, 0 |] \tag{3-5}$$

$$a_W = D_w A(|P_w|) + [| F_w, 0 |] \tag{3-6}$$

$$a_N = D_n A(|P_n|) + [| -F_n, 0 |] \tag{3-7}$$

$$a_S = D_s A(|P_s|) + [| F_s, 0 |] \tag{3-8}$$

$$a_P = a_E + a_W + a_N + a_S + a_P^0 - S_P \Delta x \Delta y \tag{3-9}$$

$$b = S_C \Delta x \Delta y + a_P^0 \phi_P^0 \tag{3-10}$$

$$a_P^0 = \frac{\rho_P^0 \Delta x \Delta y}{\Delta t} \tag{3-11}$$

here the operator $[| A, B |]$ denote the greater of A and B, the superscript ^{0} denote the known values at time t, while all other values are the unknown values at time $t+\Delta t$. The source term is linearized in the form of $S = S_C + S_P \phi_P$. The mass flow rate through the east face of a typical control volume F_e, the corresponding conductance D_e, and the Peclet number P_e are defined as

$$F_e = (\rho u)_e \Delta y \tag{3-12}$$

$$D_e = \frac{\Gamma_e \Delta y}{(\delta x)_e} \tag{3-13}$$

$$P_e = \frac{F_e}{D_e} \tag{3-14}$$

The mass flow rates, conductances and Peclet numbers for other three faces of a typical control volume are defined in the same way. The interpolation function $A(|P|)$ can be selected from various schemes such as central difference, upwind, hybrid, power law and exponential (Patankar, 1980). Here, the power law scheme is adopted, in which,

$$A(|P|) = \left[\!\left[\; 0, \left(1 - 0.1|P|\right)^5 \;\right]\!\right] \tag{3-15}$$

Note that the discretzation form of the general differential equation can be used to solve the transient problem. In our work, it is assumed that the external flow has reached a steady state in each drying time internal. Under this circumstance, we just let the Δt in equation (3-11) tends to infinite, yielding, a_P^0 equal to zero. The information of the mass transfer of the internal flow (porous medium) is passed to the external flow through the source term in equation (2-3). This will be discussed in more details in section 3.3.

3.2.2.2   Solution of the Algebraic Equations

The solution of the set of algebraic equations for an one-dimensional situation can be obtained by the standard Gaussian-elimination method. Sometimes, it is called the TDMA (TriDiagonal-Matrix Algorithm). The designation TDMA refers to the fact that when the matrix of the coefficients of these equations is written, all the nonzero coefficients align themselves along three diagonals of the matrix. For the two-dimensional situation, direct method (i.e., these requiring no iteration) for solving the algebraic equations are much more complicated and require rather large amounts of computer storage and time. For a linear problem, which requires the solution of the algebraic equations only once, a direct method may be acceptable, but in nonlinear problems, since the equations have to be solved repeatedly with updated coefficients, the use of a direct method is usually not economic. Thus, the line by line method which combines the direct method (TDMA) for one dimensional (for a chosen grid line) and the Guauss-Seidel method is used. To carry the information of the boundary conditions into domain more rapidly, the TDMA can be carried out in the grid line by line forward, then backward and column by column downward, then upward and so on.

For the solution of the algebraic equation associated to the differential equation (2-3), there is no difficulty in determining the source term because the evaporation rate at the interface is known from the solution of the network. However, difficulty arises in the calculation of the source term for the velocity field, that is, the unknown pressure field. This is so because there is no obvious equation to obtain the pressure field. The pressure field is indirectly specified via the

continuity equation (equation (2-1)). When the correct pressure field is substituted into the momentum equation, the resulting velocity field satisfies the continuity equation.

Here, the SIMPLER algorithm is used to calculate the velocity field. It consists of solving the pressure equation from a guessed velocity field to obtain the pressure field and solving a pressure-correction equation only to correct the velocities (for more details, see Patankar, 1980, 1981).

3.3   COUPLING OF EXTERNAL FLOW WITH POROUS MEDIUM

For the problem of convective drying of porous medium such as sketched in Fig. 2-1, one should pay attention to the coupling of the external and the internal flow. Generally, for the convective drying of the porous medium, the scale of external flow is different from the scale of internal flow. As have been discussed in Chapter 1, in macroscopic model of porous media, the variables of interest are not representative of transfer at the pore scale but of transfer at the scale of small volumes containing a sufficient number of pores (R.E.V.). Clearly, the scale of such kind of models is bigger than that of the external flow model. Under this circumstance, there are some doubt on the classic coupling method of external flow with internal flow. Plumb and Prat (1992) studied the size of R.E.V. of the porous medium, and they found that the Representative Elementary Volume for mass transfer is larger than that traditionally accepted for properties such as porosity and dry diffusivity.

In the present microscopic model for the porous medium, there is no doubt about scale because the equations used to describe the drying are derived at the pore scale. In other words, the variables for the porous medium are evaluated in the same scale of the variables for the external flow. This is one of the main advantages of using the microscopic model for the porous medium.

In the drying problem under consideration, the surface of the porous medium is flat. Regarding the computer storage capacity and reasonable computer time, the network size of pores and throats for the porous medium will not be bigger than 100x100 in the present simulation. The grid for the external flow could be of the same size or smaller. The control volume at the interface, for instance, can couple with one or various throats as shown in Fig. 3-7. The internal flow problem is solved separately from the external flow problem, and the coupling of the two problems is made by passing the information either of the evaporation rate of full throats or vapor flux of empty throats to the control volumes adjacent to the external flow via source term in equation (2-3). That is, the vapor transported into the external flow through the

interface is treated as it is generated in the control volume adjacent to the interface. Thus, the interface is taken as impermeable during the solution of equation (2-3). Equation (2-11) is used to calculate the evaporation rate of a full throat on the interface. The derivative of the mass fraction in equation (2-11) is calculated in different ways depending if the throat is full or empty. The two cases are shown in Fig. 3-8. For the external flow, the mass fraction is taken to be uniform along each control volume and is evaluated in its center as shown in Fig. 3-8. The distance used to obtain the derivative of the mass fraction, therefore, is somehow arbitrary.
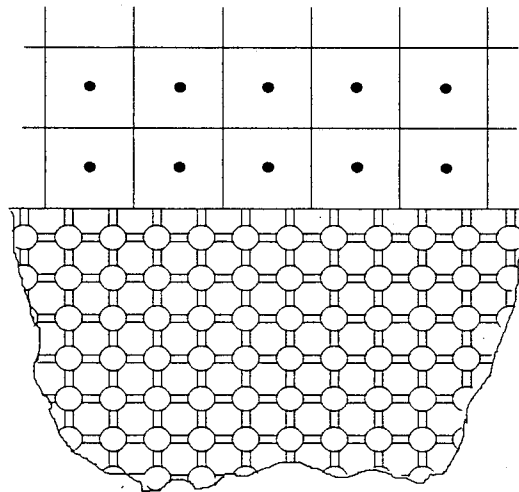
Fig. 3-7   Coupling of grid for external flow with the network
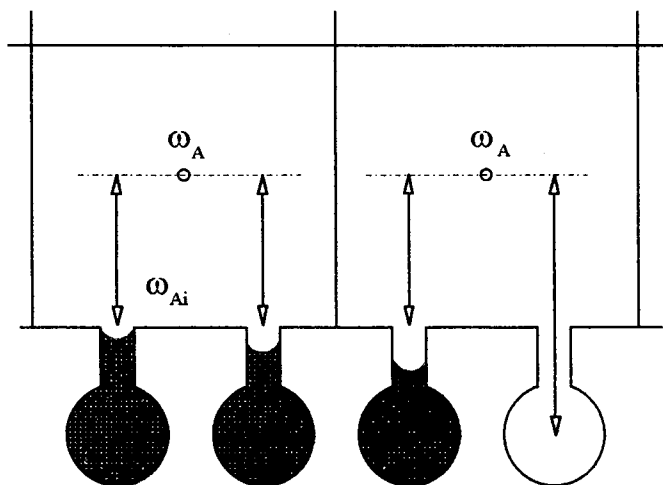
Fig. 3-8   Diagram of throats on interface

For full throats, the distance used here is that between the center point of the control volume and the surface of the meniscus (at the interface or receded meniscus). The mass fraction at the meniscus (saturated) can be calculated using equations (2-14)~(2-18). For empty throats, the vapor flux is calculated using equation (2-12). The distance employed to obtain the derivative of the mass fraction is that from the center of the control volume to the center of the empty pore.

The boundary condition at the interface for equation (2-2) is the no-slip assumption together with the blowing velocity given by equation (2-12). The interface is treated as an impermeable one for equation (2-3).

It is worthy mentioning that the two-dimensional grid used to solve the external flow, in fact, has an unity thickness in the z-direction. If the network for the porous medium is two-dimensional, i.e., the throats are rectangular and the pores are cylindrical, the network can be taken as a network with an unity thickness in z-direction as shown in Fig. 3-9. Thus, the interface of both the external flow and the porous medium have the same thickness. To calculate the vapor transported into the control volume, the intersection area of the rectangular throat (shaded area) is used.
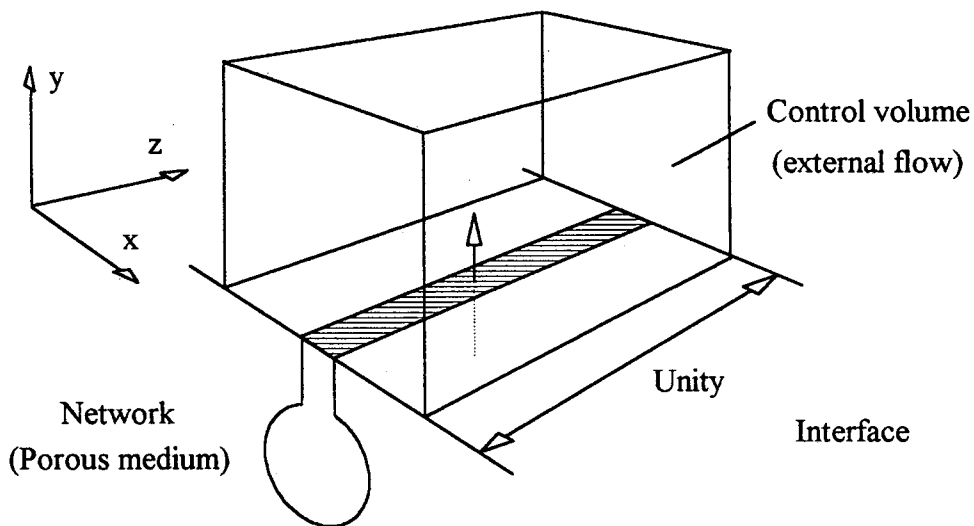
Fig. 3-9   Coupling of a 2D grid with a 2D network of rectangular throats
and cylindrical pores

However, for a two-dimensional network of cylindrical throats and spherical pores, the network thickness has a certain value (the radius of the largest pore, for example). Under this circumstance, the intersection area of the throats on the interface is their sectional area (darken

area in Fig. 3-10), but the control volume for external flow has an unity thickness. Clearly, the sectional area of the interface for the external flow and the network is incompatible. Thus, the intersection area for the network at the interface have to be modified to make it compatible with the control volume of the external flow. To do so, the diffusion rate of empty throats and the evaporation rate of full throats at the interface are modified from the sectional area of throats to the square area with a width of the diameter of the throats. Thus, the vapor transported into the control volume is calculated by multiplying the modified vapor diffusion or evaporation rate by the rectangular area with a width of the diameter and a thickness of unity (shaded area).
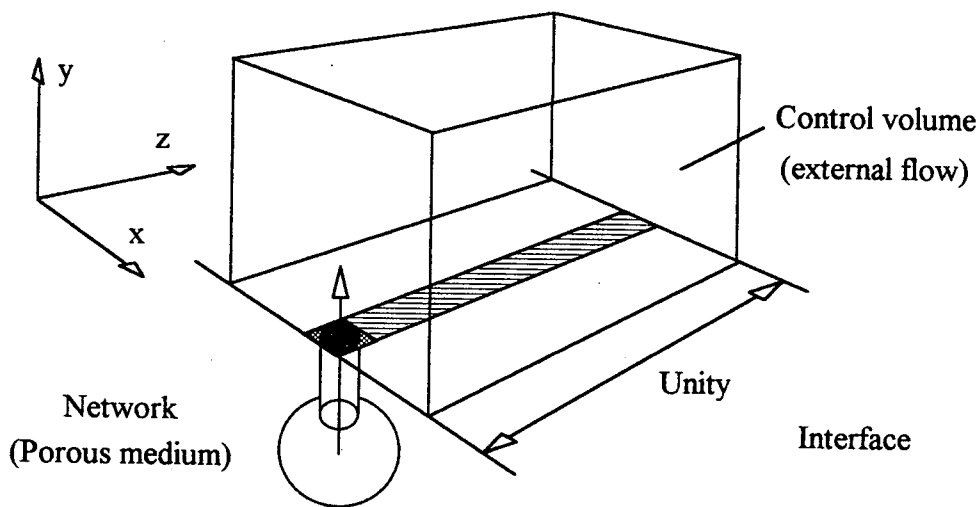
Fig. 3-10   Coupling of a 2D grid with a 2D network of cylindrical throats
and spherical pores

Of course, one could have made the control volume compatible to the network by reducing the thickness of the control volume in z-direction from unity to the same thickness of the network.

CHAPTER 4 SUBROUTINE SCANCLUSTER

4.1 INTRODUCTION

The trapped clusters phenomenon in the latter period of the convective drying problem has to be taken into account in the numerical simulation due to its great influence on the liquid phase distribution in the porous media. Because of this phenomenon, the evaporating front inside the porous medium has a complex form that changes during the drying process. In Chapter 3, it was described how the evaporated (or condensed) liquid of each cluster in a time interval can be taken off or put on. Therefore, the trapped clusters in the network should be identified, labeled and the evaporating front should be located in each time interval. To perform this process in the numerical simulation, an algorithm was developed.

The infinite and finite cluster in an infinite network is a general concept of percolation theory. The dynamic and static aspects of percolation phenomena are well known and to a large extent understood. The concept of percolation has been closely associated with the permeation of fluid through porous media. The formation of an infinite cluster of identical molecules in a network can also be described within the framework of percolation theory.

The algorithm for locating clusters in a network is discussed here as a chapter because it is not only useful for the present convective drying problem, but also for other situation. Various examples of phenomena that need this kind of algorithm are encountered in the literature. These include among others: spontaneous magnetization of dilute ferromagnets (Elliott et al., 1960), spreading of diseases in orchards (Broadbent et al., 1957), formation of polymer gels (Flory, 1953), electrical conductivity of amorphous semiconductors and metal-ammonia solutions (Eggarter et al., 1971 and Cohen et al., 1976), distribution of grain size in photographic emulsions (Kottler et al., 1950), and exciton percolation in isotopically disordered crystals and

photosynthetic units (Kopelman et al., 1975 and Kopelman, 1976). It should be noted that this list includes only a small "random sample" of a variety of percolation process occurring in nature.

Various mathematical and computational approaches to the problem, including their scope and limitations, have been outlined in numerous papers and review articles (Frisch et al., 1963, Fisher, 1964, Essan, 1973). Computational methods broadly termed as Monte Carlo methods (Broadbent et al, 1957) are applied to finite sublattices whereas percolation theory, basically, is concerned with the probability for locating an infinite cluster in an infinite lattice.

The difficulties encountered in a solution of a percolation problem utilizing the direct simulation approach are the limitation of computer storage capacity and computer speed. Hoshen and Kopelman (1976) developed a "cluster multiple labeling technique" to save storage and computer time. Its distinctive feature is the assignment of alternate labels to sites belonging to the same cluster. This technique algorithm is briefly described in the following.

The first time an marked site (it could be a site occupied by a certain molecule, or, a full pore, etc.) is encountered during the inspection of the lattice the label counter k is set to an initial value k_0. The increment Δk is a small positive integer. For the site i, its neighbors are searched first. Generally, the neighbors of site i are defined as those sites connected by bonds to site i. The number of neighbors is equal to the bond order of site i. If there are no labeled neighbors in the vicinity of site i, the site is assigned a new label after k is incremented. If there is only one labeled neighbor, site i gets the same label of its neighbor. The unique features of the cluster multiple labeling technique become apparent when there are more than one labeled neighbors, that is, the site i links two or more previously labeled cluster fragments into a single cluster. No site belonging to any of these cluster fragments is relabeled and it retains its original label throughout the inspection process. The actual readjustments occurs within the number counters of these clusters. All the labeled sites of these clusters is added to the cluster which has the smallest cluster number and the number counters of these clusters are set to a negative integer (with the same number of the smallest cluster number). With this readjustment, these clusters are coalesced into a new larger cluster without relabeling. Site labeling and cluster size classification can be accomplished by a single scan of the lattice. The additional advantage of the single scan process is that only a fraction of the columns (or layers) have to reside in the computer memory concurrently. The entire lattice need not to be stored on the computer because after a segment of columns (or layers) have been processed they are not referred to again by the program.

The idea of "cluster multiple labeling technique" can be used in the present algorithm. It should be mentioned that this algorithm requires not only the ability of locating and labeling the clusters in a square network, but also the ability of locating the pores and throats which are on the

evaporating or condensing front of each cluster. The algorithm developed by Hoshen and Kopelman (1974), which uses the "cluster multiple labeling technique", labels a same cluster using various number. Difficulties will arise at later drying stages if a cluster is labeled with more than one number, and Hoshen and Kopelman algorithm has to be altered for the same cluster to be labeled with only one number; the number of clusters in the network should be then a set of natural numbers.

4.2   SCANNING THE CLUSTER

As have been pointed out, the clusters in the porous medium have to been located for each time interval. Therefore, a subroutine SCANCLUSTER was developed specially to perform this task. The subroutine is required not only to locate the clusters in the porous medium but also to give a natural number (label) to each cluster. This subroutine was written for a network of pores and throats (the bond order is four), but it could be used to other kind of network after some modification. The algorithm is shown in Fig. 4-1. The scanning process is done row by row, from left to right and from top to bottom of the network. The first time a full throat or pore is encountered during the inspection of the network, the label counter k is set to an initial value k_0 (normally k_0 equal to 1). Three matrix are used to store the label number, one for pores, one for vertical throats and another for horizontal throats.

The network used to represent the porous medium in the present work is a square network of pores and throats. For the problem of convective drying shown in Fig. 2-1, on the border of the network there are only throats (Fig. 3-6). The scanning process is done pore by pore, and for each pore the connecting throats are also scanned.

At the beginning of the scanning, pore (1,1) is checked. If it is full, it is labeled with 1 and its four neighbor throats are labeled with the same number. This is so because it is assumed in the present model that the pore will be empty as soon as one of its four neighbor throats has been empty. As discussed earlier, this is a basic rule for the program. If the pore is empty, the full neighbor throats are labeled in sequence using different number with an increment $\Delta k=1$. Empty pores and throats are not labeled.

For the other pores of the first row, the neighbor throat of the left hand side does not need to be scanned because it has already been done in last pore. If the pore is full, the pore and other three neighbor throats are labeled with the same number of the left neighbor throat. If the pore is empty, the full neighbor throats of top, right and bottom are labeled having different numbers with an increment of $\Delta k=1$.

pore (1,1)

If pore is full, label pore and four
neighbor throats with same number
If pore is empty, label neighbor
full throats with different number
with increment of 1

pore (1,j)

If pore is full, label pore and three
neighbor throats with same number of left
throat
If pore is empty, label full throats of top,
right and bottom with different number
with increment of 1

pore (i,1)

If pore is full, label pore and three neighbor
throats with same number of top throat
If pore is empty, label full throats
of left, right and bottom in different
number with increment of 1

pore (i,j)

If pore is full, label pore, right and bottom
throats with smae number of the minimum
number of top and right throats
If pore is empty, label full throats of right
and bottom with different number with
increment of 1

Call subroutine CLUSTER to re-label a cluster
when it is found that one cluster was labeled
with different number

Call subroutine CLUSTER to rearrange the
cluster number as a natural number set

Fig. 4-1 Subroutine SCANCLUSTER

For the pores which are in the first column, the top neighbor throat is not scanned. The pore and other three neighbor throats are labeled with the same number of the top throat if the pore is full. Contrarily, the full neighbor throats of left, right and bottom are labeled using different numbers with an increment of $\Delta k=1$.

For the rest of pores, only the right and bottom neighbor throats are scanned because the left and top neighbor throats have already been scanned. If the pore is empty, the right and bottom neighbor throats are labeled with numbers different than that if they were full. There are two possibilities for a full pore. First, the left and top neighbor throats have the same number, then, the pore, right and bottom neighbor throats are labeled with this number. For the second possibility for a full pore, the left and top neighbor throats have different number. For this case, the pore and the two throats are labeled using the smaller number of the top and left neighbor throat. Note that this cluster that have different numbers for the left and top neighbor throats is really the same cluster, eventhough it is labeled with different numbers. It have to be re-labeled in a latter step because there should be an one to one correspondence between numbers and clusters.

After all full pores and throats are labeled, the next step is to change the number of clusters which were labeled with more than one number. A subroutine <u>CLUSTER</u> is written to do this job. Only full pores is scanned during the inspection because an empty pore can not link a cluster. If it is found that the four full throats of a full pore have different numbers, they have to be relabeled, since they are in the same cluster, and the same cluster should have the same number. The smaller of the numbers is found and all pores and throats which have the same number of the other throats (bigger than the smaller number) in the network are relabeled using the smaller number. As a result, each cluster will have only one number after the subroutine <u>CLUSTER</u> is called. A problem that arises is that some natural numbers disappear during this process, and the cluster number is no longer in sequence. Clearly, there is no problem to identify the clusters if the clusters have different number, even if these numbers are not in sequence. However, this is not convenient from a computational point of view because it is difficult to use the DO LOOP command if the clusters numbers that are not in sequence. To overcome this difficulty, the subroutine <u>CLUSTER</u> is used again to rearrange the cluster number.

The subroutine <u>CLUSTER</u> is called when it is found that a natural number is absent. One of the cluster which has a cluster number bigger than the absent one is relabeled by using this number. This is repeated until no cluster number is bigger than the last natural number. The last natural number is the number of clusters in network.

The pores and throats which are on the border of each cluster are found and marked in the subroutine <u>SCANCLUSTER</u>. In fact, it is these throats that represent the evaporation front inside

the network. This is an important information when evaporated liquid is taken off from each cluster. The biggest full throat from which the evaporated liquid is removed should be on the border of each cluster. Therefore, the pores and throats which are on the border of each clusters are marked by 1, and the others by 0. By using this information associated to the cluster number, one can identify the evaporating (or condensing) border of each clusters.

After subroutine SCANCLUSTER is called once, one know how many clusters are there in the network, which pores and throats are in the same cluster and which pores and throats of one cluster are on its border (evaporation or condensation front).

The subroutine SCANCLUSTER is fundamental in using the microscopic model. Its validity and efficiency, of course, has a strong influence on the simulation since it has to be used for each time interval. In what follows SCANCLUSTER will be used to scan some network demonstrating its validity and efficiency.

4.3   SOME ILLUSTRATIVE RESULTS OF SCANCLUSTER

```
 0 0 0 0 0 0 0 0 0 0 0 0 0 1 1 1 0 0 1 1 1 0 0 0 0 0 0 1 0 0
000000000000000000000000001111111000111111100000000001110000
 0 0 0 0 0 0 0 0 0 0 0 0 1 1 1 0 0 1 1 1 1 0 0 0 0 1 1 1 1
100010001010000000101000101011111010111111111000001011111111
 1 1 0 0 1 1 1 0 0 1 1 0 1 0 1 1 0 0 1 1 1 1 1 0 0 1 1 1 1 1
111110100010000000001110000011111000001110000000000111111111
 1 1 0 0 1 1 0 0 0 0 1 1 0 1 1 1 0 0 1 1 1 1 1 1 1 1 1 1 1 1
100000100000101010101111101111110000011111111111111111111111
 0 1 0 0 0 0 1 1 0 0 1 1 1 1 1 1 1 1 1 1 1 1 1 1 1 1 1 1 1 1
101110100010111110100011111111111111111111111111111111111111
 1 1 0 0 0 0 1 1 0 1 1 1 1 1 1 1 1 1 1 1 1 1 1 1 1 1 1 1 1 1
111110101000111110111111111111111111111111111111111111111111
 1 1 1 1 1 1 1 1 1 1 1 1 1 1 1 1 1 1 1 1 1 1 1 1 1 1 1 1 1 1
111111111111111111111111111111111111111111111111111111111111
 1 1 1 1 1 1 1 1 1 1 1 1 1 1 1 1 1 1 1 1 1 1 1 1 1 1 1 1 1 1
111111111111111111111111111111111111111111111111111111111111
 1 1 1 1 1 1 1 1 1 1 1 1 1 1 1 1 1 1 1 1 1 1 1 1 1 1 1 1 1 1
111111111111111111111111111111111111111111111111111111111111
 1 1 1 1 1 1 1 1 1 1 1 1 1 1 1 1 1 1 1 1 1 1 1 1 1 1 1 1 1 1
111111111111111111111111111111111111111111111111111111111111
 1 1 1 1 1 1 1 1 1 1 1 1 1 1 1 1 1 1 1 1 1 1 1 1 1 1 1 1 1 1
```

Fig. 4-2   An example of liquid distribution in network

To illustrate the validity and efficiency of subroutine <u>SCANCLUSTER</u>, a network, shown in Fig. 4-2, containing 10x30 pores will now be processed. The states of pores and throats are determined artificially according to the rule of our model. The full pores and throats are symbolized by 1, whereas the empty pores and throats have a symbol of 0.

In Fig. 4-2, the first row denotes the states of the vertical throats adjacent to the interface. The second row denotes the states of horizontal throats and pores alternatively, and so on. It can been seen from the figure that there are some dry zone at the top of the network and that some liquid clusters are trapped in the dry zone. From this information, the subroutine <u>SCANCLUSTER</u> should find out how many liquid clusters are there in the network and give each cluster a natural number. The result is given in Fig. 4-3, and as is shown, the subroutine <u>SCANCLUSTER</u> can identify liquid clusters in the network correctly. The number of clusters in the network is 34.

```
 0 0 0 0 0 0 0 0 0 0 0 0 0 1 1 1 0 0 1 1 1 0 0 0 0 0 0 1 0
000000000000000000000000111111000111111000000000000111000
 0 0 0 0 0 0 0 0 0 0 0 0 0 1 1 1 0 0 1 1 1 0 0 0 0 1 1 1
```
$900 0_{11}000_{13}0_{14}0000000_{15}0_{16}000_{17}0_{18}0111110_{19}011111111100000_{20}01111110$
```
 2 2 0 0 3 4 5 0 0 6 1 0 7 0 1 1 0 0 1 1 1 1 8 0 0 1 1 1 1
```
$222220_{21}000_{22}000000000111000001111000001110000000000111111111$
```
 2 2 0 0 10 12 0 0 0 0 1 1 0 1 1 1 0 0 1 1 1 1 1 1 1 1 1 1 1
```
$2300000 0_{24}00000_{25}0_{26}0_{27}0_{28}0111110111110000011111111111111111111111111$
```
 0 1 0 0 0 0 1 1 0 0 1 1 1 1 1 1 1 1 1 1 1 1 1 1 1 1 1 1 1
```
$_{29}01111 0_{30}000_{31}01111110_{32}00111111111111111111111111111111111111111111$
```
 1 1 0 0 0 0 1 1 0 1 1 1 1 1 1 1 1 1 1 1 1 1 1 1 1 1 1 1 1
```
$111110_{33}0_{34}00011111011111111111111111111111111111111111111111111111111$
```
 1 1 1 1 1 1 1 1 1 1 1 1 1 1 1 1 1 1 1 1 1 1 1 1 1 1 1 1
111111111111111111111111111111111111111111111111111111111111
 1 1 1 1 1 1 1 1 1 1 1 1 1 1 1 1 1 1 1 1 1 1 1 1 1 1 1 1
111111111111111111111111111111111111111111111111111111111111
 1 1 1 1 1 1 1 1 1 1 1 1 1 1 1 1 1 1 1 1 1 1 1 1 1 1 1 1
111111111111111111111111111111111111111111111111111111111111
 1 1 1 1 1 1 1 1 1 1 1 1 1 1 1 1 1 1 1 1 1 1 1 1 1 1 1 1
111111111111111111111111111111111111111111111111111111111111
 1 1 1 1 1 1 1 1 1 1 1 1 1 1 1 1 1 1 1 1 1 1 1 1 1 1 1 1
```

Fig. 4-3   Cluster numbers labeled by <u>SCANCLUSTER</u>
in a network of 10x30 pores; liquid distribution of Fig. 4-2.

Another task that <u>SCANCLUSTER</u> should perform is to find out which pores and throats of each cluster are on the border of the cluster. The pores and throats which are on the border are

marked by 1. Using this information together with the cluster number, one can identify the pores and throats which are on the border of each cluster. This map is illustrated in Fig. 4-4. Note that the top surface is the interface between the porous medium and dry air flow. The throats on this surface are on the border, of course, but only the full throats are marked. It is worthy to mention that the throats on the border are full and the pores on the border are empty.

```
0 0 0 0 0 0 0 0 0 0 0 0 0 0 1 1 1 0 0 1 1 1 0 0 0 0 0 0 0 1 0 0
00000000000000000000000011000001101100000110000000000011011010
0 0 0 0 0 0 0 0 0 0 0 0 0 1 0 0 0 0 0 0 0 1 0 0 0 0 1 0 1 1
11011101111101000111110111111100011111000000001100011110000000
1 1 0 0 1 1 1 0 0 1 1 0 1 0 0 0 0 0 0 1 0 1 1 1 0 0 1 0 0 0 0
00001111011101000001101101011000110001101101010101 10000000000
1 1 0 0 1 1 0 0 0 0 0 1 0 1 0 1 0 0 1 0 1 1 1 1 1 0 0 0 0 0
11010111010111111111100011100011010110000000000000000000000000
0 1 0 0 0 0 1 1 0 0 1 0 1 0 0 1 1 1 0 0 0 0 0 0 0 0 0 0 0 0
11101111011110001111011000000000000000000000000000000000000000
1 0 0 0 0 0 0 0 0 1 1 0 0 0 0 0 0 0 0 0 0 0 0 0 0 0 0 0 0 0
00001111111011000111000000000000000000000000000000000000000000
0 0 1 1 1 1 0 0 1 0 0 0 0 0 0 0 0 0 0 0 0 0 0 0 0 0 0 0 0 0
00000000000000000000000000000000000000000000000000000000000000
0 0 0 0 0 0 0 0 0 0 0 0 0 0 0 0 0 0 0 0 0 0 0 0 0 0 0 0 0 0
00000000000000000000000000000000000000000000000000000000000000
0 0 0 0 0 0 0 0 0 0 0 0 0 0 0 0 0 0 0 0 0 0 0 0 0 0 0 0 0 0
00000000000000000000000000000000000000000000000000000000000000
0 0 0 0 0 0 0 0 0 0 0 0 0 0 0 0 0 0 0 0 0 0 0 0 0 0 0 0 0 0
00000000000000000000000000000000000000000000000000000000000000
0 0 0 0 0 0 0 0 0 0 0 0 0 0 0 0 0 0 0 0 0 0 0 0 0 0 0 0 0 0
```

Fig. 4-4   Number map of pores and throats which are on the
border of each cluster

Observing Fig. 4-3 and Fig. 4-4, one can easily find that the SCANCLUSTER correctly locates the pores and throats which are on the border of each cluster.

A correct execution of a subroutine do not imply its efficiency. Considering that this SCANCLUSTER will be used in a network bigger than 100x100, its efficiency is as important as its accuracy. Therefore, the SCANCLUSTER will now be used on various network to study its efficiency.

4.4   *SCANCLUSTER* EFFICIENCY

The SCANCLUSTER will now be used on various network to examine its efficiency. The computer is an IBM 3090. The efficiency of the SCANCLUSTER subroutine is clearly shown in Fig. 4-5, where the time required for locating and labeling the clusters in a network is plotted *versus* the number of sites processed in network. Mere 8 seconds is required to process a network containing 10,000 (the number of clusters in this network is 298) sites illustrating the efficiency of the method. It should be noted that the 100x100 network contain 10,000 pores and 20,000 throats. The actual number of sites processed for this network is about 30,000.
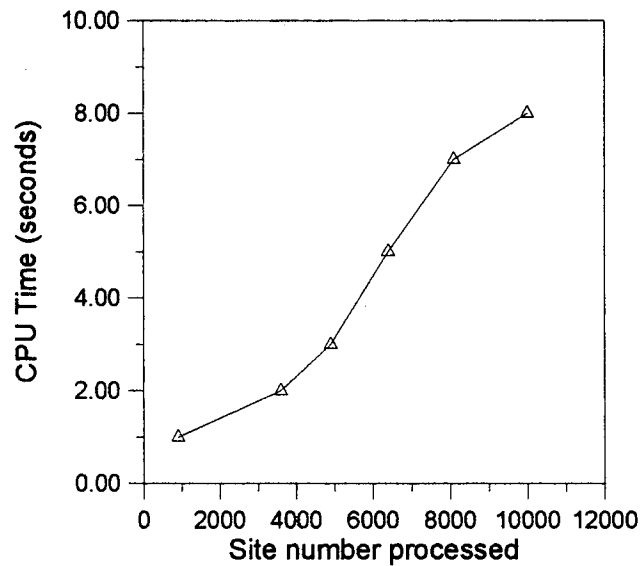
Fig. 4-5   A plot of the computer central-processor-unit (CPU) time
versus the number of sites processed in a network of 30x30 to
100x100 pores; the number of clusters in each network is different.

It should be pointed out that the CPU time required to process a network not only depend upon the number of sites in network, but also on the number of clusters. The CPU time required to process a network of 100x100 at the beginning of drying (corresponding less clusters), for example, is different from that of the same network at the later period of drying (corresponding more clusters). Fig. 4-6 gives a example of the influence of the number of clusters on the required CPU time.

Fig. 4-6 demonstrates that the number of clusters in the network have a strong influence on the required CPU time. For a 100x100 network (containing 30,000 equivalent sites), it took

only 2 seconds to execute <u>SCANCLUTER</u> in presence of 14 clusters, and it took 11 seconds for 413 clusters in the network. Considering that the maximum network which will be used to study the convective drying is 100x100 pores, the required CPU time is expected to be less than 30 seconds.
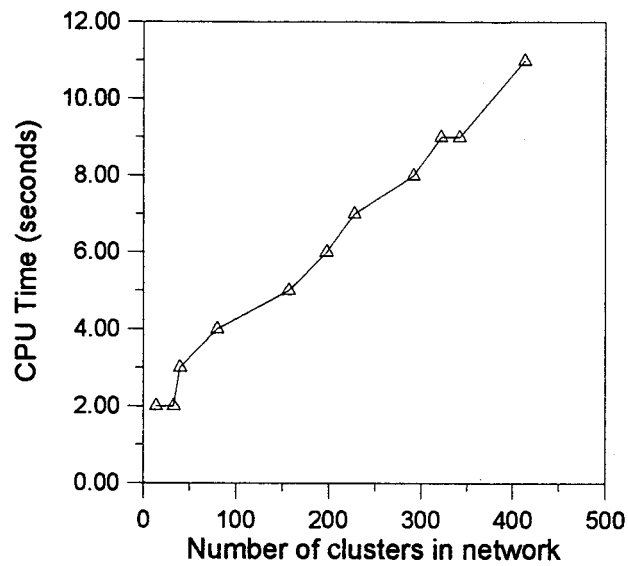
Fig. 4-6   A plot of the computer CPU time versus the number
of clusters in a network of 100x100 pores

CHAPTER 5   RESULTS AND DISCUSSIONS

All drying simulations to be explored were made on a two-dimensional network containing 4,000 throats and 2,000 pores (100x20). The pores are cylindrical and the throats are rectangular. The real size of the network is 6.0 cm (width) x 1.2 cm (depth). The thickness of the network is unity. The network is so chosen because the major interests here are focused at the beginning of the drying (near the interface of the porous medium and the external dry air flow). As have been discussed before, the dry pitches which appear at the very beginning of the drying process have a great influence upon the transfer coefficients of the interface. If the network is chosen as a square one with the same number of pores and throats (a network of 50x50, for example), it has both width and depth of 3 cm. Although the sites that should be processed for each time interval of drying are practically the same for the two network, the 50x50 network needs a longer time to be dried entirely because it has a larger depth. The drying rate is very high at the beginning while the interface is wetted with liquid and decreases sharply after the interface is dried. Thus, a 50x50 network needs more iterations for a simulation than a 100x20 network.

The radii classes of the pores and throats used to construct the network are listed in Table 5-1. One can note that the size distribution of the pores and throats is different from the data presented in chapter 3. The reason to modify the size distribution is that the porosity of the network is very small if the distance of two pores is large (600 μm, for example). On other hand, the network size will be too small if the distance of two pores is reduced.

Table 5-1   Radii classes of pores and throats used to construct the network

Radii of pores $\times 10^5$ (m)	25.00	19.89	15.30	11.29	9.556	8.429	7.301	6.325	5.060	3.933
Radii of throats $\times 10^5$ (m)	20.83	16.58	12.75	9.410	7.963	7.024	6.084	5.271	4.217	3.278

The network is initially saturated with alcohol at room temperature (20 ^{0}C). The boundary condition imposed on the open edge (the up side of the network) is the mass fraction of vapor equal to zero. The other three edges of the network are impermeable. The total pressure within the network is assumed to be atmospheric and the physical properties of alcohol used in the simulation are given in Table 5-2.

Table 5-2 Physical properties of alcohol

σ (N/m)	ρ_ℓ (Kg/m^3)	$\mathcal{D}_{AB}$ (m^2/s)	ρ_{VS} (kg/m^3)	P_{VS} (Pa)	M_A (g)
0.0217	815	0.815x10^{-5}	0.102	4159.6	60.09

Before considering the configuration sketched in Fig. 2-1, attention will focused on some behavior of the microscopic model for porous medium, such as the influence of network formation, the Kelvin effect and the evaporation-condensation phenomenon in the network. Firstly, the influence of the network formation on the drying process is studied.

5.1 INFLUENCE OF THE NETWORK FORMATION ON THE DRYING KINETICS

The network used in the microscopic model to represent the porous medium structure, as have been discussed in chapter 2, is constructed by placing pores and throats randomly in a square array. The size of pores and throats have a known distribution obtained from the experimental data. The networks constructed in this way have the same statistical characteristics such as porosity, number of pores and throats of each size class. However, the position of the pores and throats in the network can be different during the different construction because, as have been mentioned before, the pores and the throats are placed in the network randomly. Clearly, the networks constructed have some difference in a local view. The throats on the interface, for example, can have different sizes for different networks. This difference, as can be expected, will have an influence on their drying behavior. In this section the influence of network formation will be studied. All results to be presented in this section include the Kelvin effect.

5.1.1 Drying Kinetics

To study the influence of liquid phase distribution upon the drying performance, five networks were constructed by using the same pores radii and throats radii distribution. Both the pores and throats radii have ten classes within the range of 39~250 μm and 32.7~208 μm respectively. The distance between the centers of two adjacent pores is 0.6 mm. Each class of radius has the same number of throats or pores. The porosity of network is about 0.5. The drying process was simulated on these five networks under the same conditions. The drying kinetics results are presented in Fig. 5-1. The results are plotted as saturation, s, of network (volume of liquid divided by empty volume) *versus* drying time.
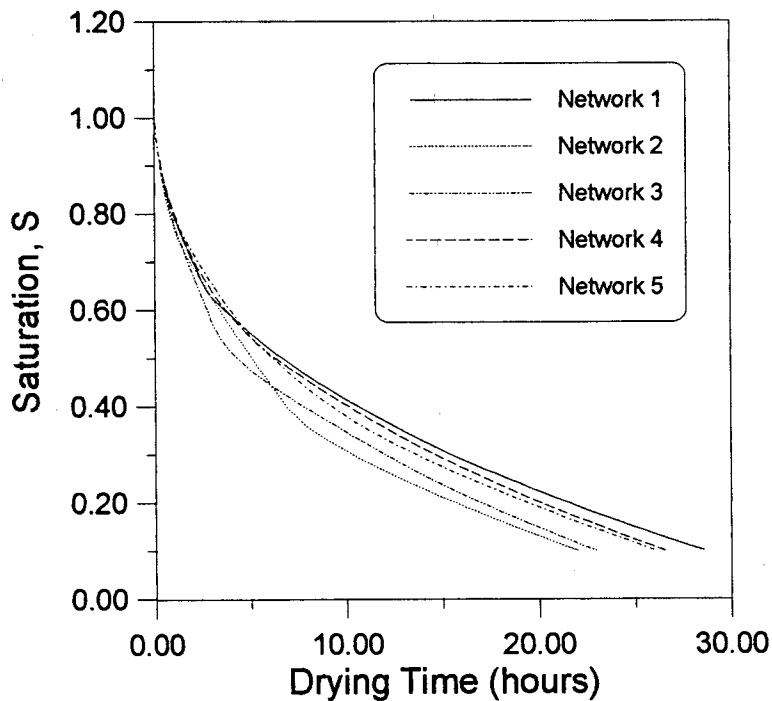
Fig. 5-1   Drying curves for five networks

It is seen from Fig. 5-1 that the drying curves for the five networks have the same characteristics. Although these five networks have the same geometrical size and the same distribution of the pores and throats sizes, the times which are needed to dry the networks to the saturation S=0.1 are different. The difference of the end drying times between the fastest one and the slowest one is about 20%. However, it was noted that the drying times can have a difference of more than 45% near the saturation S=0.4. The drying curves begin to deviate from the beginning of the drying and the deviation increases with the drying process until the saturation

reaches about 0.4. Clearly, the drying rates for each network are different during this period. After S=0.40, the drying curves become parallel, which implies that the drying rates tend to be the same for the five networks. Furthermore, an interesting evidence was noted. The network 2 dries more slowly than network 3 before S=0.6 but this tendency is then inverted after that. It seems that initially the drying rate of network 2 is small but is accelerated after S=0.6. To have a better look of it, the drying rate curves are plotted in Fig. 5-2.

5.1.2   Drying Rate

The drying rate in Fig. 5-2 is the drying time derivative of saturation (dS/dt). One can see clearly from Fig. 5-2 that the drying rates are very high at the beginning of the drying process (the interface is completely wetted with liquid) and then, decrease very quickly. The difference of the drying rates for different networks appear soon after some area of interface is dried (formation of dry pitches at the interface). This difference increases with the reducing saturation and reaches the maximum near S=0.6. After S=0.4, the drying rates of the five networks tend to be the same. This is coincident with the observation of Fig. 5-1.
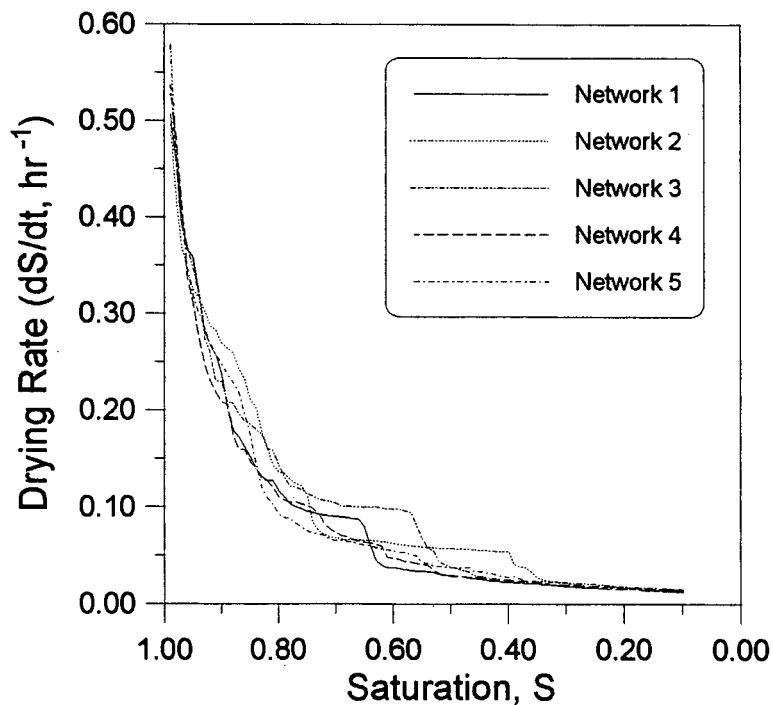
Fig. 5-2   Drying rates for five networks

Observing the drying rates of network 2 and network 3 in Fig. 5-2, one can find that the drying rate of the network 2 decreases more rapidly than that of network 3 before S=0.70. Then, the drying rate of network 2 and network 3 maintain constant with a higher drying rate of network 3. At the S=0.5, the drying rate of network 3 decreases again and becomes lower than the drying rate of network 2 which continue to be constant. This suggests that there are something occurring near the S=0.50 for network 3. In order to understand it better, the evaporating area inside the five networks during the drying process are presented in Fig. 5-3.

5.1.3   Evaporating Area in the Network

The evaporating area plotted in Fig. 5-3 is the sum of the border area of trapped clusters. It is obtained by summing up all the sectional area of the throats which are on the border of each evaporating trapped cluster. One can note that the evaporating areas at high saturations are almost the same for five networks. This is so because the initial evaporating area is exactly the sectional area of the throats on the interface. For all five networks, there is a small difference in the evaporating area at the very beginning of drying.
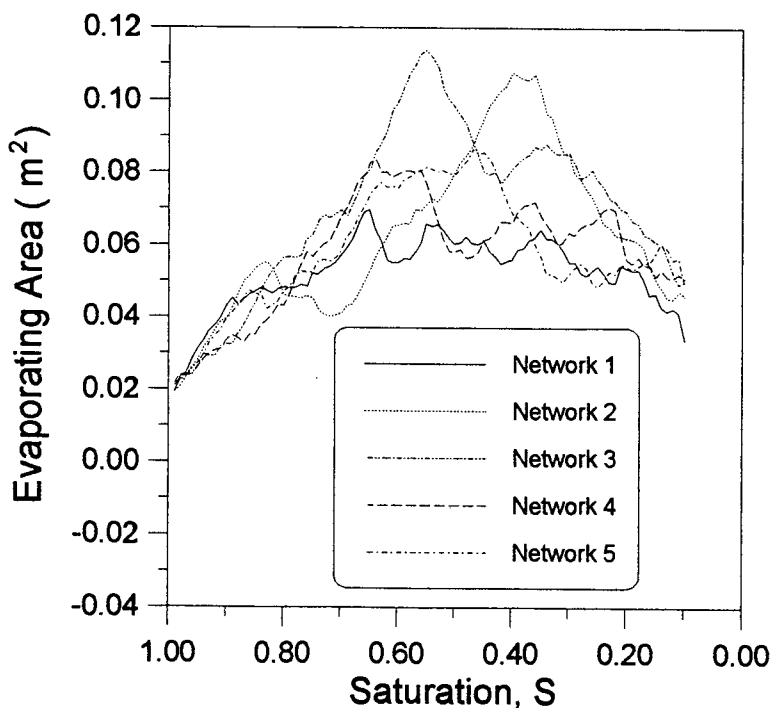
Fig. 5-3   Evaporating area inside the network during the drying

As drying proceeds, the trapped clusters in each network are not the same, i.e., the liquid phase distribution in the network during the drying simulation is different for each network. This difference results in different evaporating areas for the different networks. It is found, however, that the evaporating area curves for the five networks have the same characteristics as shown in Fig. 5-3. The evaporating area increase due to the formation of trapped clusters for S>0.70. Then, the evaporating area oscillates and for S<0.3 the evaporating area begin to decrease. The performance of the evaporating area curves will be discussed in more details latter with the liquid phase distribution maps.

It was also found that the evaporating area curves present a correspondence with the drying curves, i.e., the network which dries faster has a higher evaporating area than the network which dries slower. For the network 2 and 3, there is a peak on the evaporating area curves around S=0.4 and 0.6, respectively. As the evaporating area of network 2 begin to reach its peak value the evaporating area of network 3 begin to drop from its peak value. The cross of the two curves take place near S=0.50. It was at this point that network 2 became to dry more rapidly than network 3 as seen from Fig. 5-2. This suggests that the evaporating area inside the network plays an important role in determining the velocity of the drying process.

It is well-known that the drying rate decreases rapidly with the receding evaporating front into the porous medium. The evaporating area for network 3 reaches its peak value earlier than network 2. It means that the evaporation rate on the drying front for network 3 at the peak point should be higher than that of network 2. If the evaporating front recede uniformly, it should be nearer to the top for network 3 than for network 2 when the evaporating area reaches to the peak. As a result, the peak evaporating area should have a greater influence on the drying process for network 3. However, as seen from Fig. 5-1, although with a lower evaporation network 2 dries more rapidly than network 3. This cannot be reasoned only with information of the evaporating area because Fig. 5-3 only gives the size of the evaporating front but not its location. To obtain this information, liquid phase distribution maps are extracted during the drying simulation. From these maps, one can locate the evaporating front at each drying step.

5.1.4   Phase Distribution in the Network

Liquid phase distribution maps for network 1~5 are given in the Fig. 5-4 ~ 8. From those maps, the first thing to be noted is that the evaporating front is far from being uniform, i.e., the evaporating front does not recede into the network as a flat surface. The form of the evaporating front is very complex and different for the five networks. Even for the network 1 whose evaporating area oscillate less than other networks as seen in Fig. 5-3, the evaporating front is far
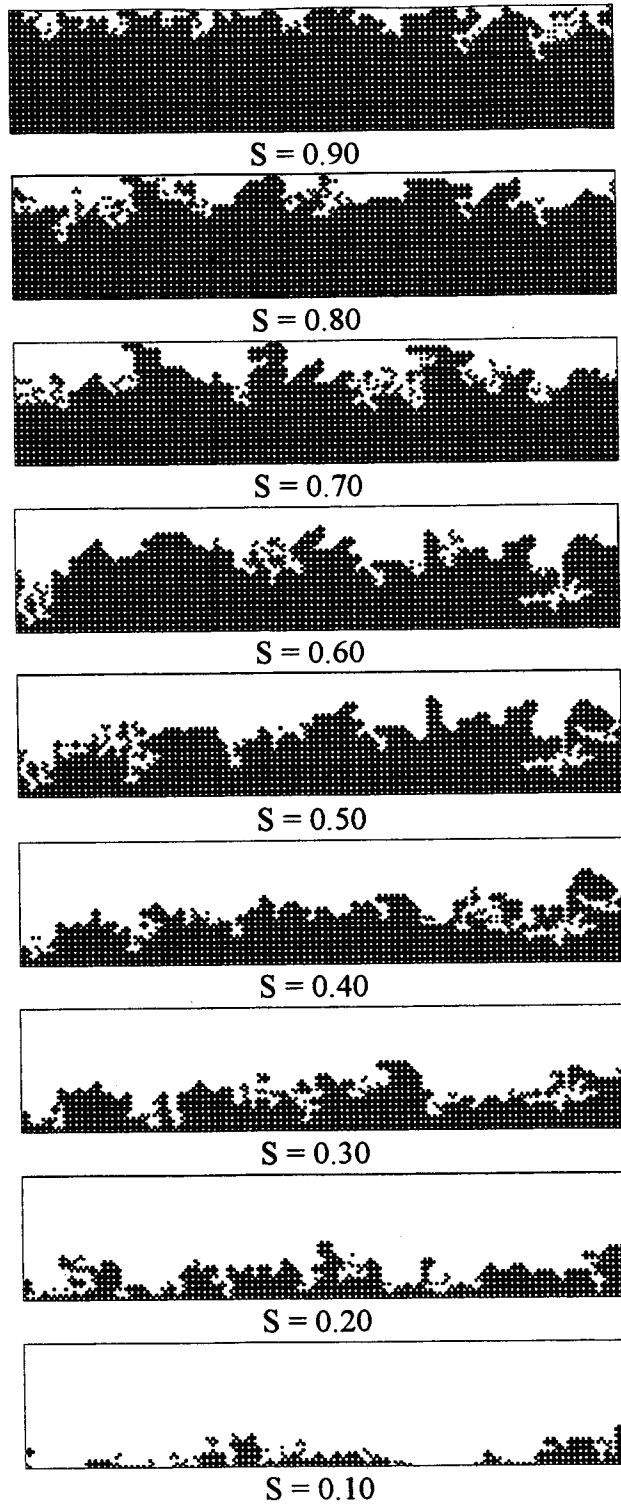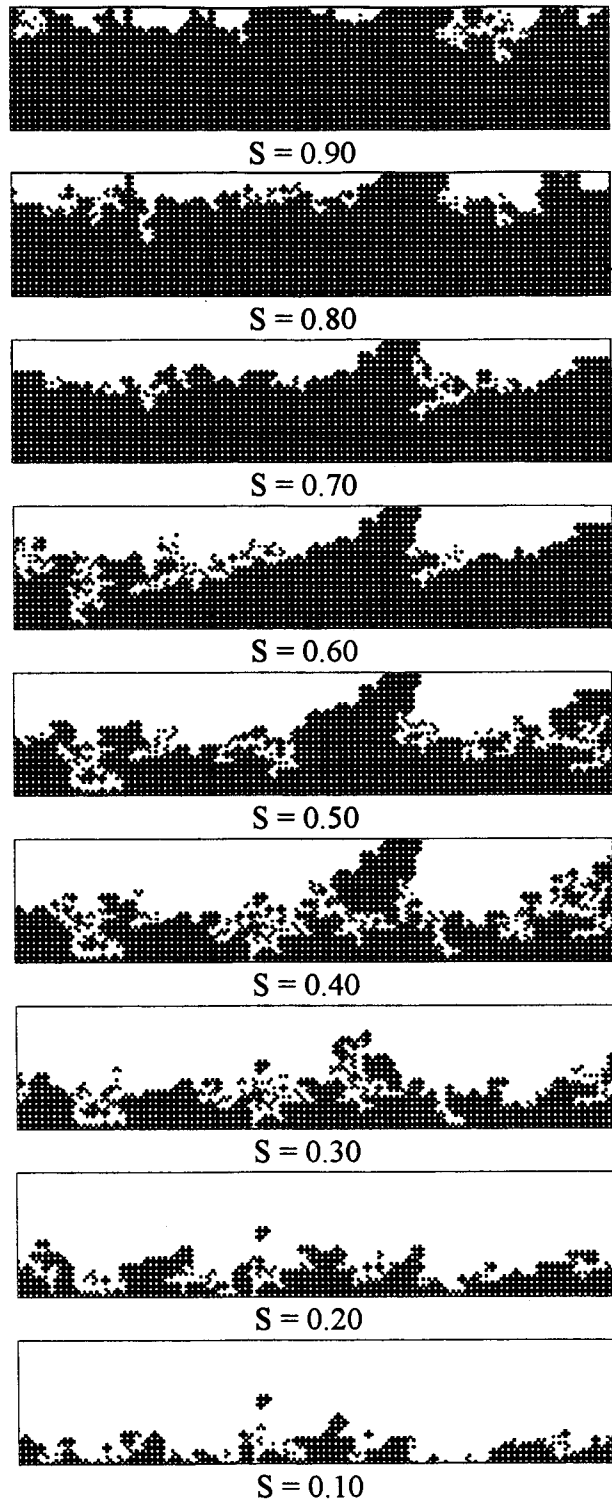
S = 0.90

S = 0.80

S = 0.70

S = 0.60

S = 0.50

S = 0.40

S = 0.30

S = 0.20

S = 0.10

Fig. 5-4   Phase distribution for network 1

S = 0.90

S = 0.80

S = 0.70

S = 0.60

S = 0.50

S = 0.40

S = 0.30

S = 0.20

S = 0.10

Fig. 5-4   Phase distribution for network 2

S = 0.90

S = 0.80

S= 0.70

S = 0.60

S = 0.50

S = 0.40

S = 0.30

S = 0.20

S = 0.10

Fig. 5-4   Phase distribution for network 3

S = 0.90

S = 0.80

S= 0.70

S = 0.60

S = 0.50

S = 0.40

S = 0.30

S = 0.20

S = 0.10

Fig. 5-4   Phase distribution for network 4

S = 0.90

S = 0.80

S= 0.70

S = 0.60

S = 0.50

S = 0.40

S = 0.30

S = 0.20

S = 0.10
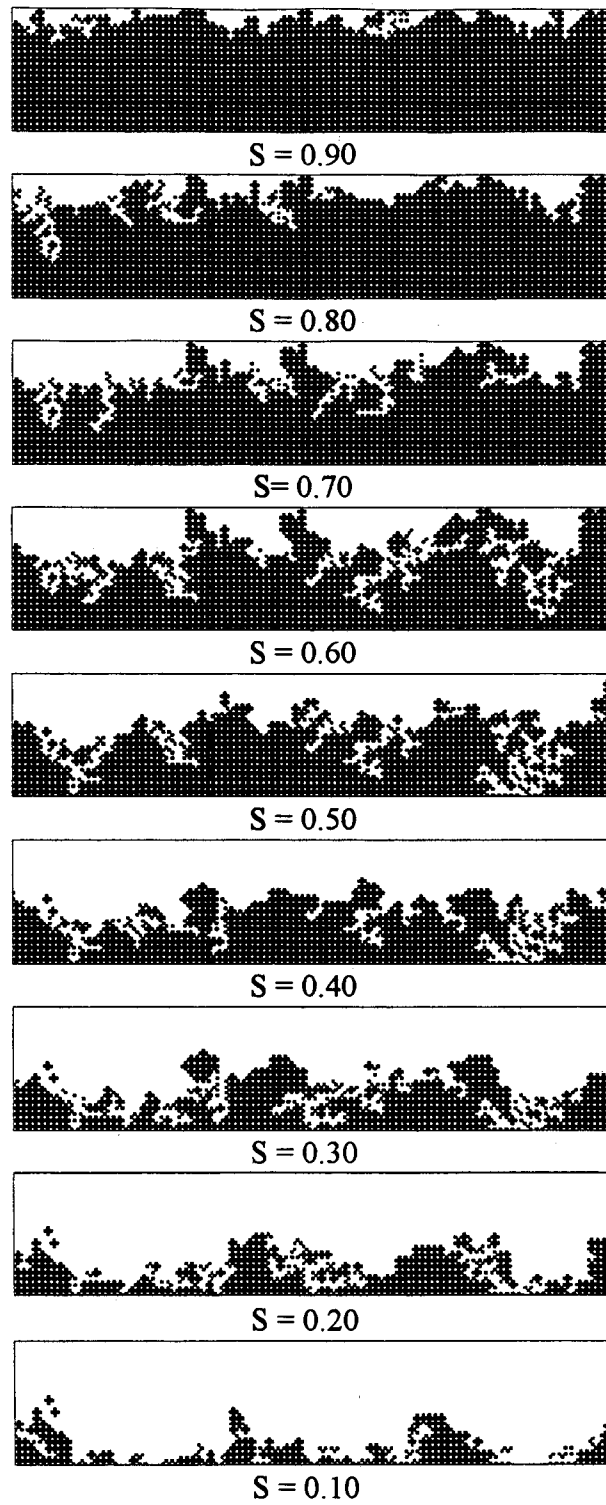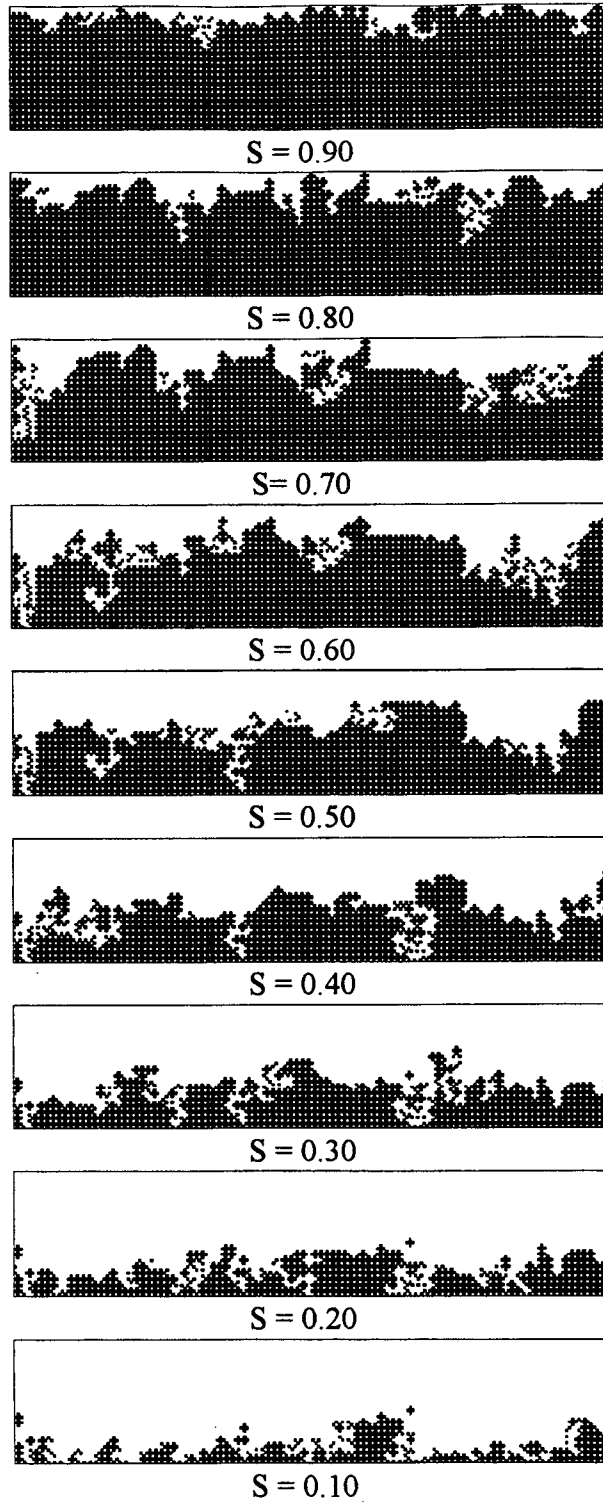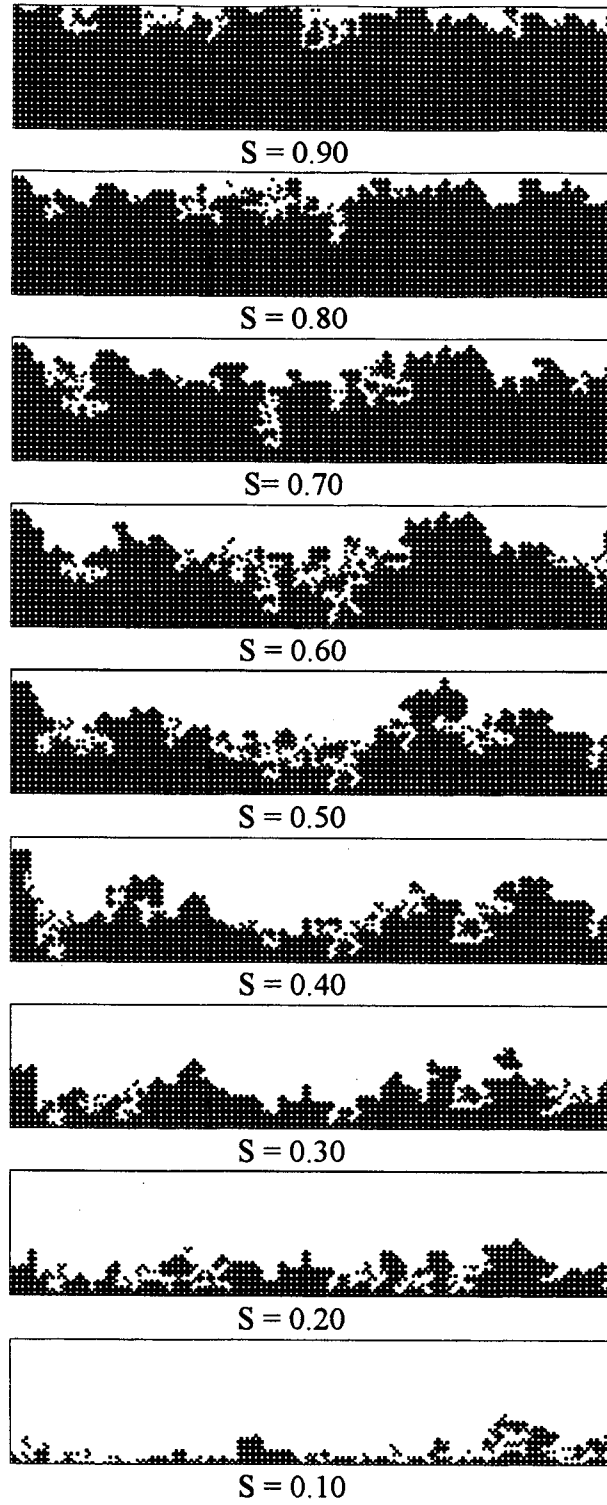
Fig. 5-4   Phase distribution for network 5

from being flat. Dry pitches at the beginning of the drying can be seen in the maps. With the receding of the evaporating front away from the top, the form of the evaporating front become more and more complex due to the appearance of more liquid clusters and the formation of some funicular drying zone.

The drying behaviors of network 2 and 3 can now be understood with the help of the liquid phase distribution maps. One can see that the top surface of network 1, 4 and 5 dried more rapidly than that of network 2 and 3. Their top surface are completely dried soon after S=0.70. For network 3, the top surface became completely dry only after S=0.60. For network 2, there is a liquid cluster on the top surface and it is completely dry only after S=0.40. The evaporating area of network 2 reached its peak value for S=0.40 because, the evaporation rate on the front kept a relatively high value due to this liquid cluster. This explains why network 2 dried more rapidly than network 3 even for later times. At a saturation of S=0.4, the evaporating front of network 2 is nearer the interface than that of network 3. With a higher evaporation rate on the evaporating front and a larger evaporating area, network 2 dries more rapidly than the other networks.

From the liquid phase distribution maps, one can understand why the evaporating area decreases after S=0.30 for all networks. Funicular drying zones reaches the bottom edge of the networks near S=0.30, and the edge effect takes place. In other words, the evaporating front is limited to develop its form freely. The edge effect reduces the clusters in the network and, consequently, the evaporating area.

The drying rate presented in Fig. 5-2, in fact, is a combination of the evaporation rate on the evaporating front and the area of the evaporating front. To illustrate the mass transfer at the top surface of the porous medium during different stages of simulation, local evaporation rate for network 2 and 3 are shown in Fig. 5-9 and Fig. 5-10.

5.1.5   Local Mass Fluxes at the Top Surface

From Fig. 5-9, it is found that the local mass fluxes of the vapor at the top surface decreases sharply after this surface is dried. The vapor fluxes at the wet surface is almost ten times bigger than the vapor fluxes at the dry surface. The mass fluxes at the top surface decrease with the receding evaporating front. For network 2, the wet pitch at the top surface maintain the global mass flux at a relatively high value. Going back to the drying rate curves in Fig. 5-2, one can observe that the drying rate curves for network 1, 2 and 3 have a feature that network 4 and 5 do not have. For the formers, the drying rate decreases rapidly at the very beginning of drying and then keeps almost constant at a certain value. Then the drying rate drops sharply again to a lower
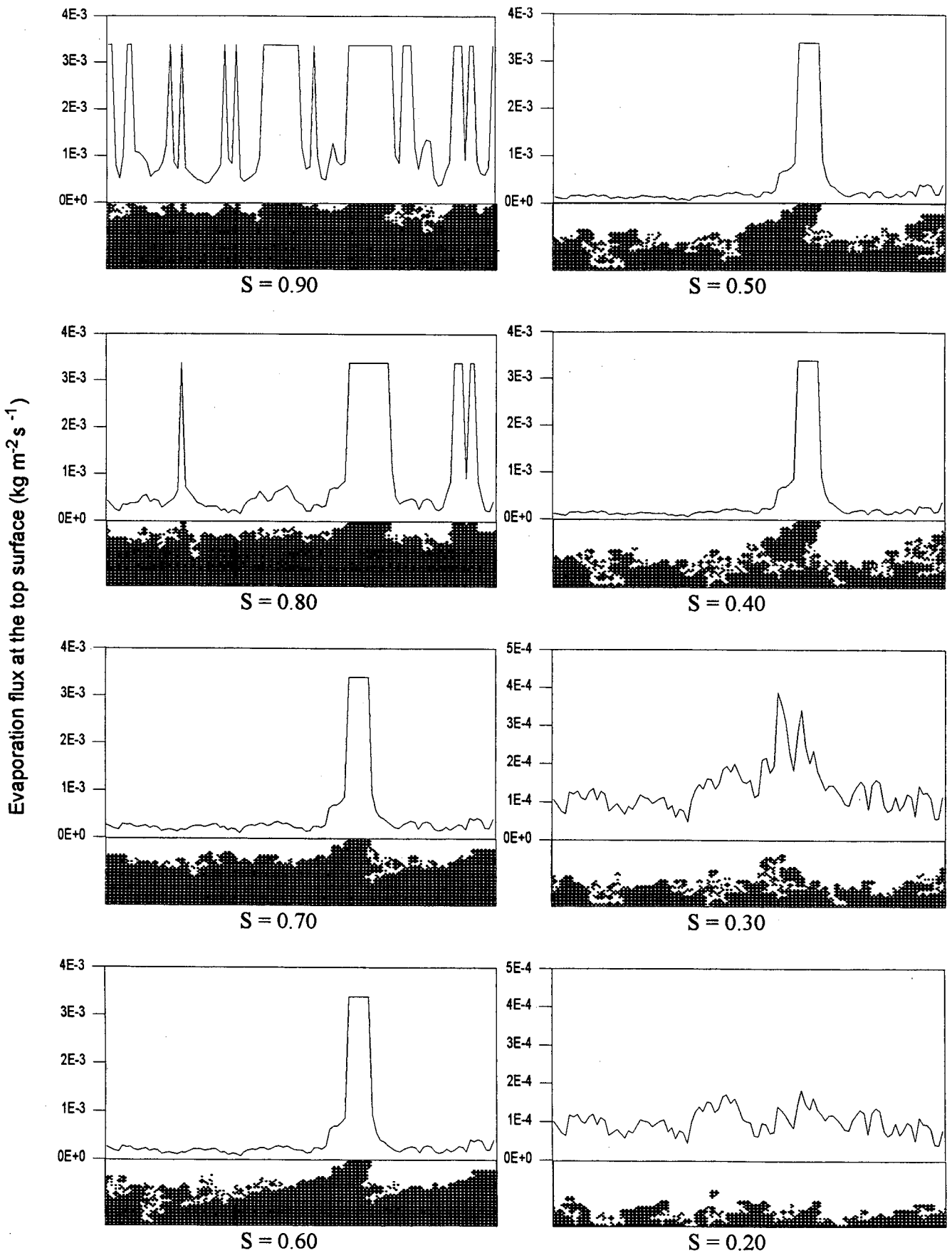
Fig. 5-9   Local mass flux profiles at the top surface for network 2 (with Kelvin effect)
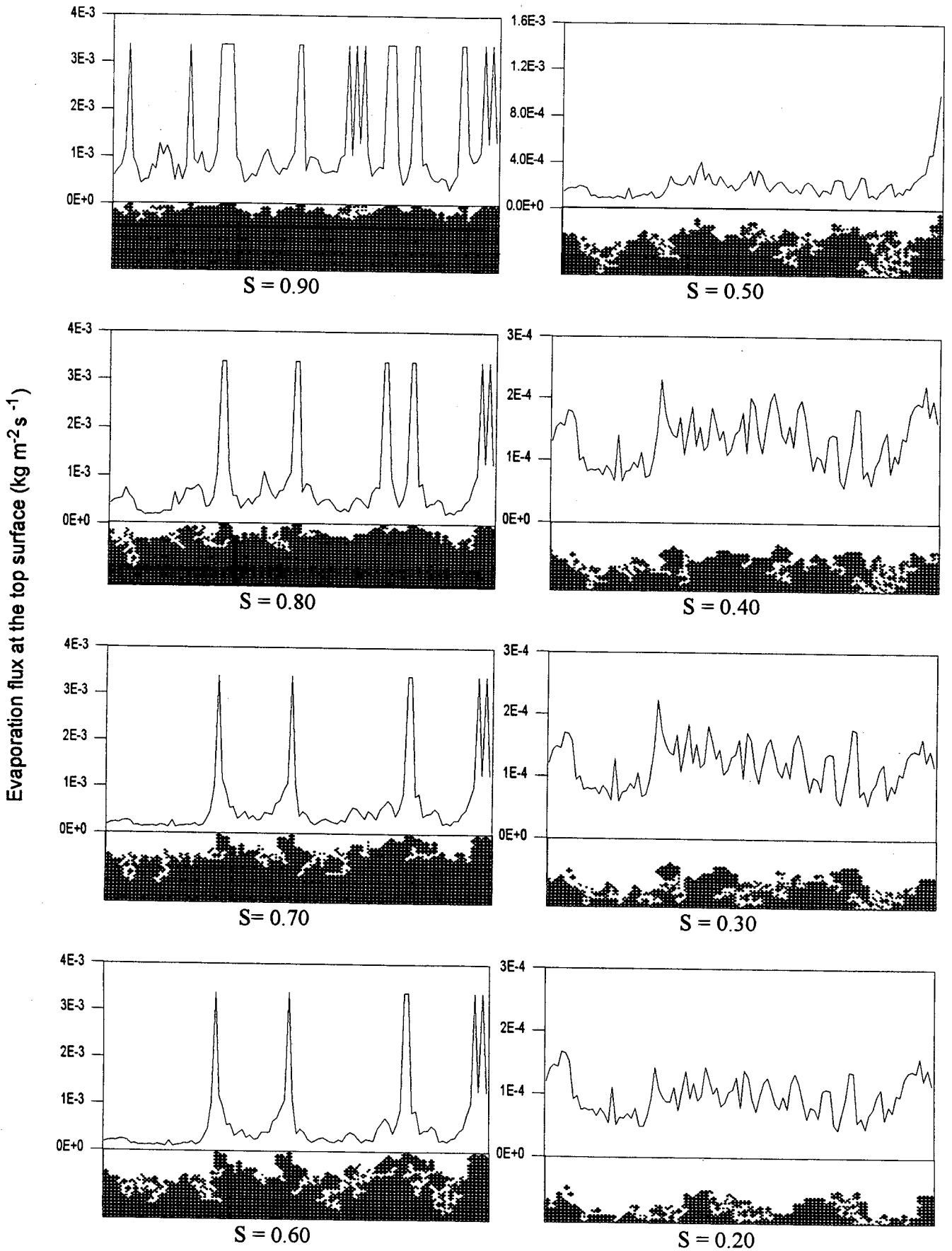
Fig. 5-10   Local mass flux profiles at the top surface for network 3 (with Kelvin effect)

value at given saturation value. This saturation value where the second drop in the drying rate takes place, in agreement with Figs. 5-4 ~ 8 and 5-9 ~ 10, is exactly the value where the top surface becomes totally dried. The constant drying rate after the first drop for network 1, 2 and 3 is different than the one that occurred earlier, which is determined by the wet area of the top surface. The larger the wet area, the higher the global mass flux at the top surface. On other hand, the longer the top surface keeps wet, the longer the constant drying rate period is.

For network 4 and 5, the second drop in the drying rate is not as clear as that for other networks. From Fig. 5-7 and Fig. 5-8, one can find that the top surface becomes totally dried very quickly (before S=0.7). Their drying curves, thus, are smoother than that of other networks.

It is worthy mentioning here that evaporation-condensation mechanisms were observed during all simulations, i.e., some clusters have a negative global evaporation rate around their border, although in a somewhat low extent. This was not reported by Prat (1993) because the Kelvin effect was not included in his drying model, i.e., all gas-liquid interface in his network are taken to be plane.

Motivated by the existence of evaporation-condensation inside the network Kelvin effect will now be explored.

5.2   INFLUENCE OF THE KELVIN EFFECT ON THE DRYING KINETICS

The difference caused by the Kelvin effect, in terms of the driving force for vapor diffusion, i.e., the partial pressure of the vapor at the gas-liquid interface, is very small. According to the Kelvin's equation, the partial pressure of the vapor at a concave meniscus is lower than the partial pressure at a flat interface. The difference of the partial pressure increases with the decreasing meniscus radius. The variation of partial pressure of alcohol vapor with the meniscus radius is given in Fig. 5-11.

One can find that the difference of the partial pressure between a flat interface (P_0) and a meniscus (P_r) is very small for meniscus radius bigger than 0.1 μm. The size of pores and throats used in our network is much bigger than 0.1 μm, and, therefore, the Kelvin effect with regard to the driving force for vapor diffusion, can be neglected. However, for a drying model in which the gas-liquid interface is taken to be flat, the partial pressure of vapor at the gas-liquid interface in the network is uniform. In other words, vapor condensation, as have been reported by Prat (1993), can not take place at these interfaces because the vapor partial pressure at the interface is always the highest inside the network. For a drying model in which the gas-liquid interface has a certain curvature, although the difference of the saturated partial pressure at the interface caused by the difference of the curvature is very small, the condensation of vapor in the network, as have been observed in the simulations, can take place during the drying simulation. The interesting point is to investigate which role the condensation-evaporation mechanism plays during the simulation.
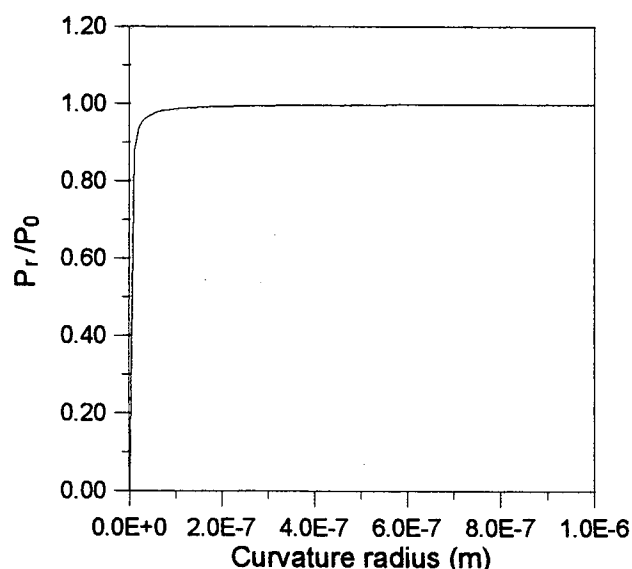
Fig. 5-11   Variation of partial pressure with curvature radius

To study the Kelvin effect on the drying kinetics, two drying models are used to simulate the drying behavior for the same network. One drying model takes into account the Kelvin effect (the gas-liquid interfaces have curvature) and the other takes the gas-liquid interfaces as flat. The five networks used here are the same of those used in the last section. The simulations are carried out under the same conditions of the last section. Again, the external flow is not considered.

5.2.1 Drying Kinetics

The drying curves for the five networks using the two different drying models are presented in Figs. 5-12 ~ 16. The first evidence that can be observed from these figures is that the Kelvin effect has a different influence on a different network. For network 1 and 2, the difference in drying time caused by the Kelvin effect is much larger than that for network 3, 4 and 5. The difference in drying time can reach more than 20% (for network 1) or less than 2% (for network 4). For all networks used here, the drying time for the two models is practically the same for S>0.7. Deviations take place near S=0.50. After this point, the drying curves for the two models separate one from the other.
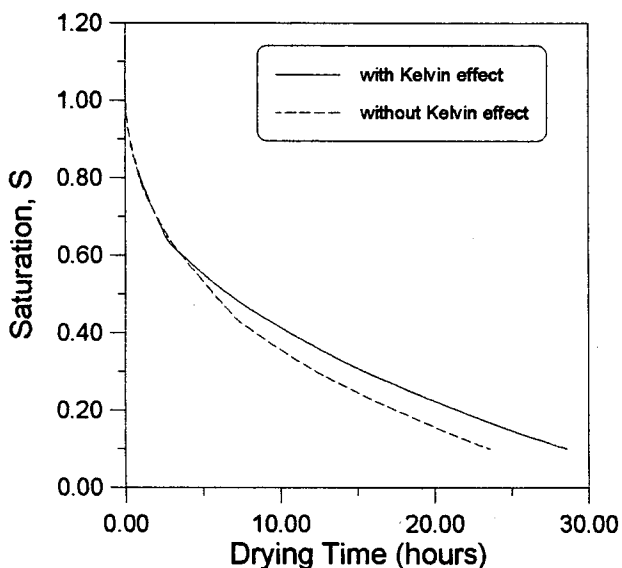
Fig. 5-12   Drying curve for network 1   Fig. 5-13   Drying curve for network 2
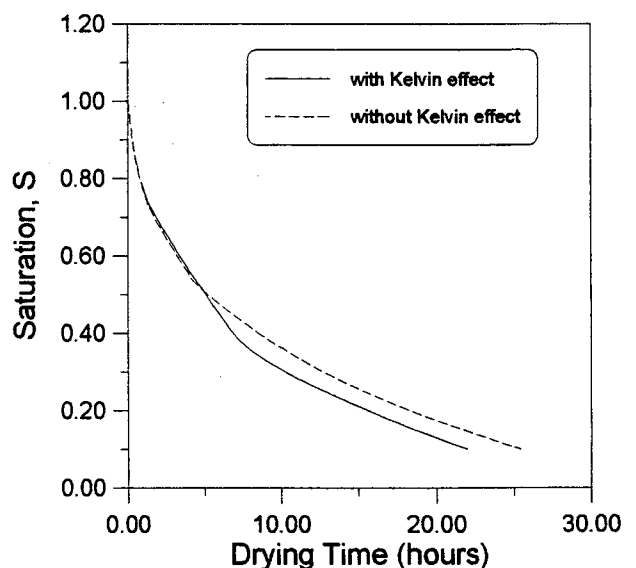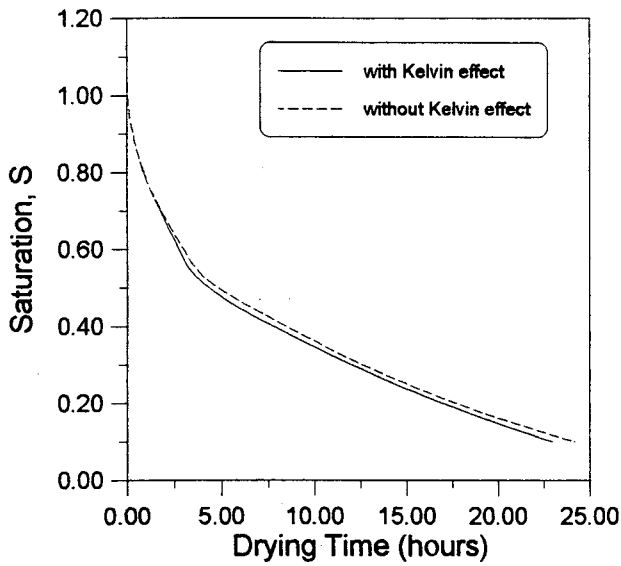
Fig. 5-14   Drying curve for network 3   Fig. 5-15   Drying curve for network 4
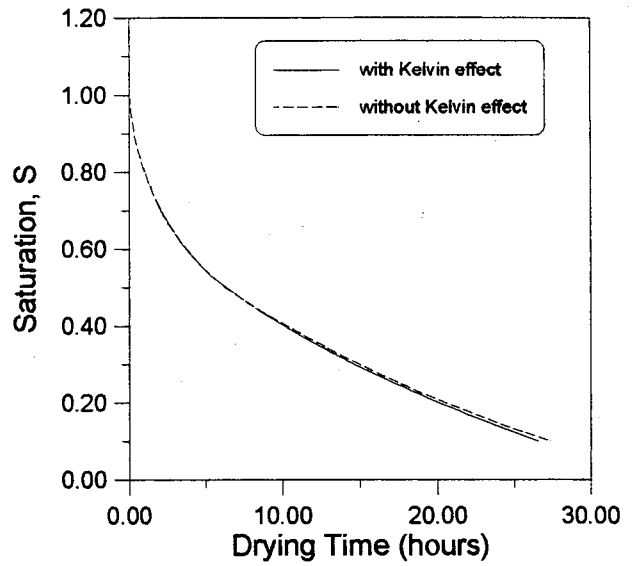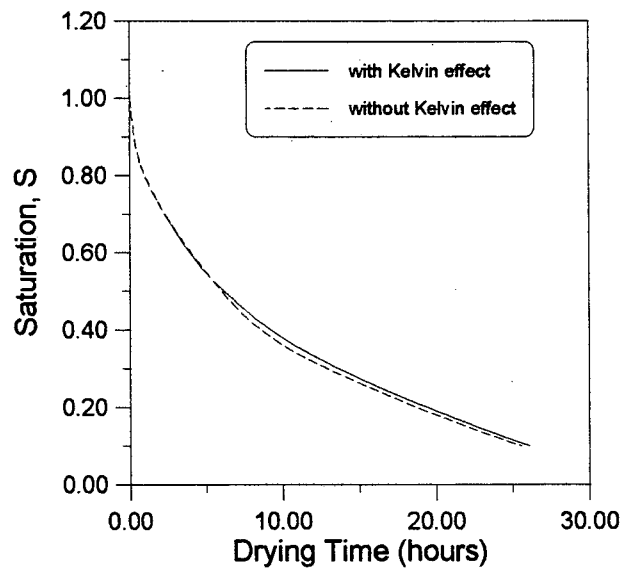
Fig. 5-16   Drying curve for network 5

The second evidence, which is more interest, is that the Kelvin effect can cause either a positive influence (accelerating the drying process) or a negative influence (reducing the drying process). This is somehow strange because, as one usually would expect, the Kelvin effect should always reduce the drying. For the two drying models used here, the boundary condition imposed on the top edge of the network is the same, i.e., the mass fraction of alcohol vapor is the zero. For the model which takes Kelvin effect into account, the saturated partial pressure of alcohol vapor

at the gas-liquid interface inside the network is lower than that of the model which do not consider the Kelvin effect and should slow the drying process. However, one can find, from Figs. 5-12 ~ 16, that the effect on network 1 and 5 (positive effect) is different than that on the network 2, 3 and 4 (negative effect). As have been explained before, the negative effect is easy to understand. Otherwise, the positive effect can not be explained only by the difference of the saturated partial pressure at the gas-liquid interface in the network. More detailed information inside the network are needed to explain why for some networks reducing the vapor pressure at the gas-liquid interface can accelerate the drying.

5.2.2 Drying Rate

The drying rate curves for the five networks are presented in Figs. 5-17 ~ 21. It can be seen that the difference of drying rate coincides with the difference of the drying time caused by the Kelvin effect. For network 1 and 2, the difference in drying curves obtained by using the two drying models is large, as seen from Figs. 5-12 and 5-13; the same occurs for the drying rate according to Figs. 5-17 and 5-18. For network 3, 4 and 5, the difference in the drying rate curves due to the Kelvin effect is small. The drying rate curves for the model without the Kelvin effect have the same characteristics of the drying rate curves for the model with the Kelvin effect, that is, the drying rate decreases rapidly to a certain value and then this value is maintained for a period. For network 1, 2 and 3, the second drop in the drying rate occurs for both models, whereas for network 4 and 5 the second drop is not clear on the drying rate curves. The occurrence of the second drop in the drying rate which indicates the moment, as have been discussed before, that the interface becomes totally dried, is not at the same saturation for the two different models. For network 1 (Fig. 5-17), the second drop on the solid line (with Kelvin effect) occurs earlier than that on the dashed line (without Kelvin effect), i.e., the interface dries more rapidly by using the model with Kelvin effect than by using the model without Kelvin effect. This implies that the liquid phase distribution is different during the simulation for the same network depending whether Kelvin effect is included or not.

Different than what was observed for network 1, for network 2 the second drop in the drying rate with Kelvin effect takes place later than without Kelvin effect. It means that the top surface kept partially wetted for a longer time by using the model with Kelvin effect. As have been discussed in the last section, the wetted surface has a much higher evaporation rate than the dried surface. This difference of evaporation rate at the top surface has a stronger influence on the drying kinetics than the difference of the saturated partial pressure caused by the curvature. As a result of the wet surface, the network dries more rapidly by using the model with Kelvin effect.
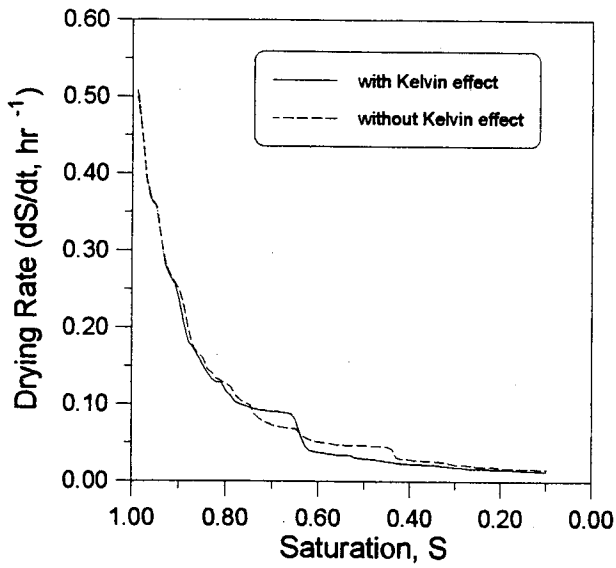
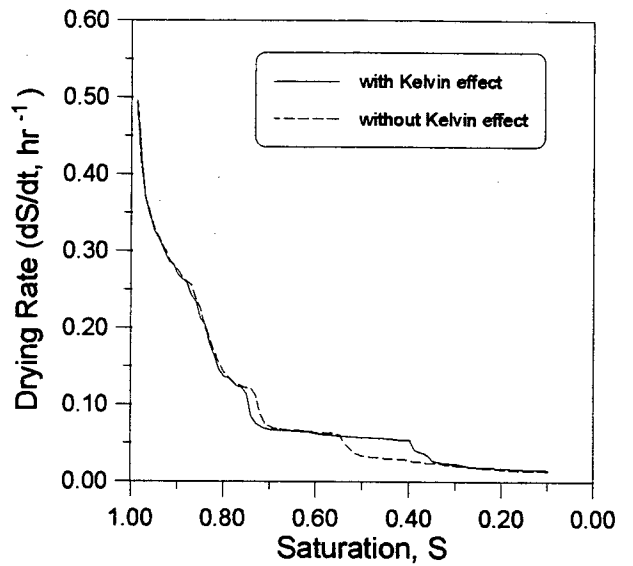Fig. 5-17   Drying rate curve for network 1

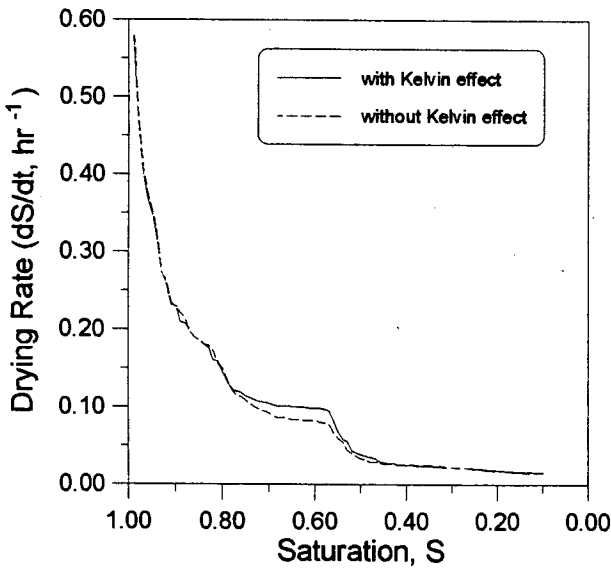Fig. 5-18   Drying rate curve for network 2

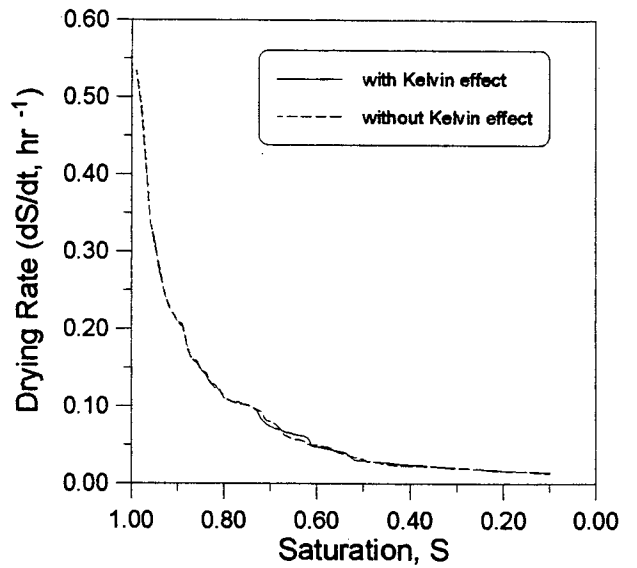Fig. 5-19   Drying rate curve for network 3

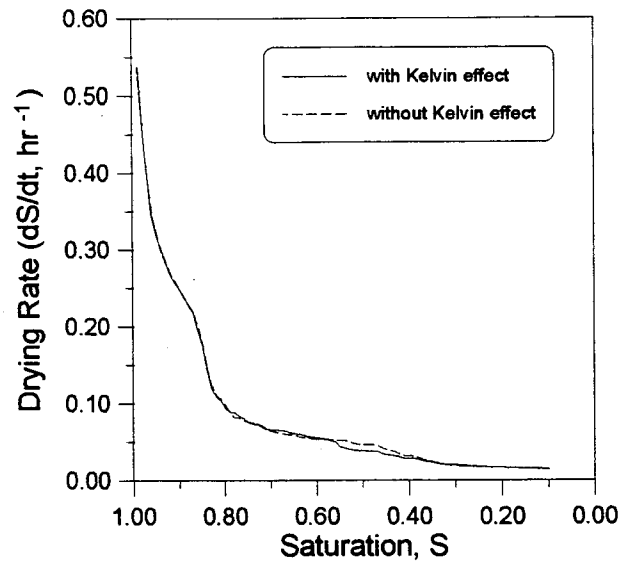Fig. 5-20   Drying rate curve for network 4

Fig. 5-21   Drying rate curve for network 5

For network 3, the second drop in the drying rate occurs almost at the same saturation for the two curves. However, the dashed line maintain a lower value of drying rate after the first drop. This might be caused by the evaporating front area or the evaporating front position in the network.

There is almost no difference on the drying rate curves for network 4 and 5.

5.2.3   Evaporating Area in the Network

The evaporating area for the five networks are plotted in the Figs. 5-22 ~ 26. It can be observed again that the curves of the evaporating area are very affected by the network. For network 1, around S=0.4 there is a peak on the curve for evaporating area when the Kelvin effect is absent while no peak is observed when the Kelvin effect is present. Contrarily, for network 2, the absence of the Kelvin effect cause the disappearance of the peak on the evaporating area curve. For network 3, 4 and 5, the curves of the evaporating area have the same feature for both models. From these figures, one can see that the evaporating area can be used to explain the drying times observed in Figs. 5-12 to 5-16. For networks 1 and 5 the drying times in absence of the Kelvin effect is shorter than those with Kelvin effect and the corresponding evaporating areas are larger. Also, for networks 2 and 3 the shorter drying times observed with the Kelvin effect is in agreement with the larger evaporating areas. However, for network 4, in spite of the larger evaporating area observed in presence of Kelvin effect, the drying time is virtually unaffected by

the Kelvin effect as seen from Fig. 5-15. This remains to be understood, and some insight will be provided in section 5.2.4. through the phase distribution in the network.
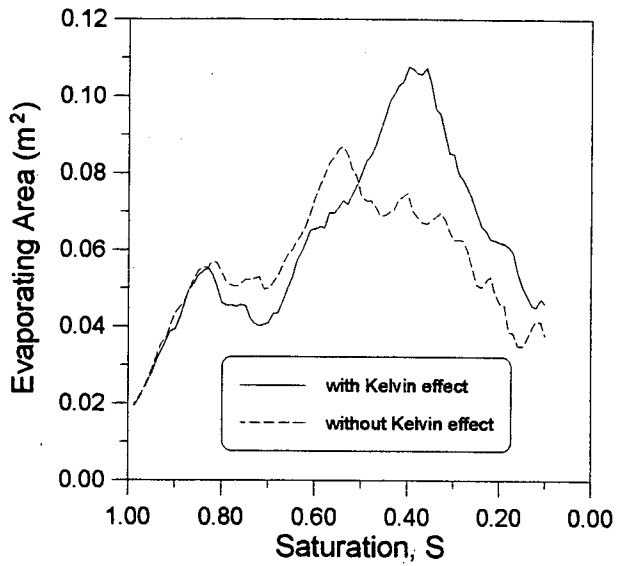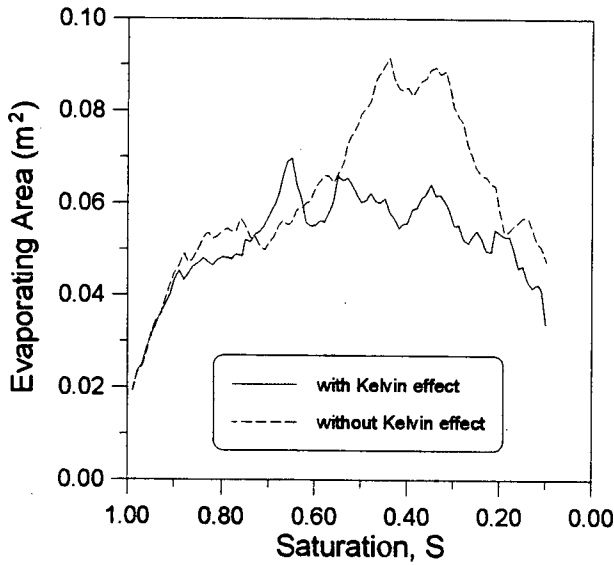

Fig. 5-22 Evaporating area curve for network 1 Fig. 5-23 Evaporating area curve for network 2
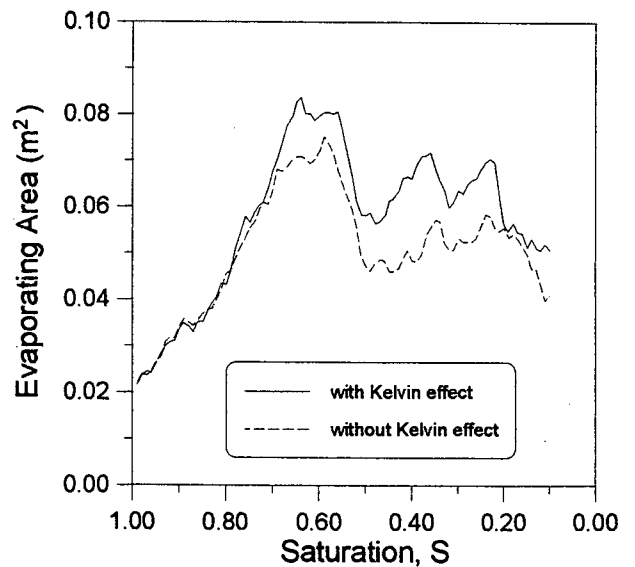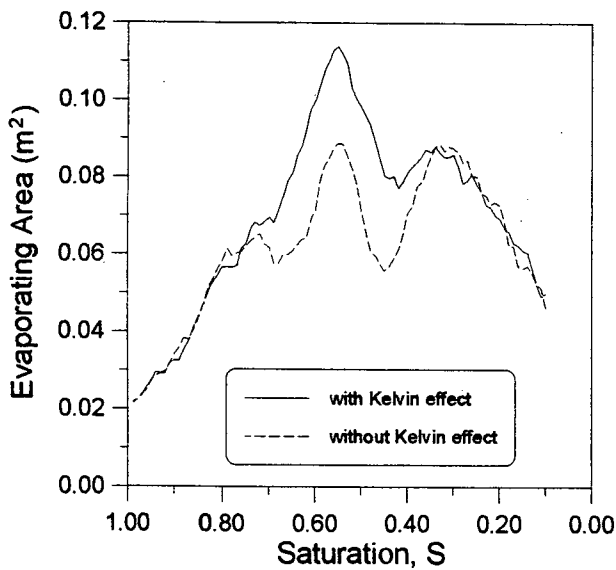

Fig. 5-24 Evaporating area curve for network 3 Fig. 5-25 Evaporating area curve for network 4
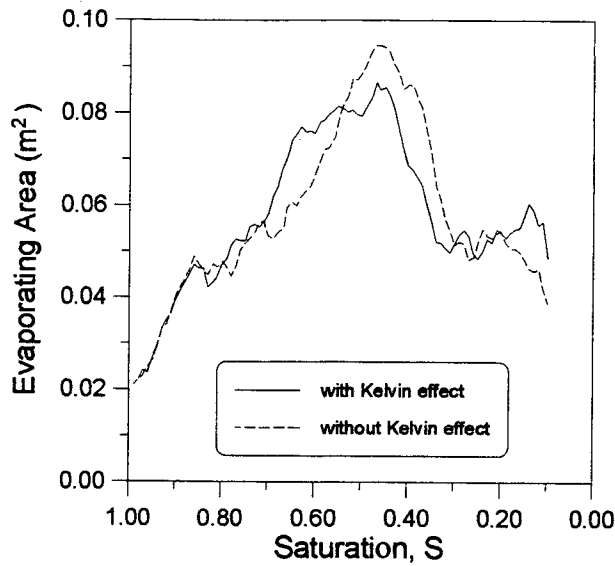
Fig. 5-26   Evaporating area curve for network 5

5.2.4 Phase Distribution in the Network

The liquid phase distribution maps, obtained from the simulations on the five network using the drying model in which Kelvin effect is absent, are presented in Fig. 5-27 to 31. Figs. 5-4 ~ 8 are presented again to facilitate the comparison of liquid distribution for the same network obtained by using the two different drying model. One can see that liquid is distributed differently for the same network at the same saturation. This means that the Kelvin effect changed the drying path in the network. For network 1 (Fig. 5-4 and Fig. 5-27), the liquid distribution in the network is somewhat similar before S=0.70. After S=0.70, in Fig. 5-4 (with Kelvin effect), the evaporating front receded from the top surface, thus, as have been discussed in last section, resulting a sharp decrease of evaporation fluxes. In Fig. 5-27 (without Kelvin effect), there is some liquid near the top surface until S=0.50. This keeps the evaporation fluxes at the top surface at a relatively high value, accelerating the drying process.

For network 2 (Fig. 5-5 and Fig. 5-28), what happened is contrary to that observed for network 1. In Fig. 5-5, the top surface became totally dry only after S=0.40. In Fig. 5-28, the interface was dried soon after S=0.60. The influence of Kelvin effect on the drying kinetics caused by the difference of liquid phase distribution is much stronger than that caused by the difference in saturated pressure at the gas-liquid interface. As a result, the network dries slowly even in the absence of the Kelvin effect. This also explained the drying behavior of network 3.

S = 0.90

S = 0.80

S = 0.70

S = 0.60

S = 0.50

S = 0.40

S = 0.30

S = 0.20

S = 0.10

With Kelvin effect   Without Kelvin effect

Fig. 5-27   Phase distribution for network 1 (without Kelvin effect)

S = 0.90

S = 0.80

S = 0.70

S = 0.60

S = 0.50

S = 0.40

S = 0.30

S = 0.20

S = 0.10

With Kelvin effect   Without Kelvin effect
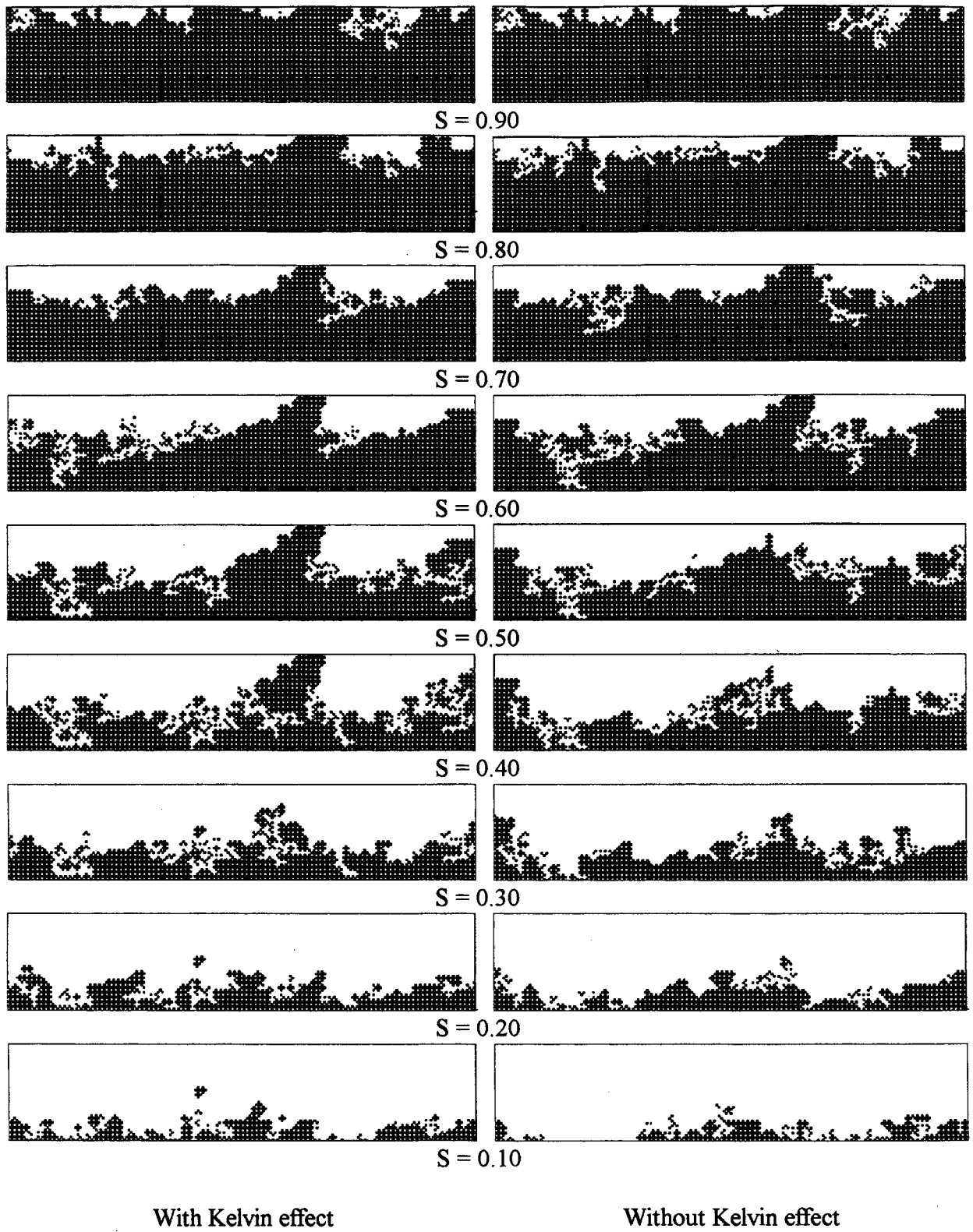
Fig. 5-28   Phase distribution for network 2 (without Kelvin effect)

S = 0.90

S = 0.80

S= 0.70

S = 0.60

S = 0.50

S = 0.40

S = 0.30

S = 0.20

S = 0.10
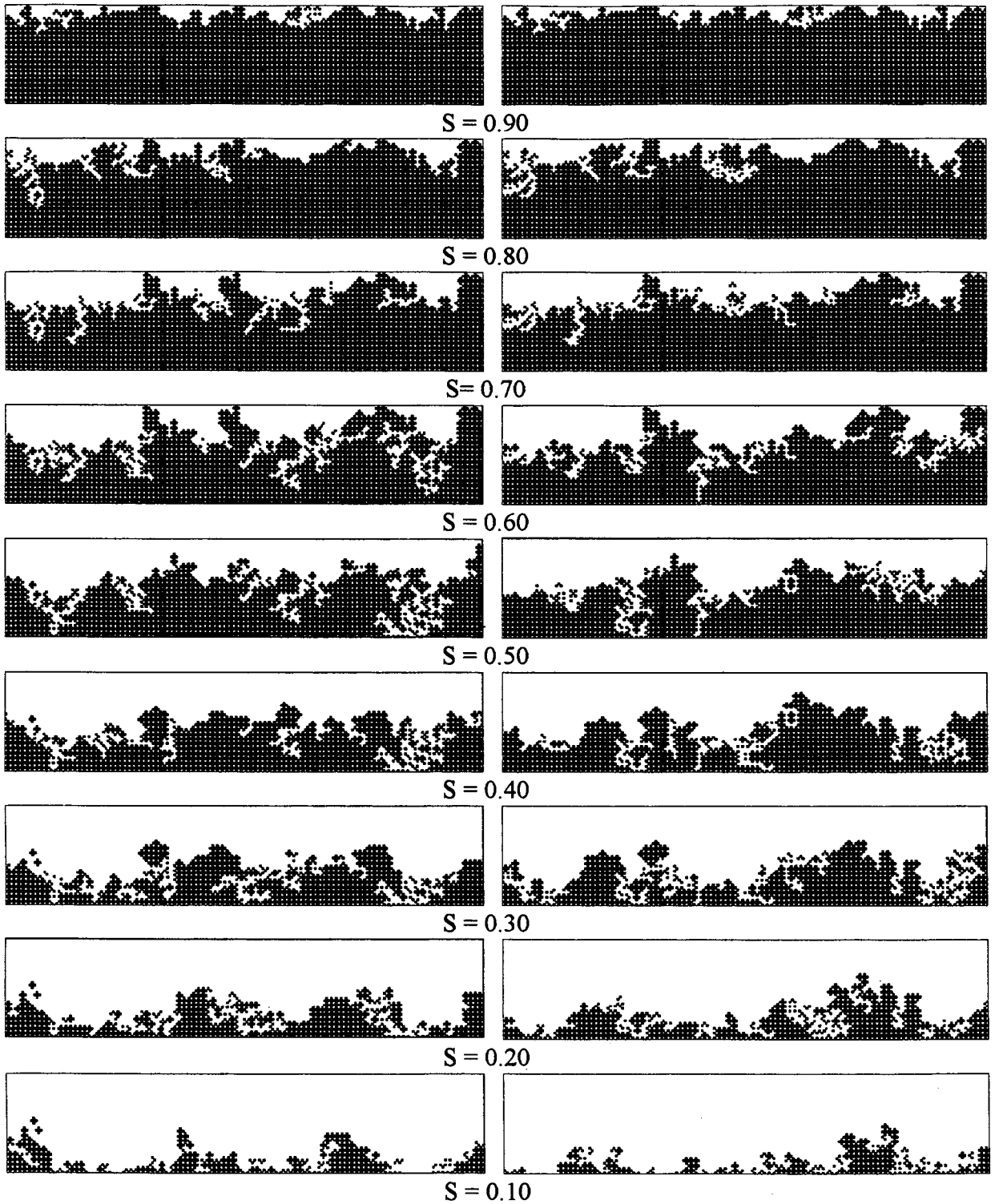
With Kelvin effect   Without Kelvin effect

Fig. 5-29   Phase distribution for network 3 (without Kelvin effect)

S = 0.90

S = 0.80

S= 0.70

S = 0.60

S = 0.50

S = 0.40

S = 0.30

S = 0.20

S = 0.10
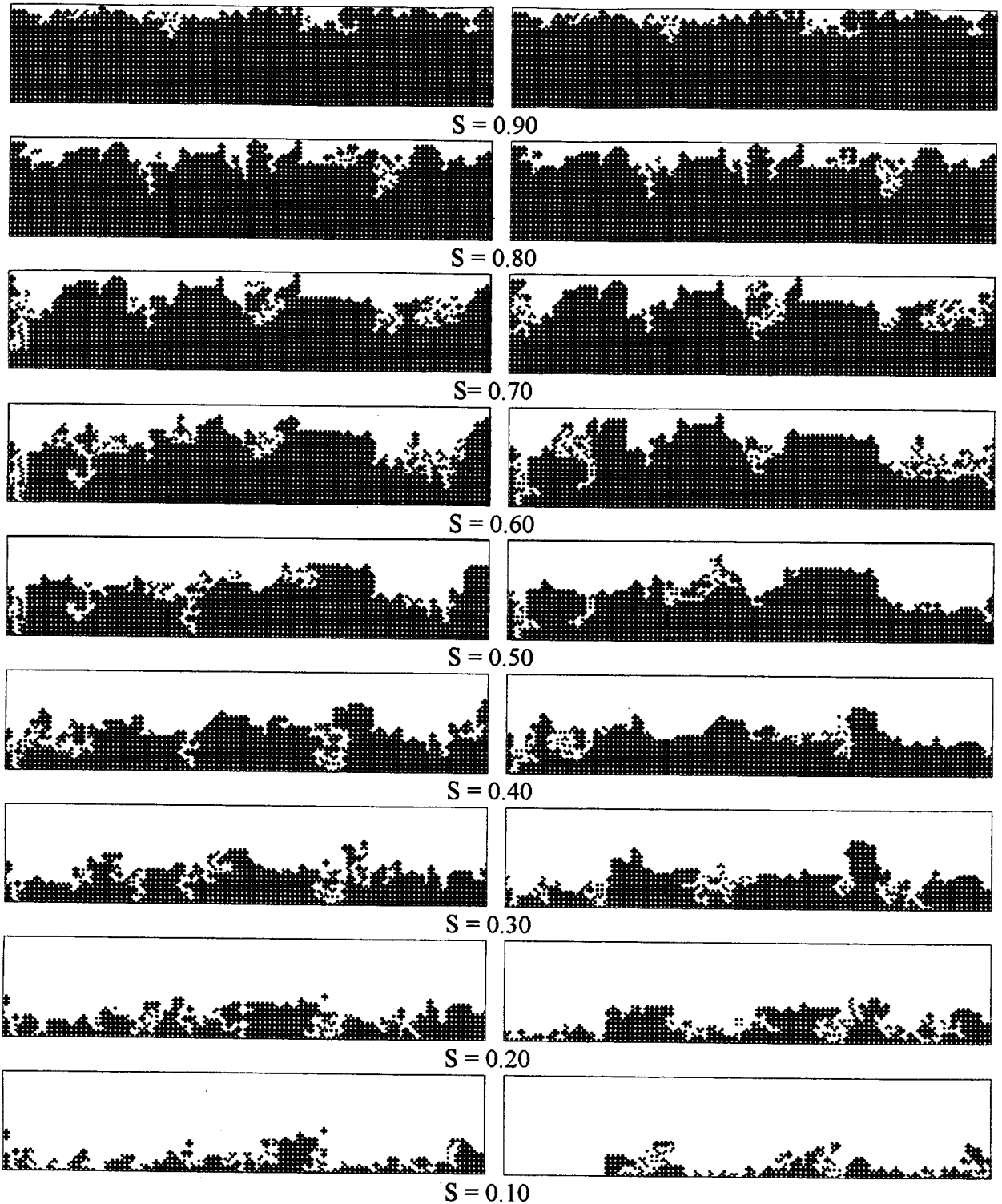
With Kelvin effect   Without Kelvin effect

Fig. 5-30   Phase distribution for network 4 (without Kelvin effect)

S = 0.90

S = 0.80

S= 0.70

S = 0.60

S = 0.50

S = 0.40

S = 0.30

S = 0.20

S = 0.10

With Kelvin effect   Without Kelvin effect

Fig. 5-31   Phase distribution for network 5 (without Kelvin effect)

From what have been discussed, one can conclude that the liquid phase distribution in the network during the drying process has a strong influence on the drying kinetics. The Kelvin effect has a strong or weak influence, depending on the network and on the manner the drying path affects the kinetics (in fact, the phase distribution). This influence can be on increasing or decreasing the drying rate.

At this point one can go back to Figs. 5-15 and 5-25 and try to understand why the drying time for network 4 was unaffected by the presence of Kelvin effect in spite of the influence of Kelvin effect on the evaporating area as seen from Fig. 5-25.

First it should be observed that for network 2 and S=0.5 the evaporating area without Kelvin effect is larger than that with Kelvin effect. However, as shown by Figs. 5-15 and 5-28 for S=0.5, with Kelvin effect the top surface has wet patches contrary to the top surface without Kelvin effect which is totally dry. Thus, even through with Kelvin effect the evaporating area is smaller than that without Kelvin effect, the drying rate for network 2 at S=0.5 is higher for the former (with Kelvin effect) than for the latter (without Kelvin effect). This finding evidences that the drying rate is affected by both the evaporating area and the resistance for the vapor diffusion from the gas-liquid interface to the top surface.

For network 4 with Kelvin effect, the evaporating area might be larger than that without Kelvin effect but the resistance for the vapor diffusion is smaller due to the phase distribution inside the network. The combination of both effects, evaporating area and vapor diffusion resistance yields drying rate for network 4 that is unaffected by the presence or not of Kelvin effect as is observed in Figs. 5-15 and 5-20.

5.3   STABILITY OF THE EVAPORATING FRONT

The stability of the evaporating front, as has been pointed out by Prat (1993), is important from the point of view of the validity of the continuum or macroscopic approach. If the continuum approach is valid with the porous medium, the evaporating front should be relatively stable during the drying process because the porous medium is usually assumed to be isotropic, i. e., the properties of the porous medium such as porosity, conductivity and permeability has the same value in any direction, at least at the scale of the representative elementary volume (R.E.V).

From the phase distribution maps of all simulations, three main regions can be observed during the drying process (Fig. 5-32):
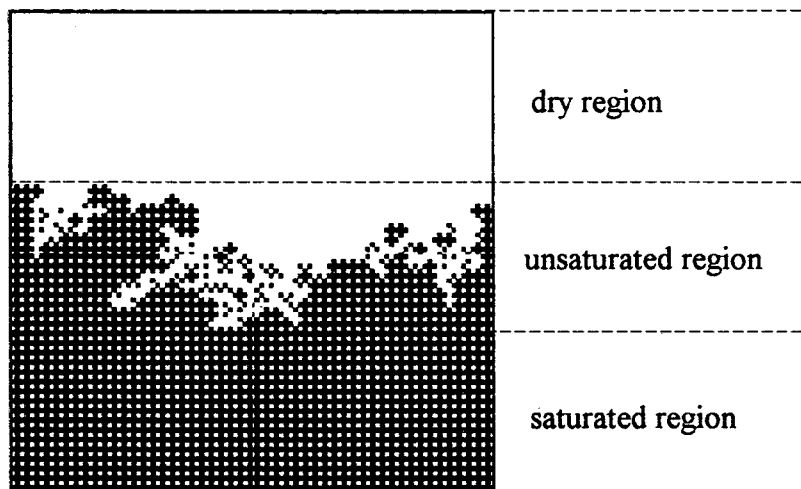
Fig. 5-32   Three main regions in term of phase distribution

• Dry region

There is no liquid in this region. The vapor is transported in the gaseous phase by vapor diffusion.

• Unsaturated region

There are some temporary trapped liquid clusters where the liquid transport is the result of a complex interaction between liquid transport within the trapped clusters and vapor diffusion in the surrounding gaseous phase. The evaporation-condensation mechanism (liquid bridge) takes place in this region.

• Saturated region

The liquid transport occurs in the liquid phase due to capillary force.

In fact, the evaporating front is formed by the evaporating throats on the border of the clusters. Its shape is quite complicated. Strictly speaking, there is an evaporating surface surrounding each temporary trapped cluster. In other words, the evaporating front is not a continuous surface but a region consisting of many separated evaporating surface. The term "evaporating front" used here is associated with the unsaturated region. The stability of evaporating front, therefore, refers to the stability (the relative depth) of this region.

Some fingering occurs after the evaporating front receded from the top surface. Although those fingering do not reach to the sample size, the evaporating front is far from being flat as assumed in many drying models encountered in the literature. The depth of the evaporating front region (unsaturated region) tends to increase while the evaporating front recede from the top surface. One can find also that the number of trapped clusters increase as drying proceeds. Some example of the variation of the temporary trapped cluster number during the drying simulation are given in Fig. 5-33 and 5-34. It is clearly shown in the figures that the trapped cluster number increase rapidly with decreasing saturation. The trapped cluster number decrease at the end of drying because of the bottom edge effect, as have been discussed before.

Similar phenomena have been observed by Masmoudi et al. (1992) and Prat (1993) in their experimental and numerical works. In the paper of Masmoudi et al., the liquid phase distribution was obtained using a transparent etched network (for more detail, one can refer to Lenormand et al., 1988). The liquid phase distribution in the network was photographed during the drying process. The influence of gravity on the cluster size and on their number in the network was investigated by Masmoudi et al. and it was found that the shape of the evaporating front is fractal, and that depth of the evaporating (invasion front, in that paper) depends clearly on the Bond number which is defined as

$$B = \frac{\Delta \rho l^2 g}{\sigma}$$

where $\Delta \rho$ represents the density difference between the displacing and displaced fluids, the l is a typical pore size diameter and the σ is the interfacial tension. Their experimental results show that the number and the maximum size of the clusters tend to increase as Bond number decrease.

One interesting feature observed by Masmoundi et al. is the relative stability of the invasion front (cluster region). This stability is observed in the experiments with the micromodel when the gravity forces are not negligible. Such a stability is also observed in the numerical simulation results of Prat (1993). As have been pointed out by Prat in his paper, the front stability could be explained in terms of the removal mechanism of the clusters through the action of

evaporation. In fact, there is no permanent trapped cluster in the network during the drying process. The small trapped clusters can be eliminated soon due to evaporation.
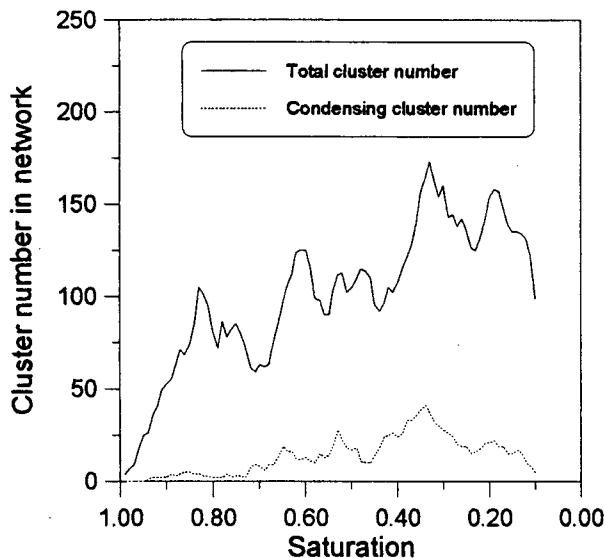

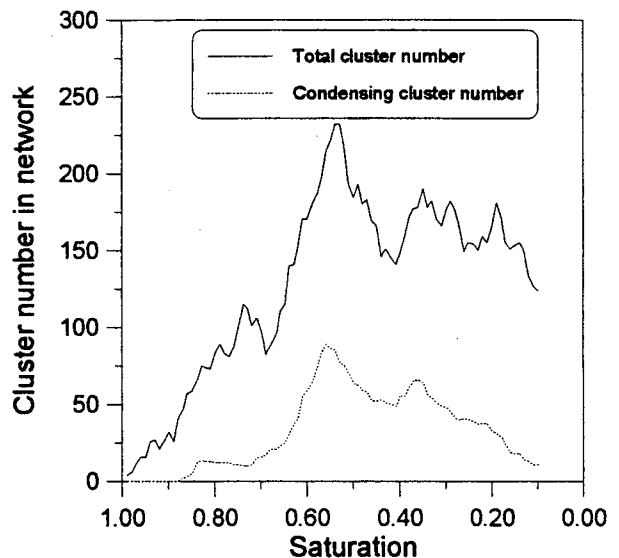Fig. 5-33 Total cluster number and condensing   Fig. 5-34 Total cluster number and condensing
cluster number in the network 2 during drying   cluster number in the network 3 during drying

One can find also, from the present simulation, that the depth of the evaporating front tend to increase while the evaporating front receded from the interface. According to Masmoudi et al., the reason for the increasing of the evaporating front depth should be associated with the decreasing of the evaporation rate in terms of a diminished power for the evaporation process (together with the diffusion process of vapor in the gaseous phase) to eliminate or erode the cluster.

The sharp decrease of the evaporation rate at the top surface after it becomes totally dry has been shown clearly in the present simulation. The present author agree with the explanation of Masmoudi et al. about the increasing of evaporating front depth. However, the evaporation-condensation mechanism was not concerned in their discussion. In the present author's opinion, the reducing of the evaporation process power is an important effect, but not the unique reason. The other reason for the increasing of the evaporating front depth, is the temporary condensing clusters. It has been confirmed in the present simulation that the evaporation-condensation mechanism takes place during the drying process. As have been shown in Fig. 5-33 and 5-34, the total cluster number and the condensing cluster number increase with the receding evaporating

front. The condensing clusters can not be eliminated in the network until they become evaporating ones. As a result, the evaporating front depth increase.

The place of condensing clusters in the network during the simulation process are given in Fig. 5-35 and 36. In these figures, the evaporating clusters are printed black and the condensing clusters red. One can see that the condensing clusters are always at the place where is surrounded by other clusters. There is no permanent condensing cluster in the network during the simulation, i.e., the cluster could be a condensing one in one drying time interval and become evaporating one in next drying time interval. As have been observed, the condensing clusters exist only when the place is surrounded by other evaporating clusters. Once after the place is open due to the elimination of some evaporating clusters around it, the condensing clusters change to be evaporating clusters and can be eliminated as time advances.

It should be reminded that gravity has not been taken into account in the present drying model. Generally, gravity becomes negligible when the pore size is small enough, that is, the capillary force is large enough comparing to the gravity force difference caused by the pores location in the network. In fact, the height of network used here is only 1.2 cm and the pore size range is 39 ~ 250 μm. The gravity force is not important for simulation.

In the paper of Masmoudi et al., the stability of the invasion front was discussed in terms of gravity by considering only the typical pore size (Bond number). It should be noted that the pore size distribution range has a great influence on the stability of evaporating front. Generally speaking, for a network with a narrow pore size range, the evaporating front should be more stable due to the small difference of capillary force. As an extreme example, the evaporating front should be flat for a network with an uniform pore size.

The experimental results of Masmoudi et al. (1992) were obtained using a network containing about 10000 ducts with seven classes of width (from 0.1 ~ 0.6 mm) distributed at random; gravity is not negligible for these pores. The network used in the present simulation has ten classes of pore and throat size. For a real porous medium, however, the pore size distribution range is quite large. The material used to obtain the pore size distribution in the present work, for example, has a pore size ranging from 5.0 to 170 μm. It can be expected that the evaporating front in a real porous medium should be wider than those observed here.

S = 0.90

S = 0.80

S = 0.70

S = 0.60

S = 0.50

S = 0.40

S = 0.30

S = 0.20

S = 0.10

S = 0.90

S = 0.80

S = 0.70

S = 0.60

S = 0.50

S = 0.40
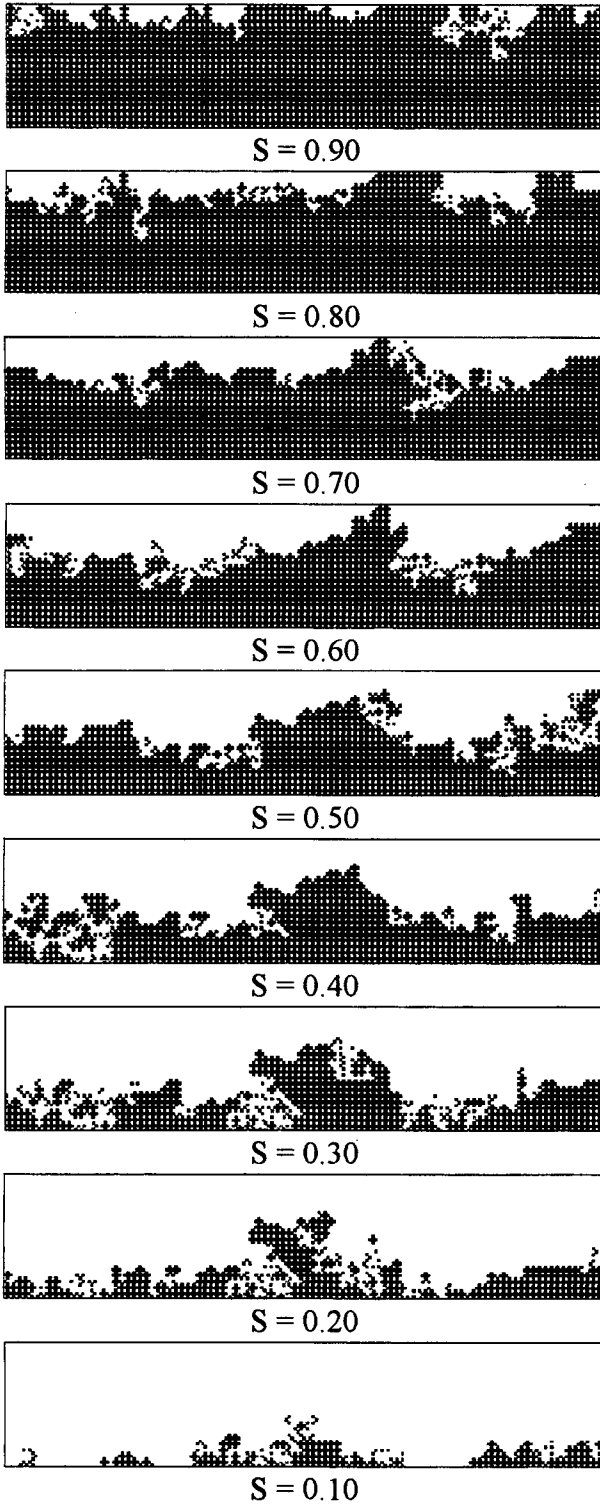
S = 0.30

S = 0.20

S = 0.10

Fig. 5-35   Place of condensing clusters
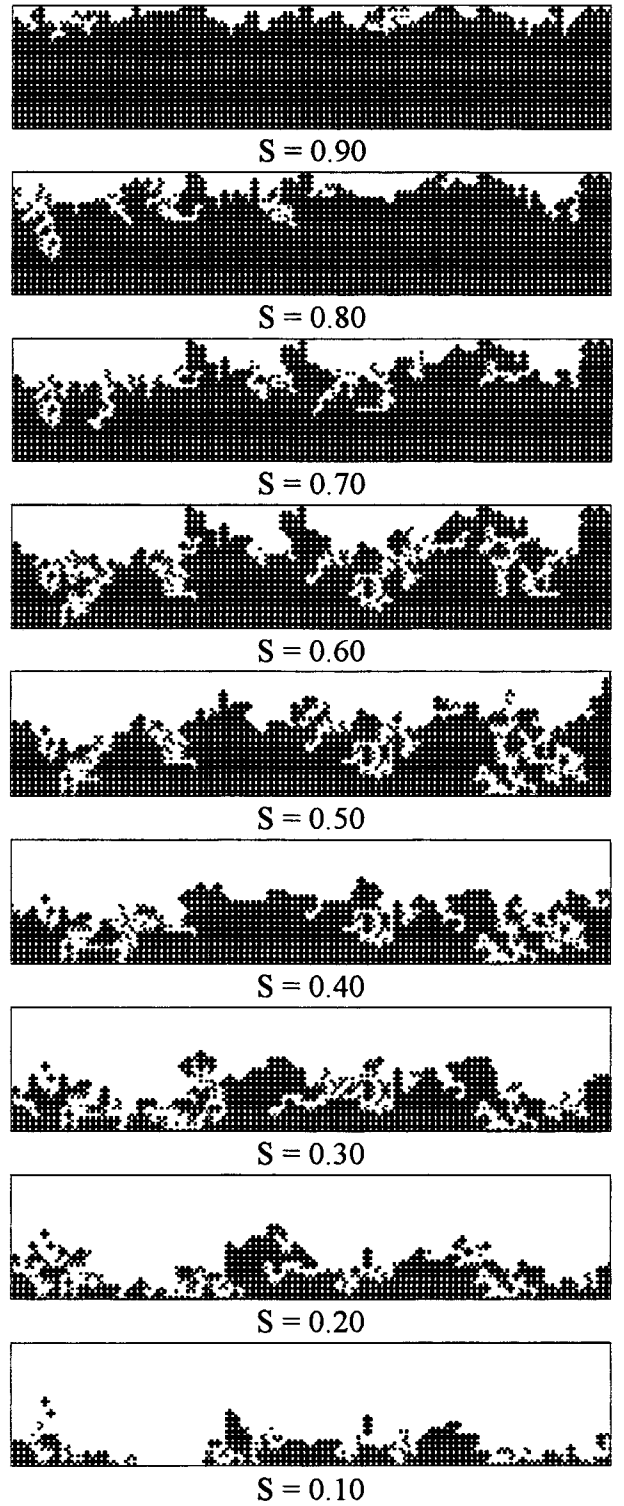in network 2 during the drying simulation

Fig. 5-36   Place of condensing clusters
in network 3 during the drying simulation

5.4   INFLUENCE OF THE EXTERNAL AIR FLOW

The complete configuration sketched in Fig. 2-1 will now be considered. In practice, the porous medium is dried by a hot dry (or moist) air flow. Under this circumstance, an external dry air flow is imposed on the surface of the porous medium. Generally speaking, the external flow should increase the mass transfer coefficient at the interface between the external flow and the porous medium. However, as have been mentioned before in chapter 2, the drying behavior at the interface between the external flow and the porous medium is still unclear. It is interesting, therefore, to study the influence of the external flow on the mass transfer at the interface.
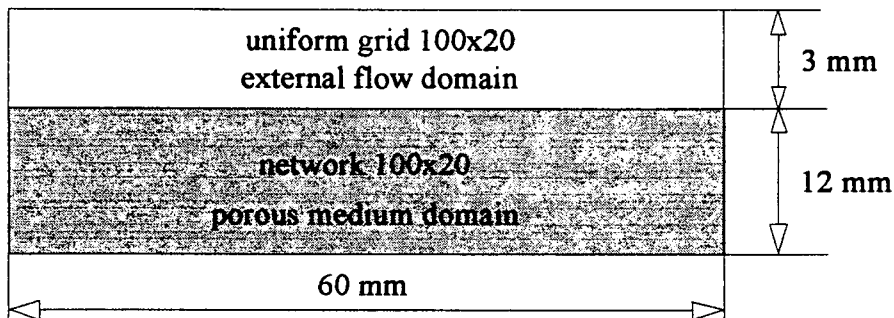
Fig. 5-37   Solution domain and the geometrical size

The solution domain to be used in the numerical calculation is presented in Fig. 5-37. The geometrical size of the domain is as shown in the figure. The network used to represent the porous medium is the same of section 5.2 and 5.3 (100x20). To facilitate the coupling of the external flow with the porous medium, an uniform 100x20 grid is used for the external flow domain. Thus, each throat is coupled with one control volume at the interface. Both network and external flow grids have an unity thickness. It is not necessary, therefore, to convert the throat surface at the interface. It should be pointed out that the main focus here is not on the numerical accuracy of the phenomenon that is being modeled. Instead a general description of the drying kinetics is being sought. For a more representative simulation in which quantitative agreement with experiments is needed a more refined grid is required.

The simulation conditions for porous medium are the same of the last section. The inlet velocity of the external flow is assumed to be uniform and the inlet mass fraction of alcohol vapor is zero. The velocity field is obtained by solving the differential equations (2-1) and (2-2) under the assumption of no-slip condition at the interface. Considering that the evaporation rate at the interface is not very high, the obtained velocity field is used for the whole simulation without

updating it, that is, the quantity of the evaporated alcohol vapor from the porous medium is assumed to be small enough to not influence the velocity field. This can save the computation time significantly and, as explored by Prata and Sparrow (1987) in a somehow similar problem, has a negligible effect on both the flow field and the evaporation rate. After the velocity field is calculated, the moisture field is obtained by solving the differential equation (2-3) with the prescribed evaporation rate at the interface. The moisture field is updated for each drying time interval with the updated evaporation rate at the interface. The procedure of the alcohol removal from the network is the same of that described in last section. The drying simulation is made on network 1 for the inlet velocity of 1 ~ 50 m/s, and for the aforegiven parameters the flow is laminar.

5.4.1 Drying Kinetics

The drying kinetics curves for inlet velocity of 1 ~ 50 m/s is presented in Fig. 5-38. One can see that the difference of drying time caused by the external flow is small. The difference of the total drying time is not larger than 10%. Just as have been observed in the results of the phase distribution, the drying curves begin to deviate one from the other at the very beginning of drying until S=0.60. The maximum difference of drying time can reach 50% (between U=1.0 and 50.0 m/s). After the saturation of S=0.60, the deviation stops developing and the drying time curves for the various inlet velocities become almost the same.

It is surprising to observe that the relationship between the drying time and the inlet velocity is not monotonic. The network dries fastest when the inlet velocity is U=10.0 m/s and the total drying time for U=5.0 m/s is larger than that for U=3.0 m/s. This is, of course, unexpected from the point of view of the continuum approach. One can note that the drying curves become nearly parallel while the saturation equals to about 0.60. To have a better look at the beginning of the drying process, Figs. 5-39 ,40 and 41 were prepared.

It is observed from Figs. 5-39 to 41 that for S > 0.7, the drying time decreases as the inlet velocity increases, as expected. This evidences the external flow influence on the drying kinetics during this period. Also noted from the figures is that the influence of external flow decreases with increasing inlet velocity. That is, the impact on drying of an increase of the inlet velocity diminishes as the inlet velocity increases. One can see that near the S=0.65, drying is accelerated for U=7.0 and 10.0 m/s and the corresponding curves for these inlet velocities cross the curve for U=50.0 m/s. In especial, the curve for U=7.0 m/s crosses the curve for U=50.0 m/s four times. It becomes to dry more quickly than U=50.0 m/s near S=0.65 and back to dry more slowly near S=0.50. It becomes to dry faster again at S=0.25 and to dry slower near S=0.20. Also worth

noting is that close to S=0.25 the curve for 5.0 m/s that was yielding drying times smaller than those of U=3.0 m/s crosses it and starts to dry more slowly. Those findings will be discussed with the results for the evaporating area.
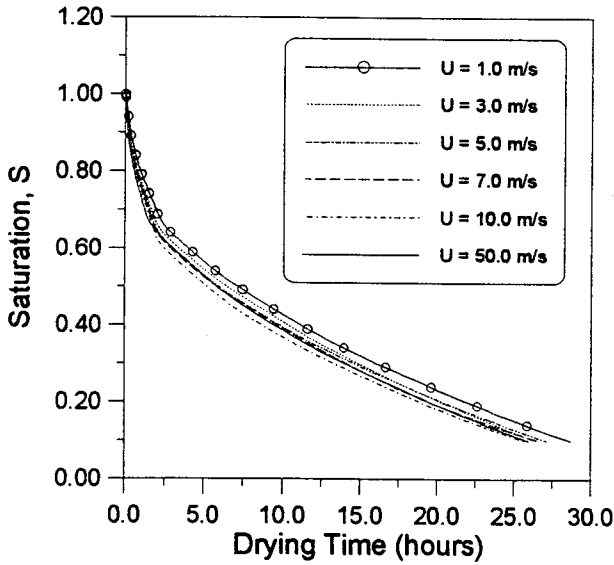

Fig 5-38   Drying curves for various
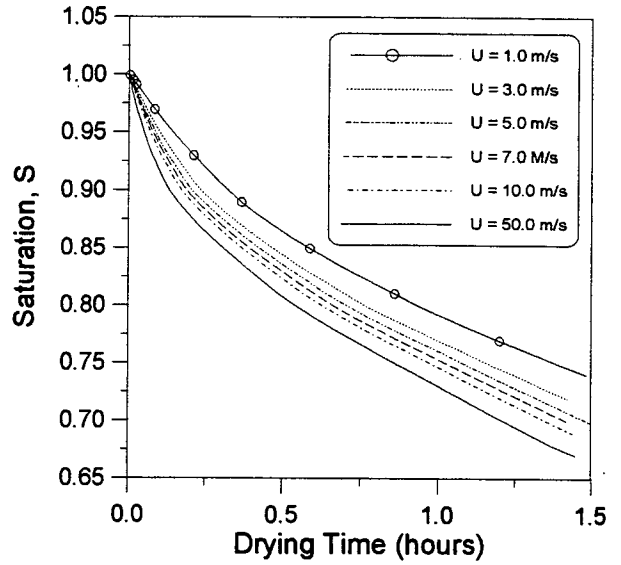inlet velocity of external flow

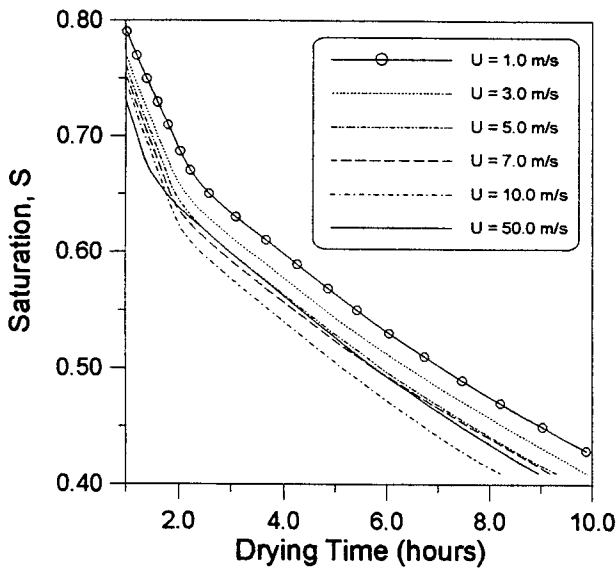Fig. 5-39   Drying curves of beginning part
for various inlet velocity

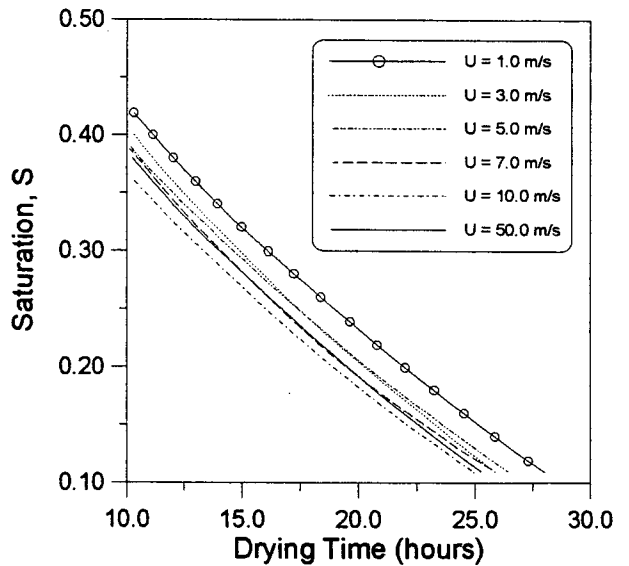Fig. 5-40   Drying curves of middle part
for various inlet velocity

Fig. 5-41   Drying curves of latter part
for various inlet velocity

5.4.2 Drying Rate

The drying rate curves shown in Fig. 5-42 is, as also presented in the last section, the drying time derivative of saturation (dS/dt) *versus* saturation. It can been found that the difference of drying rate caused by the external flow velocity occurs before saturation reaches the 0.60 value. The maximum difference on the drying rate takes place at the initial of drying. This difference decreases with the reducing saturation. A second drop in the drying rate can been observed for all inlet velocities investigated. From Fig. 5-43, one can find that the second fall in drying rate occurs between S=0.70 and 0.60. As have been discussed in the last section, this point indicates the moment that the top surface becomes totally dry. The second drop takes place at smaller saturation for U=10.0 m/s than for the others velocities. This coincides with the drying kinetics where the network dries most quickly for U=10.0 m/s than for the others velocities. After the second fall, the drying rate for all cases tend to be the same. This indicates that the external flow has influence on the drying kinetics only when the top surface is totally or partially wetted. For a dry surface the internal vapor diffusion resistance overcomes the external convective resistance, and becomes the dominant mechanism for drying.
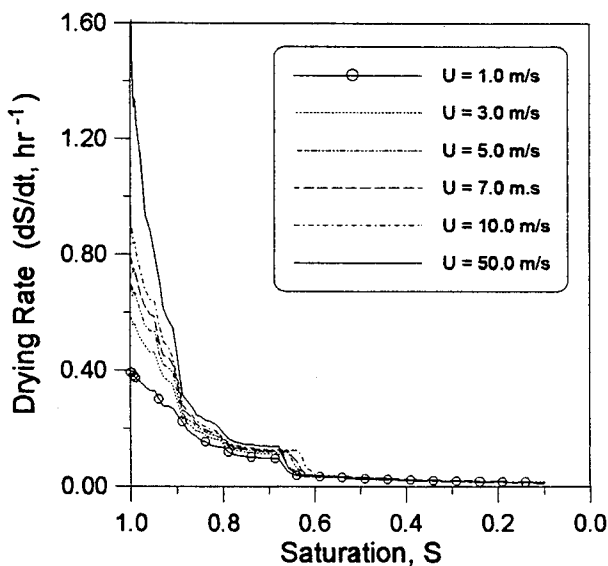
Fig. 5-42   Drying rate curves for various
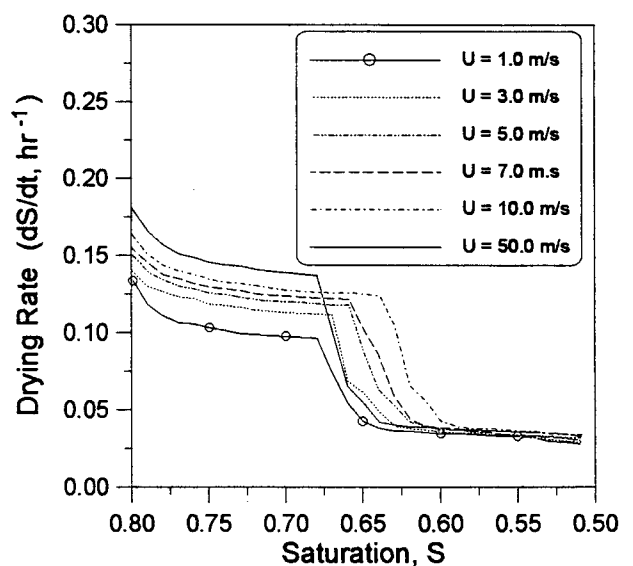inlet velocity of external flow

Fig. 5-43   Drying rate curves for various
inlet velocity of external flow

5.4.3 Evaporating Area in Network

The evaporating area inside the network, from which the information of evaporating front can be obtained, is plotted in Fig. 5-44. It is found that the evaporating area for all inlet velocities investigated has the same overall pattern. The evaporating area at the very beginning is the same for all inlet velocities since this area is exactly the wet area when the top surface is saturated. As the same network is used for all velocities, the wet area of top surface is the same. The evaporating area increase with the decreasing saturation until the first peak is reached. It can be also seen that the peak value and the corresponding saturation peak value is different for various inlet velocities. The evaporating area decreases after this point since all the evaporating front begin to recede from the top surface, as a result, the evaporating front becomes flatter. The first peak point corresponds to the moment that the top surface becomes totally dry. The second peak of evaporating area is believed to be caused by the formation of more trapped clusters in the network. The evaporating area during the simulation for each inlet velocity is different. This suggests an influence of the inlet velocity on the phase distribution in the network. Attention will be returned to this matter in section 5.4.6.

A careful examination of Fig. 5-44 indicates that the curve for U=7.0 m/s crosses the curve for U=50.0 m/s four times, just as have been observed in Fig. 5-38. The first peak for U=7.0 m/s occurs later and is higher than U=50.0 m/s, corresponding to the first cross in which U=7.0 m/s becomes to dry more quickly than U=50.0 m/s. The second peak takes place on the curve for U=50.0 m/s during S=0.60 ~ 0.40 resulting in a faster drying while no peak is observed on the curve for U=7.0 m/s. The evaporating area for U=7.0 m/s becomes higher than that for U=50.0 m/s near S=0.40 and lower again near S=0.20, corresponding to the other two cross of the drying curves, as mentioned before. It is worth noting that although the evaporating area for U=7.0 m/s is not much higher than that for U=50.0 m/s, considering the large inlet velocity difference, the case for U=7.0 m/s succeeds in drying faster than U=50.0 m/s during S=0.40 ~ 0.20, indicating that the external flow influence is weak during the latter drying period.

The variation of the wet area percentage of the top surface with the saturation is presented in Fig. 5-45 to show the moment that the top surface becomes totally dried. It can be seen that the variation of wet area percentage of the top surface with the saturation is almost the same for all inlet velocities. The top surface dries quickly at the very beginning and only 5.0% of top surface is wetted when S=0.90. The top surface approximately maintains this percentage of wet area until S=0.65. Recalling what have been observed on the drying rate curves, the drying rate decreases sharply before S > 0.90 and then becomes almost constant until the second drop. To show more clearly how the wet area percentage at the top surface approaches zero, Fig. 5-46 was prepared. It should be noted that the curve for U=50.0 m/s is overlapped on the curve of U=1.0 m/s. It can

be seen that the sequence that the top surface becomes totally dry coincides with the sequence of second drop in drying rate in Fig. 5-43 and the first peak point of evaporating area in Fig. 5-44.
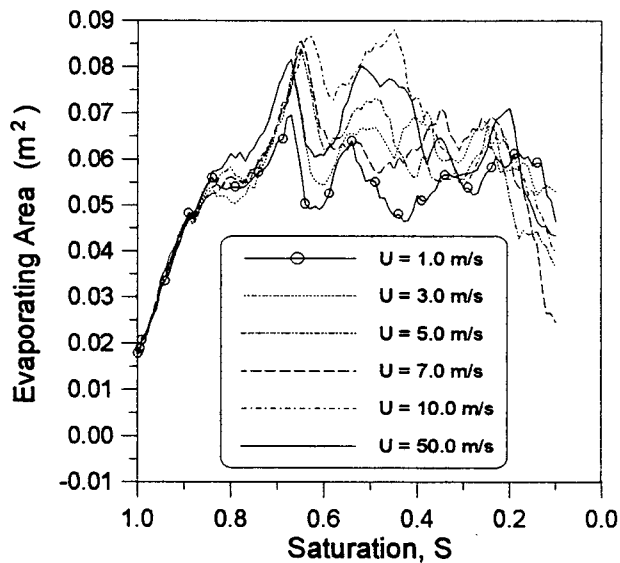

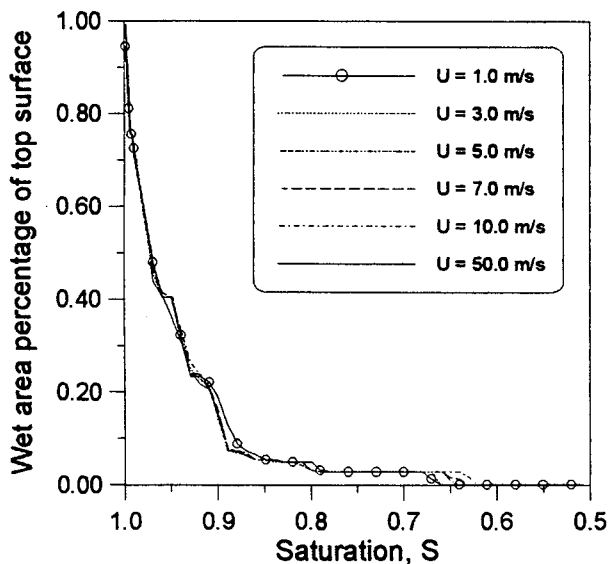Fig. 5-44   Evaporating area in network for various inlet velocity

Fig. 5-45   Wet area percentage of top surface
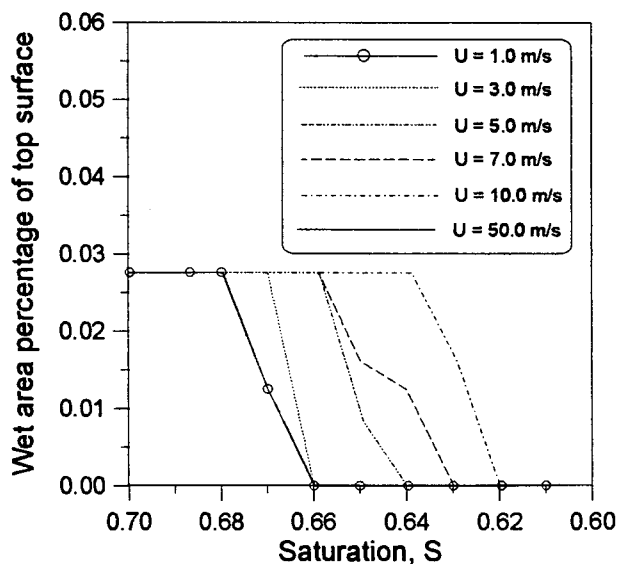*versus* saturation for various inlet velocity

Fig. 5-46   Wet area percentage of top surface
versus saturation for various inlet velocity

5.4.4 Local Evaporation Rate at the Top Surface

As have been pointed out in the last section, the drying rate curves presented in Figs. 5-42 and 43 give the average value of the mass fluxes at the top surface, and one cannot have an idea of the local mass fluxes from those figures. The local mass fluxes at the top surface during the drying process are important in studying the influence of dry patches on the drying kinetics, and in exploring the influence of the surface saturation on the mass transfer coefficient. In applying the continuum approach to predict drying of unsaturated porous medium much debate has appeared in the literature concerning the variation of the local Sherwood number on the top surface and the validity of the analogy between heat and mass transfer (see for example, Lee et al., 1992, Rogers and Kaviany, 1990, Tao and Kaviany, 1989 and Chen and Pei, 1989). To shed some light into this issue, the local mass fluxes at the top surface for some cases at certain saturations are presented in Fig. 5-47 ~ 49. The inlet velocity of the external flow is 1, 5 and 10 m/s, respectively.

From these figures, one can see the influence of the external flow on the mass fluxes along the top surface. The local mass fluxes profiles are different from those presented in Fig. 5-9 and 10, where the mass fraction of alcohol vapor at the top surface was taken to be zero, and as a result, the local mass fluxes of the wetted interface was uniform. With an external flow over the surface of the porous medium, the local mass fluxes of the wetted top surface decrease downstream. This mass fluxes profile is expected and follows the typical mass transfer pattern observed from a boundary layer over a flat surface (Kays and Crawford, 1993). The mass fraction of alcohol vapor at the entrance of the external flow domain is zero, and the evaporation rate at the wetted surface is highest. The evaporated alcohol vapor is carried downstream in the domain resulting in an alcohol laden air along the top surface, decreasing the evaporating rate. As can been observed from the figures the boundary layer effect has virtually no influence on the evaporation flux when the top surface is no longer wet. Once again, the difference of mass fluxes for wetted and dry top surface is very large.

After the top surface have been dried, the external flow has a weak influence on the mass fluxes profile. Contrary to the wetted surface, the local mass fluxes downstream can be higher than that upstream. This is so because for a dry top surface the mass flux is more affected by the resistance to vapor diffusion inside the network, as explored before.

A careful examination of the phase distribution maps and the corresponding local mass fluxes at the top surface indicate the influence of the external flow, in spite of its weakness, after the top surface have been dried. From Fig. 5-43, one can find that, at the latter periods of drying, the mass flux upstream can be higher than that downstream, considering the large distance between the evaporating front and the top surface.
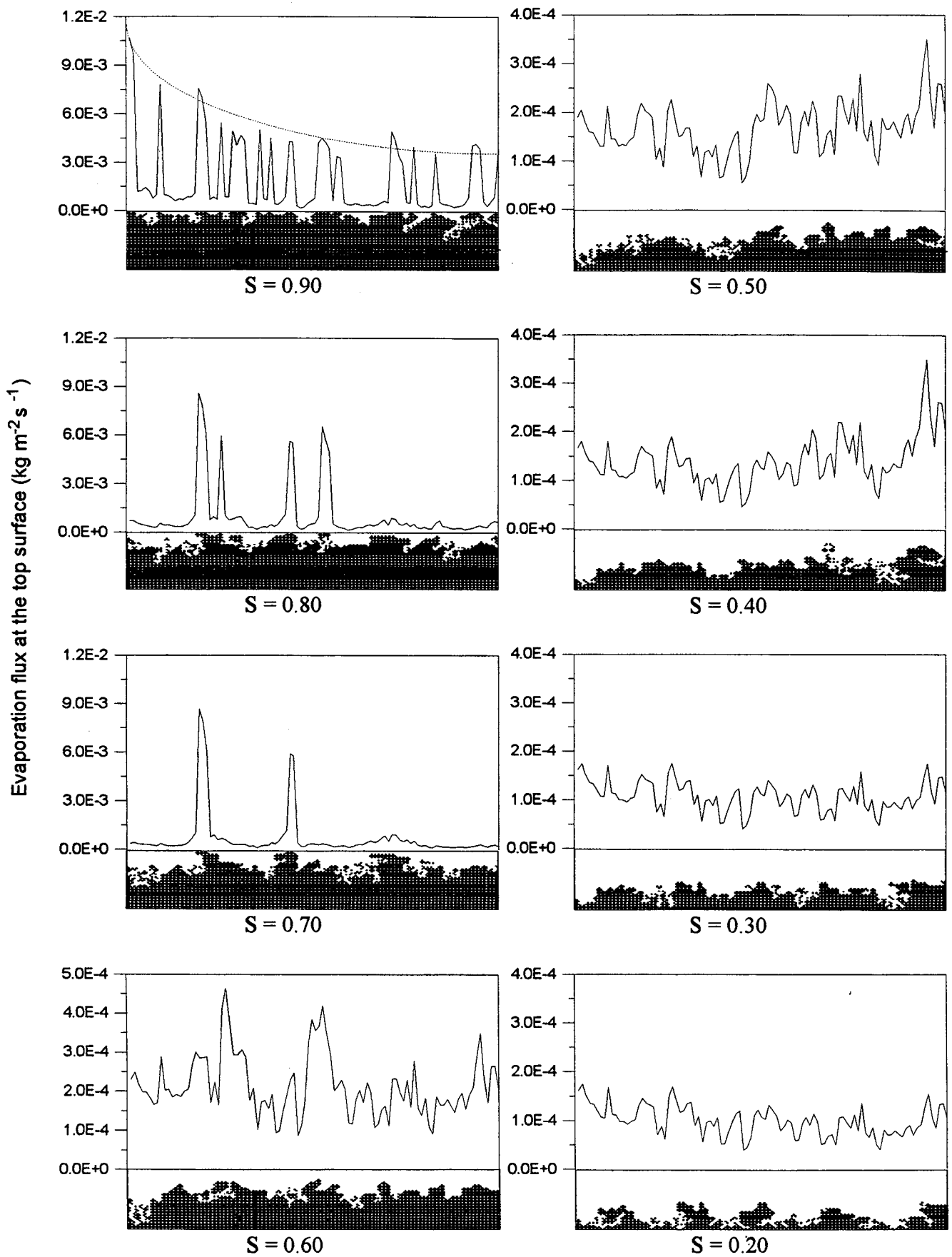
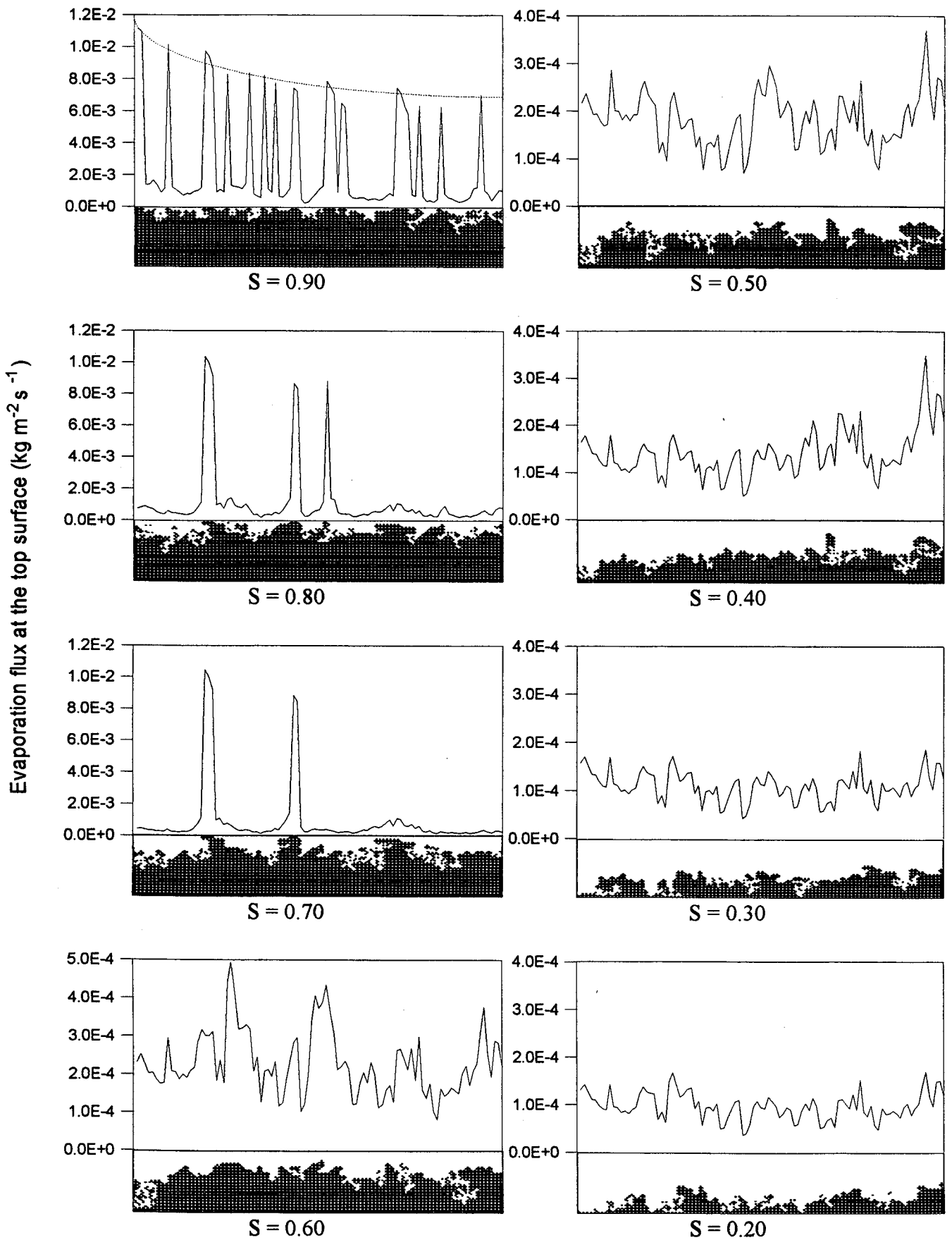Fig. 5-47   Local mass flux profiles at the top surface for U=1.0 m/s

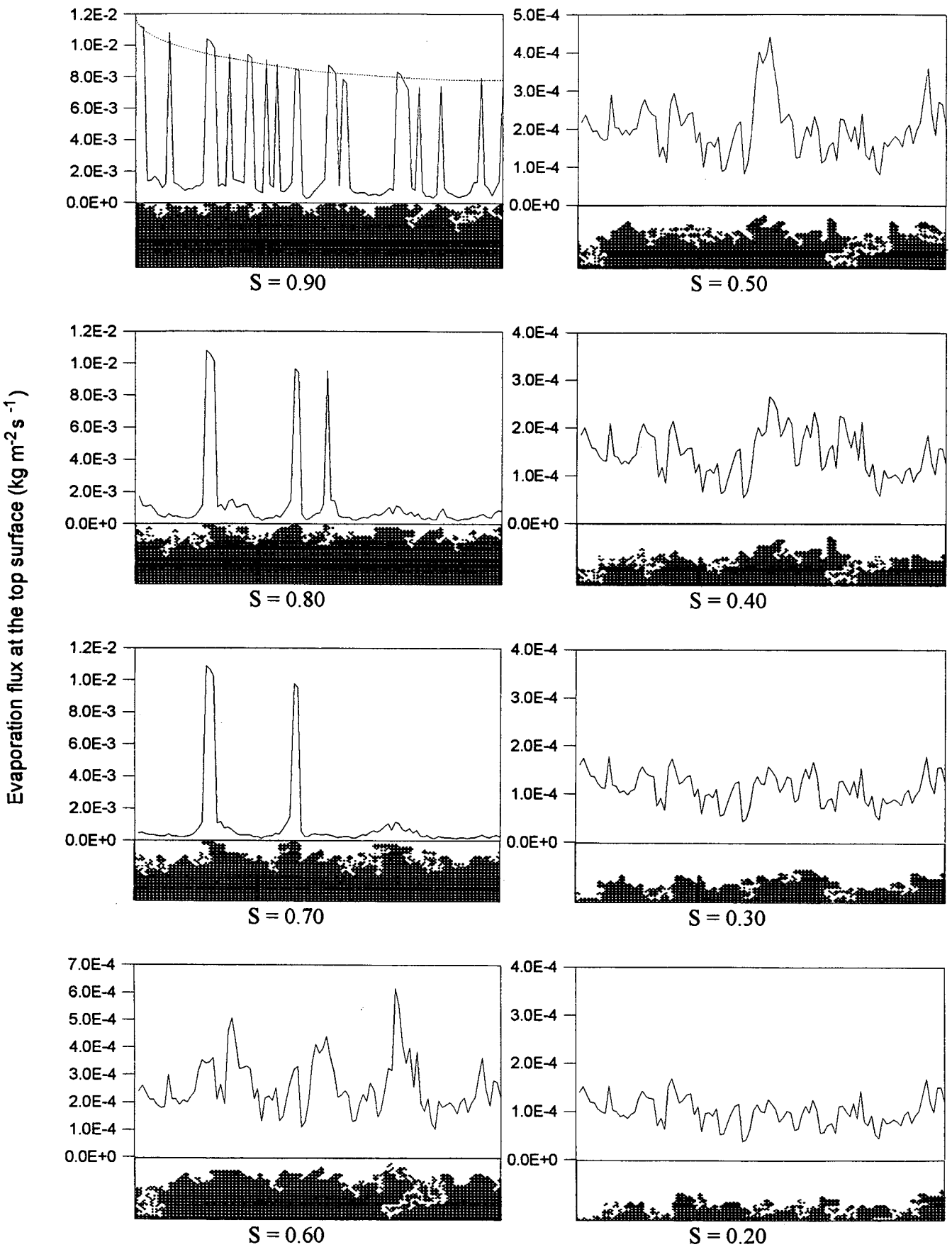Fig. 5-48   Local mass flux profiles at the top surface for U=5.0 m/s

Fig. 5-49   Local mass flux profiles at the top surface for U=10.0 m/s

Other interesting finding extracted from Fig. 5-47 ~ 49 is that the mass fluxes profiles at the top surface for latter drying periods (S < 0.30) are almost the same for the three different inlet velocities, even though the evaporating fronts in the network have different shapes. As have been discussed before, the evaporating front in the network during the drying process is far from being flat. This heterogeneity in the evaporating front has a strong influence on the mass fluxes at the top surface while the top surface is totally or partially wet. This influence reduces with the receding evaporating front from top surface. From what are observed here, it seems that the heterogeneity of evaporating front is no longer important for latter drying periods. Recalling that the present network has only a depth of 1.2 cm, this finding suggests that from the point of view of the validity of the continuum approach, the stability of evaporating front is not so important as one might think, once the top surface has been totally dried.

At high saturation, comparing the mass fluxes profiles at the top surface for different inlet velocities, one can find that the difference in the mass fluxes caused by the external flow decrease with increasing inlet velocity, as explored in Fig. 5-50. Again this is an expected result and follows from the boundary layer theory.
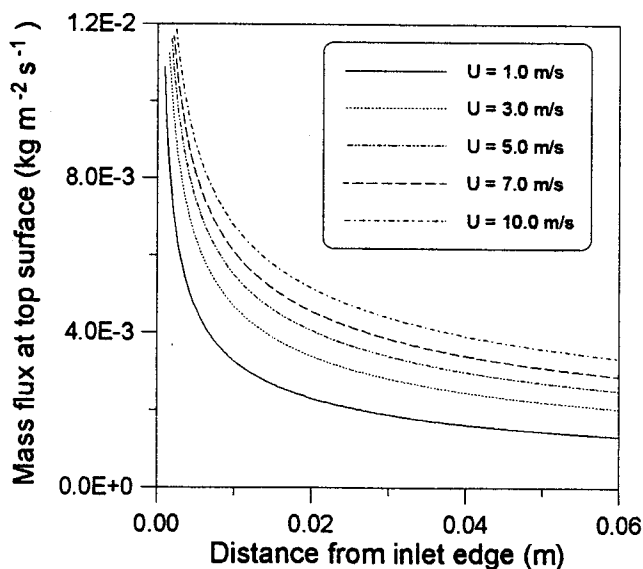

Fig. 5-50   Mass fluxes profile for various inlet velocity at S ≈ 1.0

5.4.5 Local Mass Transfer Coefficient at Top Surface

As have been discussed by Lee et al. (1992), the convective mass transfer coefficient calculated from the analogy between heat and mass transfer holds only if the top surface is completely covered with liquid resulting in the saturated vapor conditions at all points on the surface. If the surface is partially wet, then the average vapor pressure at the surface should be less than the saturated value. Thus, it is interesting to explore the near surface physics using the present drying model. For this purpose, the local convective mass transfer coefficient at the surface for $S \approx 1.0$ are presented in Fig. 5-51 ~ 55 for inlet velocities of 1.0 ~ 10.0 m/s and compared with the convective mass transfer coefficient calculated from the correlation of boundary layer theory.

In each figure six set of results are presented. The solid line is obtained from the boundary layer theory; large slashed line represents the numerical results assuming that the top surface is totally covered with liquid; triangles are numerical results for actual situation as seen in Figs. 3-7 to 3-9, that is, part of the top surface is wetted and part is solid; slash-dotted line is curve fitting for the triangles; circles are numerical results for actual situation averaged over the surface of each control volume; small slashed line is curve fitting for the circles. More details about each one of the set of results will be provided in the next paragraphs.

The mass transfer coefficient in Fig. 5-51 ~ 55 is defined as

$$k = \frac{J_A}{\rho_{vs} - \rho_\infty}$$

where k is the convective mass transfer coefficient, J_A is the vapor flux density, ρ_{vs} is the saturated vapor density and ρ_∞ is the inlet vapor density.

To show the validity of the present numerical results, the local mass transfer coefficient calculated using the 100x20 uniform grid with assumption of the saturated vapor density at all points on the top surface (total wet surface) are also presented in Fig. 5-51 ~ 55 and compared with that calculated from the correlation of boundary layer theory. According to boundary layer theory, the local mass transfer coefficient for laminar flow can be calculated using the following correlation

$$Sh_x = 0.332 \, Re_x^{1/2} \, Sc^{1/3} \qquad \text{for Sc>1} \qquad (5-1)$$

where Sh_x is the local Sherwood number, (kx/D), Re_x is the local Reynolds number, $(\rho U_\infty x/\mu)$, and Sc is the Schmit number, (v/D).

It can be found from these figures that the deviation between numerical and analytical results concentrates near the upstream and increases with the inlet velocity. This is so because, as have been mentioned at the beginning of this section, the grid used for external flow is not refined enough for describing the vapor density derivative near the inlet edge where the boundary layer is very thin. With a higher inlet velocity, the boundary layer near the inlet edge is thinner resulting in a larger deviation between the numerical and analytical results. However, the numerical results are reasonable for a qualitative analysis.

It can be also seen that the local mass transfer coefficients calculated numerically for the actual situation (S=1.0) under all investigated inlet velocities are higher than that calculated from the boundary layer theory. It is an expected result since the top surface of network is not totally covered by liquid even when the saturation at the top surface is equal to 1.0. The wet surface is about 30% of the total surface at S=1.0. Clearly, the saturation conditions can be only used on wet surface and at the solid surface the vapor pressure is practically zero. Comparing with the totally wet surface, less vapor enter into the external flow resulting in a lower mass fraction in the boundary layer and, consequently, a higher local convective mass transfer coefficient. The local mass transfer coefficient presented in Fig. 5-51 ~ 55 for the actual situation is the local value for wet surface. In other words, the area for mass transfer considered here is not the total top surface, but the sectional area of throats on the top surface. Recalling the Fig. 3-9 that shows the coupling of the porous medium with the external flow, the local mass transfer coefficient for wet surface is obtained using the mass flux density at the wet surface, not the average value for the total surface.

The local mass transfer coefficient calculated from average mass flux density for actual situation shows a very interesting behavior. One can note from Fig. 5-51 ~ 55 that these local mass transfer coefficients agree well with the correlation value for all investigated inlet velocities. Again, the deviation occurs only near the inlet edge and increases with increasing inlet velocity. It seems that the local mass transfer coefficient obtained from analogy can be used at the very beginning of the drying even though the top surface of porous medium is not totally covered with liquid. It should be pointed out that the wet surface is somehow distributed periodically on the top surface of network and is in accord with the point of view of the continuum approach. As the evaporating front receding from top surface, of course, the wet patches are no longer distributed periodically on top surface and, as have been shown in Fig. 5-47 ~ 49, the local mass transfer coefficient will be quite different from that obtained using the correlation.
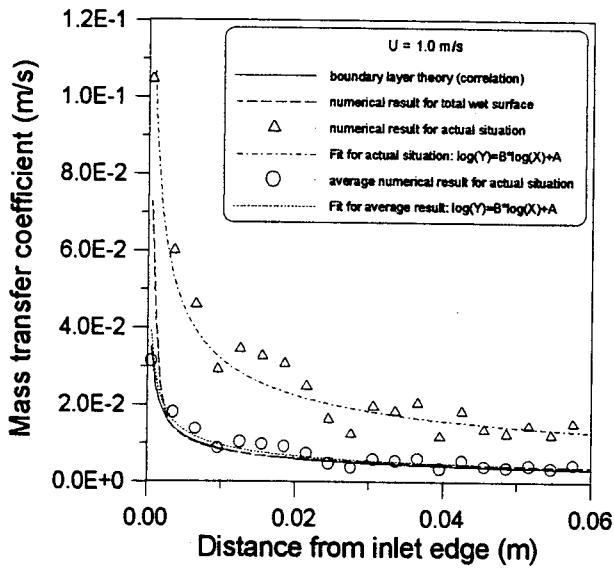
Fig. 5-51   Local mass transfer coefficient
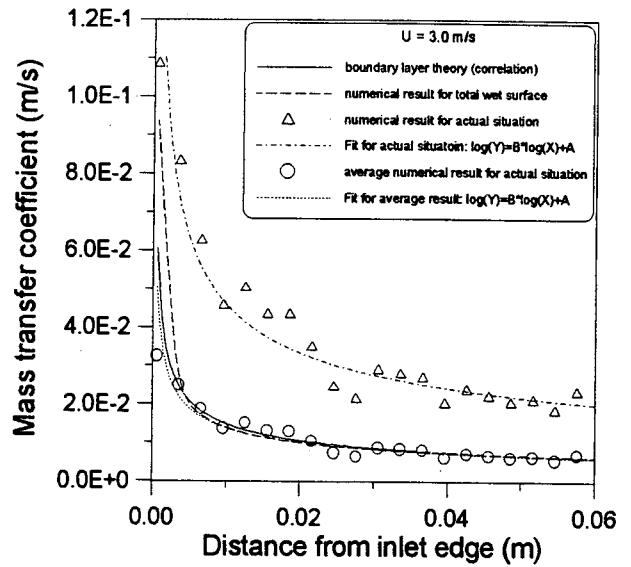at the top surface for U=1.0 m/s

Fig. 5-52   Local mass transfer coefficient
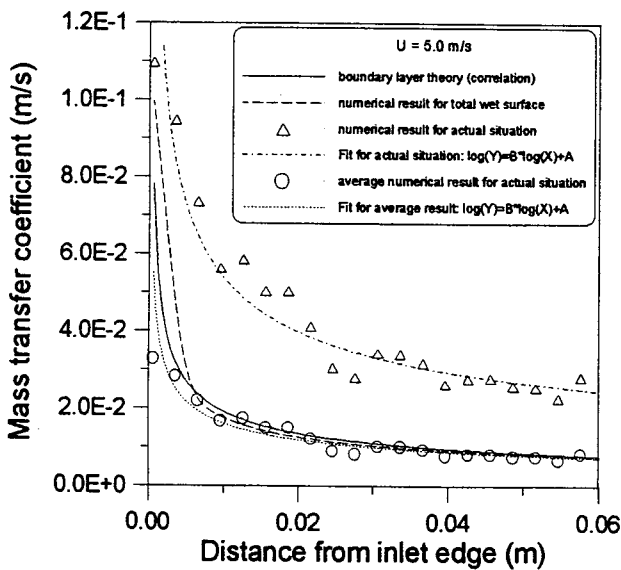at the top surface for U=3.0 m/s

Fig. 5-53   Local mass transfer coefficient
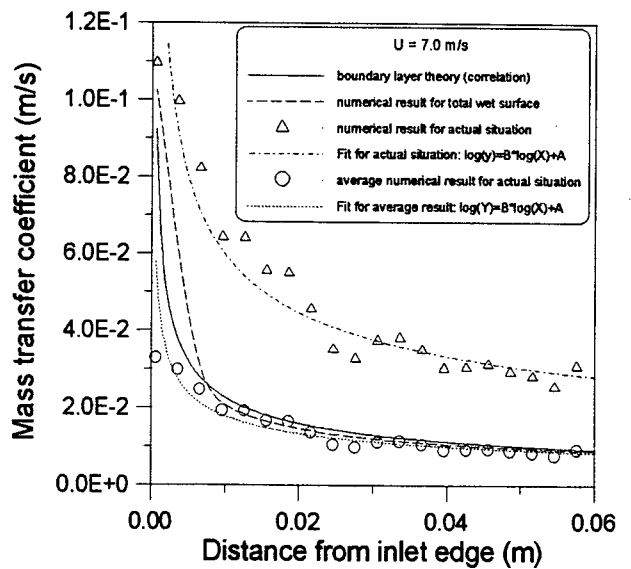at the top surface for U=5.0 m/s

Fig. 5-54   Local mass transfer coefficient
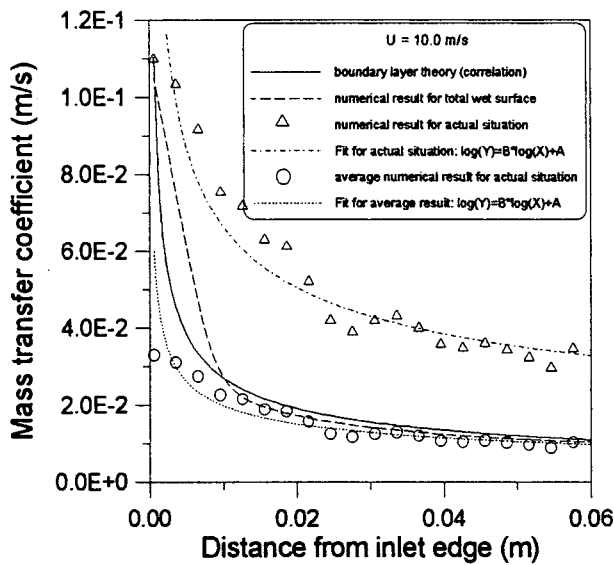at the top surface for U=7.0 m/s

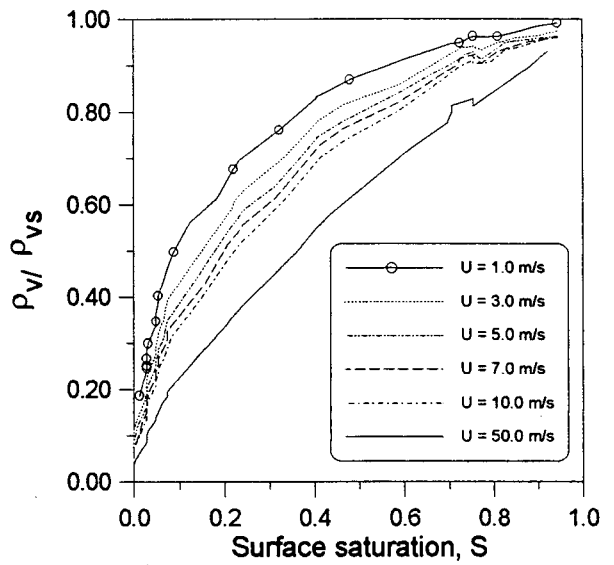Fig. 5-55 Local mass transfer coefficient
at the top surface for U=10.0 m/s

Fig. 5-56 Calculated vapor density
as a function of surface saturation

The variation of the vapor density at the top surface with the surface saturation for various inlet velocities is presented in Fig. 5-56. The vapor density is back calculated using the convective mass transfer coefficient obtained under the saturated conditions at the top surface. One can find that the vapor density at the top surface is less than the saturated value for all surface saturation. This is in accord with the observation of Lee et al. (1992) in their experiment results. Also noting is that the vapor density for the same surface saturation decreases with an increasing inlet velocity.

5.4.6 Moisture Field and Boundary Layer

The boundary layer for the alcohol vapor mass fraction during the drying simulation are presented in Fig. 5-57 ~ 59 for some cases. The numbers in the figures are not the mass fraction but the relative humidity value of the alcohol vapor (P/P_0) due to the small values of the mass fraction. The size of external domain is 60 x 3 mm, and in the figures presented here the y-direction is amplified to show the boundary layer more clearly.

From Fig. 5-57, one can see that the boundary layer thickness decreases as drying proceeds. The mass fraction near the top surface decreases rapidly with the receding evaporating front during the early drying period. After the interface is totally dried, the mass fraction near the

top surface reduce to a very low value, and the boundary layer thickness remains almost unchanged.

Some evaporation focuses are observed when the top surface is partially wetted at the early drying period. As have been discussed before, the mass flux is very affected whether the top surface is dry or wet. This difference can be of the order of ten times. The evaporated alcohol vapor goes into the external flow mainly from the wet patches. When the external flow velocity is not very high, the alcohol vapor evaporated from the wet patches is not carried away by convection quickly enough, and the mass fraction near these wet patches become higher than that of the adjacent regions, yielding a mass fraction gradient along the top surface that can be in the downstream or upstream direction, depending on the mass fluxes and on the velocity of external flow.

Comparing Figs. 5-57, 58 and 59, one can see that the thickness of the boundary layer decreases with increasing inlet velocities due to the stronger convection. The boundary layer thickness for U=5.0 m/s, for example, is just a half of that for U=1.0 m/s. The thickness of the boundary layer for U=10.0 m/s, however, is only a little smaller than that for U=5.0 m/s. The same behavior is observed for the mass fraction near the top surface, which is reduced from about 0.481 to 0.301 while the inlet velocity increases from 1.0 to 5.0 m/s. The top surface mass fraction only decreases from 0.301 to 0.251 as the external flow velocity increases from 5.0 to 10.0 m/s, indicating that the external flow influence decrease with increasing inlet velocity.

It can be also noted that the evaporation focuses observed at low inlet velocity is no longer so obvious when the inlet velocity is relatively high. This is so because the alcohol vapor evaporated from the wet patches (focuses for low inlet velocity case) can be carried downstream by convective for the higher inlet velocities, and the vapor evaporated from wet patches, therefore, can not be accumulated to form the focuses of alcohol vapor.

The boundary layers for case of U=1.0 m/s are drawn in Fig. 5-60 in color to show more clearly the evaporation focuses at the top surface. One can see that there are some high alcohol vapor concentration regions at the top surface (red areas) while the surface is partially wetted. These focuses of alcohol vapor are coincident with the wetted surface where the evaporation fluxes are very high. After the top surface is totally dried, no focus is observed at the interface.

It should be noted that different scales for the mass fraction were employed for the various saturation in drawing Fig. 5-60. The same color indicates different mass fraction value in different drying stages. One can refer to Fig. 5-57 to have an idea about the mass fraction value during the drying process.

S = 0.90

S = 0.40

S = 0.80

S = 0.30

S = 0.70

S = 0.20

S = 0.60

S = 0.10

S = 0.50
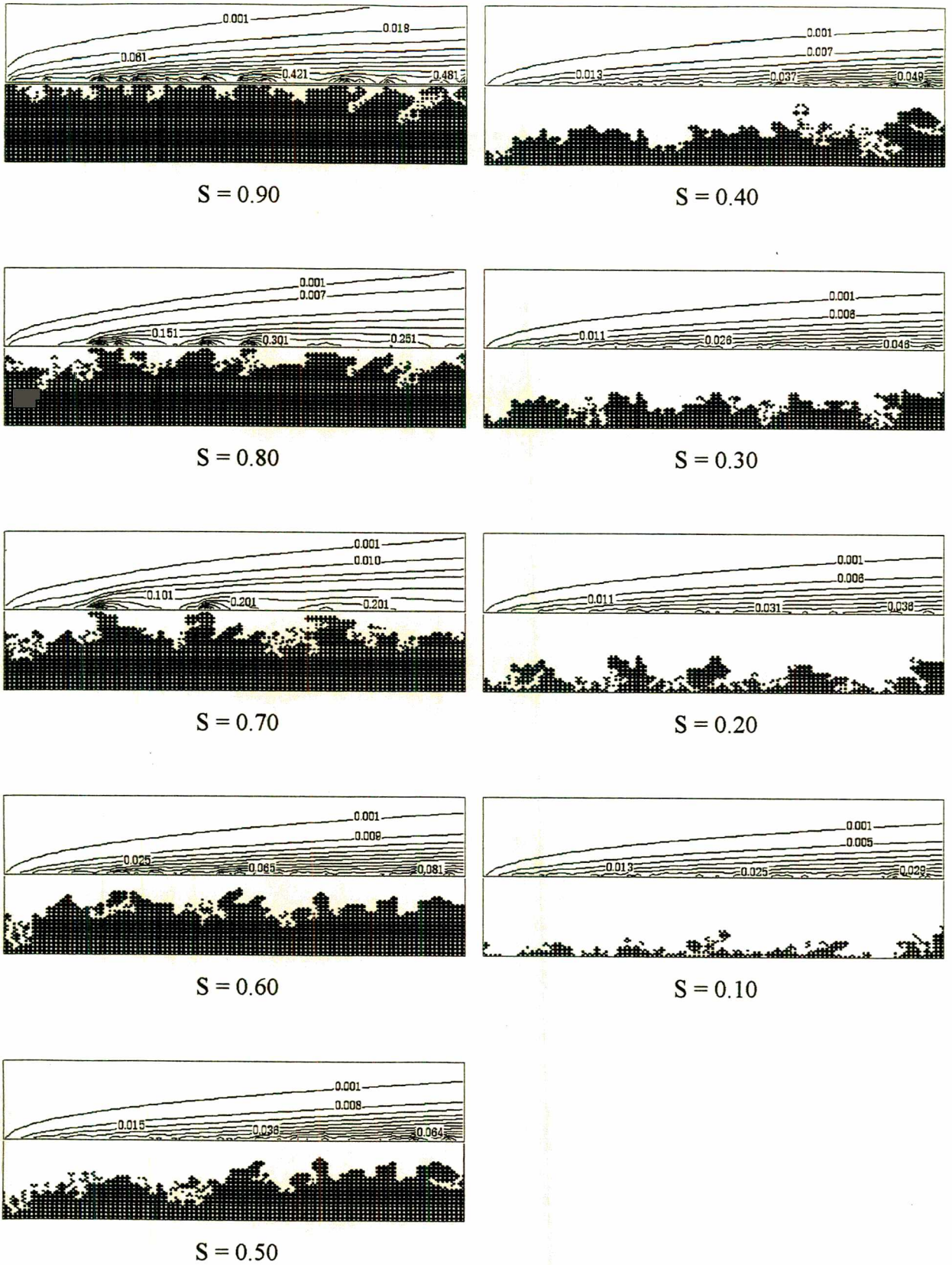
Fig. 5-57   Mass fraction boundary layer for U=1.0 m/s

S = 0.90

S = 0.40

S = 0.80

S = 0.30

S = 0.70

S = 0.20

S = 0.60

S = 0.10

S = 0.50
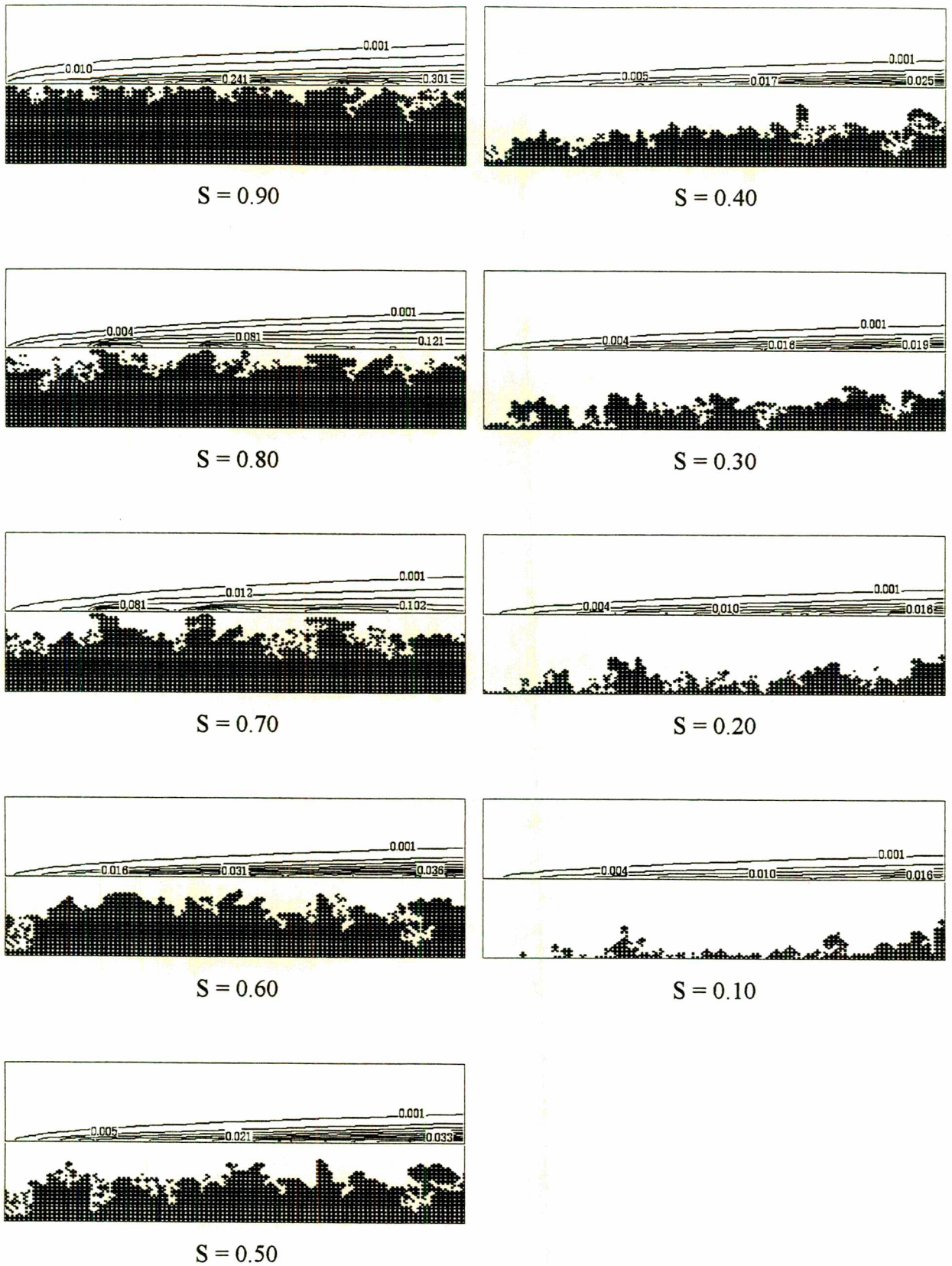
Fig. 5-58   Mass fraction boundary layer for U=5.0 m/s

S = 0.90

S = 0.40

S = 0.80

S = 0.30

S = 0.70

S = 0.20

S = 0.60

S = 0.10

S = 0.50
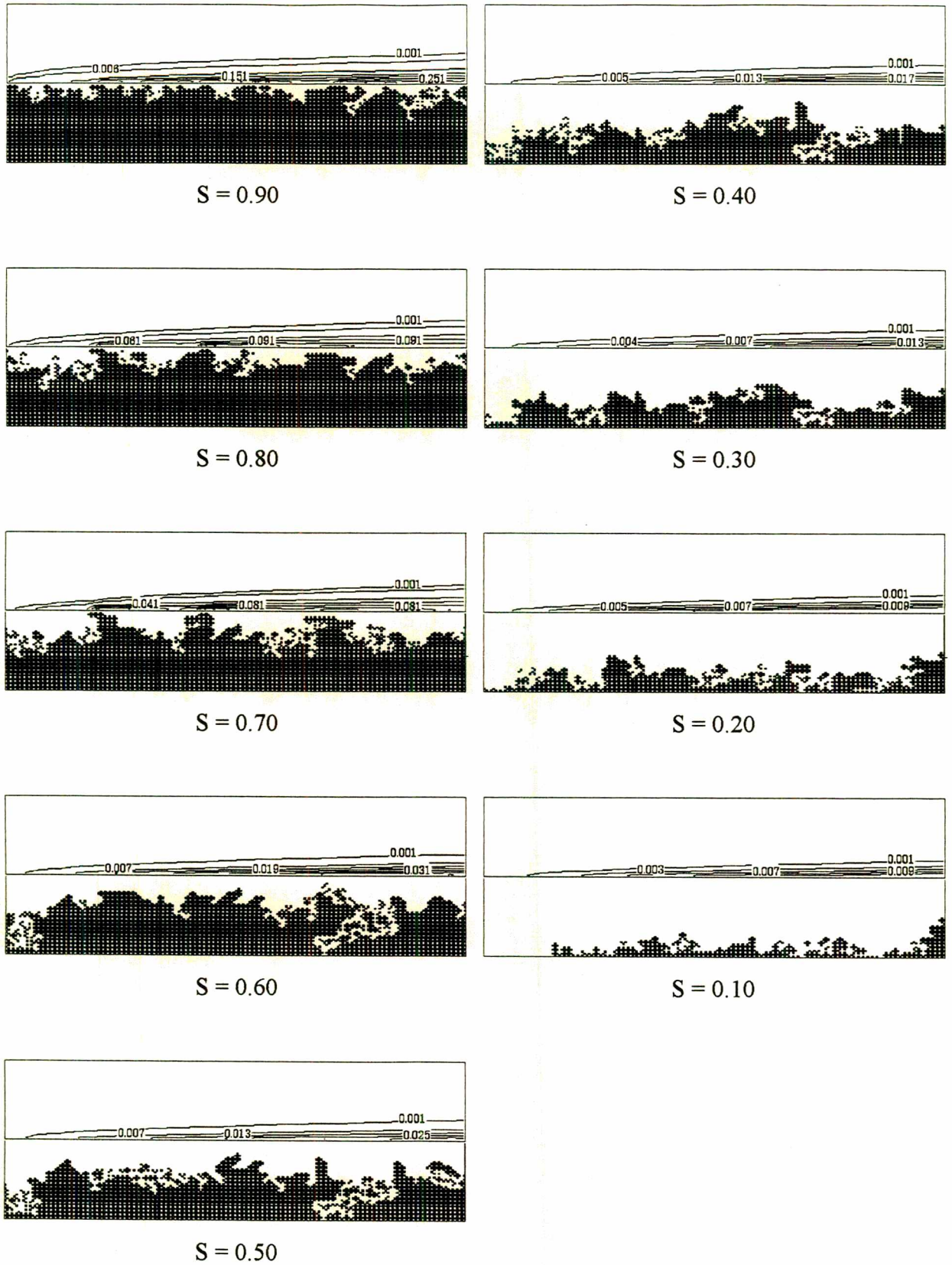
Fig. 5-59   Mass fraction boundary layer for U=10.0 m/s

S = 0.90

S = 0.40

S = 0.80

S = 0.30

S = 0.70

S = 0.20

S = 0.60

S = 0.10

S = 0.50

Fig. 5-60   Mass fraction boundary layer for U=1.0 m/s (color)

CHAPTER 6   CONCLUSIONS

A microscopic drying model for capillary porous medium is presented in this thesis. This microscopic model is based on a network approach for porous medium and is intended to study the mass transfer behaviors inside the porous medium at the pore level during the drying process. It can be used, for example, to study the effect of heterogeneities of phase distribution in porous medium, that cannot be attained by a macroscopic drying model due to the continuum approach. Moreover, the Kel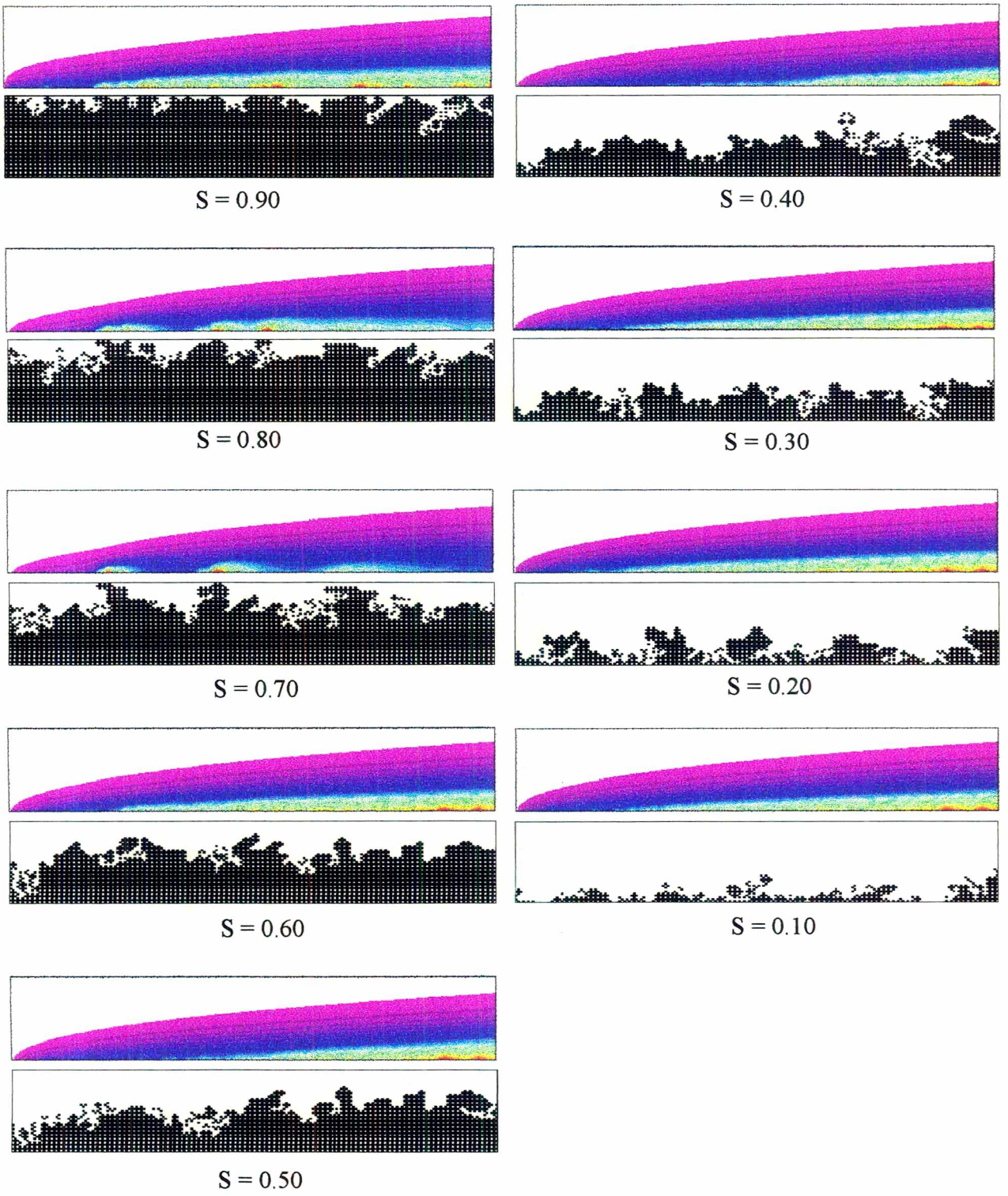vin effect can be studied in a quantitative manner. The influence of dry patches at the interface on the local mass fluxes can be shown clearly in the present simulation since the microscopic model is able to describe the phase distribution at the top surface.

The phase distribution effect, the Kelvin effect and the influence of inlet velocity of the external flow upon the drying process are studied in the present thesis using this microscopic model. From the simulations the following conclusions can be extracted.

- Three distinguished regions are observed in simulation, i.e., dry region, unsaturated region and saturated region. The evaporating front region (unsaturated region) is relatively stable, although it is far from being a flat surface. Many temporary liquid clusters appear in the unsaturated region as drying proceeds and the cluster number increases with increasing distance of the evaporating front from the top surface. In other words, the depth of the evaporating front region increases during the drying process. This observation indicates that the two-zone model used to describe the simultaneous heat and mass transfer during the falling rate period is more realistic than the single zone model.

- Phase distribution (moisture heterogeneities) has a great influence on the drying rate through the formation of the funicular dry zone, specially at the beginning of the drying process. This influence decreases with the receding of the evaporating front from the top

surface. The drying process becomes vapor diffusion dominated after the interface is totally dried and the influence of phase distribution heterogeneities decrease.

- Evaporation-condensation inside the porous medium is observed in the present simulations. Some clusters are condensing at one drying time interval and can not be eliminated by evaporation action. These condensing clusters always appear surrounded by other evaporating clusters. They can become evaporating clusters and thus be eliminated as drying proceeds.

- Concerning to the microscopic model, the Kelvin effect makes a very small difference in terms of the diffusion driving force caused by the meniscus curvature. The Kelvin effect, however, is very important from the point of view of the evaporation-condensation mechanism. The appearance of condensing clusters changes the drying path due to the liquid removing process. Consequently, the phase distribution is altered during the drying process. This influence is not the same for different network.

- Dry patches phenomena (surface saturation) have a strong influence on the local mass fluxes at the interface. The difference of mass fluxes for wet and dry surface can reach to ten times.

- Constant rate period is not observed for the simulations performed in the present work because that only 30% of top surface is covered with liquid even as top surface saturation equals to 1.0. A second drop in the drying rate is found, which indicates the moment that the top surface becomes totally dried.

- Numerical local mass transfer coefficient for the totally wetted top surface agree with the analytical value. The local mass transfer coefficient calculated from average mass flux density for actual situation shows a very interesting behavior. The local mass transfer coefficient agree well with the correlation value for all investigated inlet velocities even though the top surface is not totally covered with liquid, but periodically distributed.

- Inlet velocity of the external flow over the top surface of the porous medium affects the local mass fluxes. This is significant only while the interface is totally or partially wet. The influence of the inlet velocity decreases with the receding evaporating front. Concerning the stability of the evaporating front, it seems that this is only important at the beginning of drying.

It should be pointed out that the network size used in the present work (100x20) is not large enough to assure statistical homogeneity. As can be seen in chapter 5, different networks which are constructed with the same size distribution of pores and throats, but with a different random generator, do not show the same drying kinetics. In fact, the random generator will settle the spatial distribution of clusters of small diameter throats: when these clusters are located near the top surface, the effect is to increase the drying rate, as a consequence of smaller vapor diffusion resistance. The networks considered in the present work are, nevertheless, important for describing the effect of heterogeneities in the spatial distribution of pores on drying kinetics, specially at the very beginning of drying. In fact, spatial heterogeneities are frequently found in samples used for drying as a result of sample manufacturing. These heterogeneities have a great influence on the early stage of drying, when the drying depth is of same magnitude order as the mean heterogeneity length.

It is worthy reminding that the microscopic drying model presented here is, in some meanings, a simplified model. Naturally, there are many improvements that should be done for the model. The mechanism for liquid transfer considered here, for instance, is only the capillary force. The formation of liquid films on the porous surface at unsaturated regions, as have been observed by Prat in his experiments (1993), is not taken into account and may modify the drying kinetics. The gravity effect, which can play a role either as stablisant or destabilisant of evaporating front, is ignored. The model can not address all drying situations and heat transfer is not taken into account in the present model. To describe the porous medium better, the model should be extended to three dimensions.

REFERENCES

- Adler P. M., *"Porous Media, Geometry and Transpots"*, Beetterworth-Heinemann, Boston, 1992

- Bachmat Y. and Bear J., "Macroscopic Modeling of Transport Phenomena in Porous Media, 1: The Continuum Approach", *Transport Porous Media*, Vol. 1, pp. 213-240 (1986)

- Bear J. and Bensabat J., "Advective Fluxes in Multiphase Porous Media Under Non-Isothermal Conditions", *Transport Porous Media*, Vol. 4, pp. 423-448 (1989)

- Bories S. A., "Fundamentals of Drying of Capillary-Porous Bodies", *Convective Heat and Mass Transfer in Porous Media*, Kakaç S. et al. (eds), Kluwer Academic Publishers, Netherlands, pp. 391-434 (1991)

- Broadbent S. R. and Hammersley J. M., "Percolation Processes, Crystals and Mazes", *Proc. Cambridge Philos. Soc.*, Vol. 53, pp. 629-641 (1957)

- Burganos V. N. and Sotirchos S. V., "Diffusion in Pore Networks: Effective Medium Theory and Smooth Field Approximation", *AIChE Journal*, Vol. 33, pp. 1678-1689 (1987)

- Chandler R., Koplik J., Lerman K. and Willemsen J. F., "Capillary Displacement and Percolation in Porous Media", *J. Fliud Mech.*, Vol 119, pp. 249-267 (1982)

- Chatzis I., "A Network Approach to Analyse and Model Capillary and Transport Phenomena in Porous Media", *Ph. D. Thesis*, University of Waterloo, Canada (1980)

- Chatzis I. and Dullien F. A. L., "Modelling Pore Structure by 2-D and 3-D Networks with Application to Sandstones", *J. Can. Petrol. Technol.*, Vol. 16, pp. 97-108 (1977)

- Chen P. and Pei D. C. T., "A Mathematical Model of Drying Processes", *Int. J. Heat Mass Transfer*, Vol. 32, pp. 297-310 (1989)

- Cohen M. H., Webman I. and Jortner J., "Optical and Microwave Properties of Metal-ammonia solution", *J. Chem. Phys.*, Vol. 64, pp. 2013-2019 (1976)

- Conner W. C. and Lane A. M., "Measurement of the Morphology of High Surface Area Solids: Effect of Network Structure on the Simulation of Porosimetry", *J. Catalysis*, Vol. 89, pp. 217-225 (1984)

- Conner W. C., Lane A. M., Ng K. M. and Goldblat M. J., "Measurement of the Morphology of High Surface Area Solids: Porosimetry of Agglomerated Particles" *J. Catalysis*, Vol. 83, pp. 336-345 (1983)

- Constantinides G. N. and Payatakes A. C., "A Three-dimensional Network Model for Consolidated Porous Media. Basic Studies", *Chem. Engng. Commun.*, Vol. 81, pp. 55-81 (1989)

- Crausse P., "Etude Fondamentale des Transferts Couplés de Chaleur et de Masse en Milieu Poreux Non-saturé", Thèse Doctorat d'Etat, I.N.P.T. (1983)

- Crausse P., "Etude Fondamentale des Transferts Couplés de Chaleur-Masse en Milieu Poreux", *Int. J. Heat Mass Transfer*, Vol. 24, pp. 991-1000 (1981)

- Dias M. M. and Payatakes A. C., "Network Models for Two-Phase Flow in Porous Media, Part I: Immiscible Microdisplacement of Non-Wetting Fluids", *J. Fluid Mech.*, Vol. 164, pp. 305-336 (1986)

- Dias M. M. and Payatakes A. C., "Network Models for Two-Phase Flow in Porous Media, Part II: Motion of Oil Ganglia", *J. Fluid Mech.*, Vol. 164, pp. 337-358 (1986)

- Dullien F. A. L. and Batra V. K., "Determination of the Structure of the Porous Media", *Ind. Eng. Chem.*, Vol. 62, pp. 25-53 (1970)

- Eggarter T. P. and Cohen M. H., "Mobility of Exess Electrons in Gaseous He: A Semiclassical Approach", *Phys. Rev. Lett.*, Vol. 27, pp.129-132 (1971)

- Elliott R. J., Heap B. R., Morgan D. J., and Rushbooke G. S., "Equivalence of the Critical Concentrations in the Insing and Heisenberg Models of Ferromagnetism", *Phys. Rev. Lett.*, Vol. 5, 366-367 (1960)

- Essan J. W., in *Phase Transitions and Critical Phenomena*, edited by Domb C. and Green M. S., Academic, New York (1973)

- Fatt I., "The Network Model of Porous Media, I. Capillary Pressure Characteristics", *Trans. AIME*, Vol. 207, pp. 44-181 (1956)

- Fernandes C. P., "Caracterização Morfotopologia de Espaços Porosos: Reconstituição Multi-Escala e Simulação de Processo de Invasão de Fluidos Não-Molhantes", *Tese de Doutorado*, Depto. Eng. Mecânica, Univ. Federal de Santa Catarina (1994)

- Fisher M. E., *Proceedings of the IBM Scientific Computing Symposium on Combinatorial Problems*, New York (1964)

- Flory P. J., *Principles of Polymer Chemistry*, Cornell U. P, Ithaca, N. Y.,Chapter 9 (1953)

- Frisch H. L. and Hammersley J. M., "Percolation Processes and Related Topics", *J. Soc. Ind. Appl. Math.*, B11, pp. 894-918 (1963)

- Gray W. G., "General Conservation Equations for Multi-Phase Systems: 4. Constitutive Theory Including Phase Change", *Adv. Water Resour.*, Vol. 6, pp. 130-140 (1983)

- Hoshen J. and Kopelman R., "Percolation and Cluster Distribution I. Cluster Multiple Labeling Technique and Critical Concentration Algorithm", *Phys. Rev. B*, Vol. 14, pp. 3438-3445 (1976)

- Ioannidis M. A. and Chatzis I., "Network Modelling of Pore Structure and Transport Properties of Porous Media", *Chem. Engng. Sci.*, Vol. 48, pp. 951-972 (1993)

- Kaviany M., *"Principles of Heat Transfer in Porous Media"*, Springer Verlag, New York (1991)

- Kays W. M. and Crawford M. E., *"Convective Heat and Mass Transfer"*, 3rd edition, McGraw-Hill, New York (1993)

- Kloubek J., "A New Method for the Investigation of Porous Structures using Mercury Porosimetry", *Powder Technology*, Vol. 29, pp. 89-97 (1981)

- Kopelman R., "Excitons Ternary Mixed Molecular Crystals: 'A Prototype for the Primary Step of Photosynthesis?'", *J. Lumin.*, Vol. 12, pp. 775-780 (1976)

- Kopelman R., Monberg E. M., Ochs F. W. and Prasad P. N., "Exciton Percolation. Isotopic-mixed $_1B^{2u}$ Naphthalene", *Phys. Rev. Lett.*, Vol. 34, pp. 1506-1509 (1975)

- Kottler F., "The Distribution of Particle Sizes. Part I", *J. Franklin Inst.*, Vol. 250, pp. 339-356 (1950)

- Kottler F., "The Distribution of Particle Sizes. Part II", *J. Franklin Inst.*, Vol. 250, pp. 419-441 (1950)

- Lapidus G. R, Lane A. M., Ng K. M. and Conner W. C., "Interpretation of Mercury Porositry Data Using a Pore-Throat Network Model" *Chem. Engng. Commun.*, Vol. 38, pp. 33-56 (1985)

- Larson R. G., Davis H. T. and Scriven L. E., "Displacement of Residual Nonwetting Fluid from Porous Media", *Chem. Engng. Sci.*, Vol. 36, pp. 75-85 (1981)

- Larson R. G., Scriven L. E. and Davis H. T., "Percolation Theory of Two Phase Flow in Porous Media", *Chem. Engng. Sci.*, Vol. 36. pp. 57-73 (1981)

- Lee W. C., Plumb O. A. and Gong L., "An Experimental Study of Heat and Mass Transfer During Drying of Packed Beds", *Journal of Heat Transfer*, Vol. 114, pp. 727-734 (1992)

- Lenormand R., Touboul E. and Zarcone C., "Numerical Models and Experiments on Immiscible Displacements in Porous Media", *J. Fluid Mech.*, Vol. 189. pp. 165-187 (1988)

- Luikov, A. V., *Heat and Mass Transfer in Capillary - Porous Bodies*, Pergamon Press, Oxford, United Kindom (1966)

- Maneval J. and Whitaker S., "Effects of Saturation Heterogeneities on the Interfacial Mass Transfer Relation", *Proc. Sixth Int. Drying Symp.*, pp. 499-506 (1988)

- Masmoudi W., Prat M., "Heat and Mass Transfer between a Porous Medium and a Parallel External Flow. Application to Drying of Capillary Porous Materials", *Int. J. Heat Mass Transfer*, Vol. 34, pp. 1975-1989 (1991)

- Masmoudi W., Prat M. and Bories S., "Drying: Percolation Theory or Continuum Approach. Some Experimental Evidences", *in: Heat and Mass Transfer in Porous Media*, (Edited by Quintard M. & Todorovic M.), pp. 817-828, Elsevier, New York (1992)

- Moyne C. and Degiovanni A., "Water Vapor Diffusion and Thermal Conductivity of Wet Porous Media", *9th International Heat Transfer Conference*, Vol. 5, pp. 213-313 (1990)

- Moyne C., Batsale J. C. and Degiovanni A., "Approche Experimentale et Theorique de la Conductivite Thermique des Milieux Poreux Humides - II. Theorie", *Int. J. Heat and Mass Transfer*, Vol. 31, pp. 2319-2330 (1988)

- Patankar S. V., *"Numerical Heat Transfer and Fluid Flow"*, Hemisphere Publishing Corporation, Washington, (1980)

- Patankar S. V., "A Calculation Peocedure for Two-dimensional Elliptic Situations", *Numerical Heat Transfer,* Vol. 4, pp.409-425 (1981)

- Pathak P., Winterfeld P. H., Davis H. T and Scriven L. E., SPE 8846. *Improved Oil Recovery Symposium.* Tulsa, Oklahoma, (1980)

- Payatakes A. C., Dias M. M., "Immiscible Microdisplacement and Ganglion Dynamics in Porous Media", *Rev. Chem. Eng.,* Vol. 2, pp. 85-174 (1984)

- Payatakes A. C., Ng K. M. and Flumerfelt R. W., "Oil Ganglion Dynamics during Immiscible Displacement: Model Formulation", *AIChE Journal,* Vol. 26, pp. 430-443 (1980)

- Payatakes A. C., Tien C. and Turian R. M., "New Model for Granular Porous Media: I. Model Formulation", *AIChE Journal,* Vol. 19, pp. 58-67 (1973)

- Peishi C. and David C. T. P., "A Mathematical Model of Drying Processes", *Int. J. Heat and Mass Transfer*, Vol. 32, pp. 297-310 (1989)

- Philip J. R., de Vires D. A., "Moisture Movement in Porous Media under Temperature Gradient", *Trans. Amer. Geophys. Union*, Vol. 38, pp. 222-232 (1957)

- Philippi P. C. and Souza H. A., "Modelling Moisture Distribution and Isothermal Transfer in A Heterogeneous Porous Material", *Int. J. Multiphase Flow*, Vol. 21 (1995)

- Plumb O. A. and Prat M., "Microscopic Models for the Study of Capillary Porous media", *Drying'92*, edited by Mujumdar A. S., Elsevier Science Publishers B. V., pp. 397-406 (1992)

- Plumb O. A., Spolek G. A. and Olmstead B. A., "Heat and Mass Transfer in Wood During Drying", *Int. J. Heat and Mass Transfer*, Vol. 28, pp. 1669-1678 (1985)

- Prat M., "Percolation Model of Drying Under Isothermal Conditions in Porous Media", *Int. J. Multiphase Flow*, Vol. 19, pp. 691-704 (1993)

- Prata A. T. and Sparrow E. M., "Evaporative Mass and Heat Transfer from a Lid-driven Cavity", *Numerical Heat Transfer*, Vol. 13, pp. 27-48 (1987)

- Prata A. T. and Sparrow E. M., "Diffusion-Driven Nonisothermal Evaporation", *J. Heat Transfer*, Vol. 107, pp. 239-242 (1985a)

- Prata A. T. and Sparrow E. M., "Forced Convection Evaporation from a Cavity Containing a Liquid Whose Surface is Curved by Capillarity: Computations in Interlocking Rectangular and Cylindrical Domains", *Numerical Heat Transfer*, Vol. 8, pp. 667-688 (1985b)

- Prata A. T., "*Convecção Avançada*", Course Material (1990)

- Prata A. T. and Prat M., "Influence of Cavity and Viscosity on the Evaporation from a Capillary Tube System", submitted for publication (1995)

- Press W. H., Teukosky S. A., Vetterling W. T. and Flannery B. P., *"Numerical Recipes. The Art of Scientific Computing"*, 2nd ed., Cambridge University Press, Cambridge (1992)

- Quadri M. B., "Dinâmica de Resposta de Tensiômetros: Desenvolvimento Experimental e Modelação Numêrica", *Dissertação de Mestrado*, Depto. Engenharia Mecânica, Univ. Federal de Santa Catarina (1988)

- Reidand R. C. and Sherwood T. K., *The Properties of Gases and Liquids*, McGrawHill, New York, pp. 267-276 (1958)

- Rogers J. A. and Kaviany M., "Variation of Heat and Mass Transfer Coefficients during Drying of Granular-Beds", *J. Heat Mass Transfer*, Vol. 112, pp. 668-674 (1990)

- Rogers J. A. and Kaviany M., "Funicular and Evaporative-Front Regimes in Convective Drying of Granular Beds", *Int. J. Heat and Mass Transfer*, Vol. 35, pp. 469-480 (1992)

- Sclichting H., *"Boundary-Layer Theory"*, 6th edition, McGraw-Hill, New York (1968)

- Slattery J. C. and Bird R. B., "Calculation of the Diffusion Coefficient of dilute Gases and of the Self-diffusion Coefficient of Dense Gases", *AIChE Journal*, Vol. 4, pp. 137-142 (1958)

- Slattery J. C., "Two-Phase Flow Through Porous Media", *AIChE Journal*, Vol. 16, pp. 345-352 (1970)

- Tao Y. X and Kaviany M., "Simultaneous Heat and Mass Transfer from a Two-Dimensional, Partially Liquid-Covered Surface", *J. Heat Transfer*, Vol. 113, pp. 874-882 (1991)

- Tsakirouglou C. D. and Payatakes A. C., "A New imulator of Mecury Porosimetry for the Characterization of Porous Materials", *J. Colloid Interface Sci*, Vol. 137, pp. 315-339 (1990)

- van Brakel J., "Porespace Models for Transport Phenomena in Porous Media; Review and Evaluation with Special Emphasis on Capillary Liquid Transport", *Powder Technology*, Vol. 11, pp. 205-236 (1975)

- van Brakel J., Modry S. and Svata M., "Mercury Porosimetry: State of the Art", *Powder Technology*, Vol. 29. pp. 1-12 (1981)

- Whitaker S., "Flow in Porous Media I: A Theoretical Derivation of Darcy's Law", *Transport Porous Media*, Vol. 1, pp. 3-25 (1986a)

- Whitaker S., "Flow in Porous Media II: The Governing Equations for Immiscible, Two-Phase Flow", *Transport Porous Media*, Vol. 1, pp. 105-125 (1986b)

- Whitaker S. and Chow W. T-H, "Drying Granular Porous Media - Theory and Experiment", *Drying Tech.*, Vol. 1, pp. 3-33 (1983)

- Whitaker S., "Simultaneous Heat and Momentum Transfer in Porous Media: A Theory of Drying", *in: Advances in Heat Transfer*, Irvine T. J. and Hartnett J. P., eds., Academic Press, New York, Vol. 13, pp. 119-200 (1977)

- Wilkinson D., "Percolation Model of Immiscible Displacement in Presence of Buoyancy Forces", *Phys. Rev.*, A. 30-1, pp. 520-531 (1984)

- Wilkinson D. and Barsony M., "Monte Carlo Study of Invasion Percolation Clusters in Two and Three Dimension", *J. Phys. A: Math. Gen.*, Vol. 17, pp. L129-135 (1984)

- Yanuka M., "Percolation Processes and Porous Media. II. Computer Calculations of Percolation Probabilities and Cluster Formation", *J. Colloid Interface Sci.*, Vol. 127, pp. 35-47 (1989)